University Of Pardubice
Faculty Of Chemical Technology

A Model for remotely estimating water quality parameters in inland water bodies based on Landsat ETM+ data

Ing. Kwasi Asare Baffour Danquah

Doctoral Dissertation
2018

University Of Pardubice
Faculty Of Chemical Technology

A Model for remotely estimating water quality parameters in inland water bodies based on Landsat ETM+ data

Ing. Kwasi Asare Baffour Danquah

Supervisor: *Prof. Ing. Jaromira Chylkova, CSc*

Specialist Supervisor: *Ing. Tomas Brunclik Ph.D.*

Study Program: *Chemical and Process Engineering*

Study Field: *Environmental Engineering*

Doctoral Dissertation

2018

Declaration

I hereby declare that I have written the dissertation on my own. All the literary sources and the information used are listed in the bibliography. I was familiar with the fact that rights and obligations arising from the Act No. 121/2000 Coll., the Copyright Act, apply to my thesis, especially the fact that the University of Pardubice has the right to enter into a license agreement for use of the paper as a school work pursuant to §60, Section 1 of the Copyright Act, and the fact that should this thesis be used by me or should a license be granted for the use to another entity, the University of Pardubice is authorised to claim a reasonable fee to cover the costs incurred during the making of the paper, up to the real amount thereof.

I agree with the reference-only disclosure of my thesis in the University Library.

In Pardubice on June 29, 2018

_____

Kwasi Asare Baffour Danquah

Acknowledgement

My sincere gratitude goes to Associate Prof. Ing. Jaromira Chylkova, CSc. my supervisor, Ing. Tomas Brunclik Ph.D. specialist supervisor for this work, for their profound, diligent and professional guidance throughout the period of this research work and in the course of my doctoral studies.

Sincere thanks also to Prof. Ing. Petr Mikulasek, CSc. for his support and patience during my entire doctoral studies. Thanks to Dr. Stewart Green of the University of the West England, Bristol for his suggestions to make this work a success. My appreciation also goes to Dr. Philip Llewellyn Starke for taking the pains to proof read my script.

I would like to thank my wife Jeannie Seen Danquah and family for their motivation and support throughout my studies.

Finally to my colleagues at the Institute of Environmental and Chemical Engineering as well as friends who during the course of my studies and research work offered suggestions, valuable advice and opinions.

Dedication

I dedicate this work to my late grandmother Wilhelmina Akosua Asaah, my wife Jeannie Seen Danquah, parents, siblings and friends who have in diverse ways helped me through the course of my work.

Abstract

Monitoring of water quality parameters of inland water bodies and small inland water bodies specifically can be operationally expensive and involving. This work tries to explore how remote sensing could be used as a tool in monitoring selected water quality parameters in small inland water bodies in the Czech Republic. Models were created based of Landsat 7 ETM+ imagery based on acquisitions from autumn of 2011 until the Spring of 2015 to estimate water quality parameters. The images used were scenes of WRS-2, path and row 191/25 as well as 190/25 respectively. Samples were taken from 13 water bodies (Bunkov, Melice, Jezero, Oplatil, Pohranovsky rybnik, Velka Cerna, Opatovicky pisnik, Ujezdsky rybnik, Bohumilecsky rybnik, Spravcicky pisnik, pisnik Hradek, Bohdanecsky rybnik, Placicky rybnik), with water body area between 8-90 ha, around Pardubice and Hradec Kralove in the Czech Republic. The samples were analysed for chlorophyl-a, Total Carbon, Total Nitrogen, Total Organic Carbon, Temperature and Secchi Disk Depth. The 3×3 average window was used to limit the effect of noise on the images and water only mask was used in order to limit the process to open water areas specifically.

Models were developed based on best fit charts of water quality parameter vs. satellite band combination using linear function in the regression analysis. Models created for the water quality parameters had their performance tested based on r^2, RMSE and NRMSE. Band combination L3/L1 or the vice versa had best fit for most the models created. The exception was temperature which was based on surface radiance (brightness temperature in [K]).

Where L1-L3 are visible bands of atmospherically corrected Landsat 7 SR product. The models created are intended to help institutions that are mandated in monitoring water bodies.

Keywords

Landsat ETM+; Remote Sensing; Model; Inland Water Quality; Water Monitoring; In-Situ; Parameters; Monitoring; Limnology.

Abstrakt

Monitorování parametrů kvality vody u vnitrozemských vodních těles může být provozně nákladné a náročné. Tato práce se snaží prozkoumat, jak by bylo možné použít dálkového průzkumu země jakožto nástroje kmonitorování vybraných parametrů kvality vody v malých vodních tělesech v České Republice. Kodhadu parametrů kvality vody byly vytvořeny modely na základě snímků Landsat 7 ETM+ pořízených od podzimu 2011 do jara 2015. Byly použity tyto snímky: scény WRS-2, path a row 191/25 a také 190/25. Vzorky byly odebrány z 13 vnitrozemských vodních těles (Buňkov, Mělice, Jezero, Oplatil, Pohranovský rybník, Velká Černá, Opatovický písník, Újezdský rybník, Bohumilečský rybník, Spravčický písník, písník Hrádek, Bohdanečský rybník, Placicky rybnik) o ploše mezi 8-90 ha, vokolí Pardubic a Hradce Králové v České Republice. U vzorků byl analyzován chlorofyl-a, celkový uhlík, celkový dusík, celkový organický uhlík, teplota a průhlednost. Komezení obrazového šumu byl použit obrazový filtr 3x3 a komezení procesu čistě na otevřené vodní plochy byla použita maska vodních ploch.

Byly vyvinuty modely založené na grafech závislosti parametru kvality vody na kombinaci spektrálních kanálů satelitního senzoru za použití lineární regrese. Modely vytvořené pro parametry kvality vody byly hodnoceny na základě r2, RMSE a NRMSE. Uvětšiny vytvořených modelů nejlépe korelovala kombinace pásem L1 a L3. Výjimkou byla teplota, která byla založena na termálním kanálu přepočteném na jasovou teplotu [K].

L1-L3 jsou viditelná pásma atmosféricky korigovaného produktu Landsat 7 SR. Vytvořené modely mají pomoci institucím, které jsou pověřeny monitorováním vodních ploch.

Klíčová slova

Landsat ETM+; Dálkové snímání; Model; Kvalita vnitrozemských vod; Monitorování vody; In-situ; Parametry; Monitorování; Limnologie

Table of Contents

List of Figures

List of Tables

List of Abbreviations and Symbols

5S – Simulation of Satellite Signal in Solar Spectrum

6S – Second Simulation of Satellite Signal in Solar Spectrum

ATCOR – Atmospheric Correction

AVHRR – Advanced Very High Resolution Radiometer

CDOM – Coloured Dissolved Organic Matter

CHL-A – Chlorophyll-a

CWM – Centred Weighted Median

DN – Digital Numbers

DOS – Dark Object Subtraction

DP – Dark Pixel

ERE – Effective Resolution Element

ETM+ - Enhanced Thematic Mapper Plus

FWHM – Full-Width at Half-Maximum

GIS – Geographical Information System

GPS – Geographical Positioning System

HAB – Harmful Algal Blooms

IFOV – Instantaneous Field Of View

ISO – International Organization for standardization

ISODATA – Iterative Self – Organising Data Analysis Techniques, with a terminal A

L1-L8 – Spectral bands for Landsat 7 ETM+

LEDAPS – Landsat Ecosystem Disturbance Adaptive Processing System

MERIS – Medium Resolution Imaging Spectrometer

MODIS – Moderate Resolution Imaging Spectroradiometer

MODTRAN – Moderate Resolution Atmospheric Transmission

MSS – Multi-Spectral Scanner System

NASA – National Aeronautic and Space Administration

NDWI – Normalised Difference Water Index

NIR – Near Infra Red

NRMSE – Normalised Root Mean Square Error

OLI – Operational Land Imager

PDF – Probability Density Function

PMT – Photo Multiplier Tube

PSF – Point Spread Function

RGB – Red Green Blue

RS – Remote Sensing

RMSE – Root Mean Square Root Error

RVIN – Random–Variation Impulsive Noise

SLC – Scan Line Corrector

SM – Standard Median

SNR – Signal to Noise Ratio

SPKN – Speckle Noise

SPN – Salt and Pepper Noise

SPOT – HRV- Satellites Pour l'Observation de la Terre- Visible High Resolution

SRF – Spectral Response Function

SRP – Spatial Resolution Power

SDD – Secchi Disk Depth

SWIR – Short-Wave InfraRed

TC – Total Carbon

TIC – Total Inorganic Carbon

TIFF – Tagged Image File Format

TM – Thematic Mapper

TN – Total Nitrogen

TOAR – Top Of Atmosphere Reflectance

TOC – Total Organic Carbon

TP – Total Phosphorus

TSM – Total suspended Matter

US EPA – United States Environmental Protection Agency

USGS – United States Geological Survey

WM – Weighted Median

WRS – World Reference System

INTRODUCTION

Background

Water bodies kept as reservoirs, ponds and lakes need to be carefully managed as their quality has a lot of effects on those using it. The state of water bodies could be attributed to both human activities as well as natural phenomenon. These activities physically, chemically and biologically affect water quality [1]. The human activities that affect the quality of inland water bodies might emanate from diversion of water courses, building of dams, draining of wetlands, intentional and accidental channelling of waste in these water bodies, as well as other factors [1]. Natural phenomenon that affect the quality of inland water bodies could be from excessive erosion, torrential rainfalls, mud flow, land slides and others [2]. Globally, the origin of penury is attributed in part to the deterioration of water quality caused by the development of Harmful Algal Blooms (HABs), such as cyanobacteria blooms. The increasing development of such HABs reflects the advanced state of aquatic ecosystem eutrophication caused by urban, agricultural, and industrial developments. Once established in lakes, cyanobacteria populations are extremely difficult to control except through the long-term reduction of nutrient inputs from the watershed and from internal sources. The users could be humans or aquatic life and making sure these water bodies have a standard quality is a tedious and sometime time consuming and laborious as well as costly work to do. In addition, standard *in situ* sampling and sample analyses are very expensive. Example, more than $650,000 CAN was spent to collect and analyse *in situ* samples from 150 water bodies in the province of Quebec alone during 2009 [3]. Measuring of quality parameters are done in-situ and ex situ. If you have a number of water bodies to deal with, one can imagine the work involved. Chlorophyll can be one of such parameters to measure with respect to water quality and there are other water quality parameters such as Total Carbon, Total Organic Carbon, Total Nitrogen, Temperature, Secchi Disk Depth, Coloured Dissolved Organic Matter. Remote sensing, with its synoptic viewing, consistent recurrence and capacity to provide information over a range of wavelengths represents an attractive alternative method to monitor algal blooms. Satellite sensors that provide data in visible and near infrared (NIR) wavelengths can be used to estimate water quality parameters based on its high absorption of the blue and red part of the electromagnetic spectrum, and its high reflectance of the green and NIR wavebands. Thus, bio-

optical models that relate the apparent optical properties of water bodies to their inherent optical properties can be used to estimate water quality parameters [4]. Case 1 Some years past, it could be said that, the use of satellite data had been limited to open ocean waters classified as Case-1 waters, in which phytoplankton and co-varying material of biological origin are the principal constituents responsible for variations in ocean inherent optical properties [5] and algal pigments are often the only component optically active in the water [6]. Case1 water bodies are those waters whose properties are optically obtained basically by the use of phytoplankton, as well as related coloured dissolved organic matter and waste degradation products [7].In some lake waters, the use of airborne and satellite remote sensing has demonstrated to provide more reliable temporal-spatial information about water quality and the extent of cyanobacterial blooms than does conventional monitoring [8]. Most of these water bodies that are mostly monitored are the big lakes, ponds as well as reservoirs. The reliance on Landsat data will help in creating models that cover the various water bodies that are to be monitored for the various water quality parameters (TC, TOC, TN, Chl-a, SDD, T). Landsat ETM+ data was chosen due to its availability at no cost for research [9]. There exists a huge potential in the use of remote sensing as a tool in the monitoring of inland water quality.

Context

The monitoring of inland water bodies is generally a tedious and continuous process. There is therefore the need for methods that are most appropriate as well as less expensive to use. To monitor every inland water body is nearly impossible relying on traditional methods of inland water quality monitoring. Most of the lakes, ponds, reservoirs that are monitored are the bigger ones. There is a problem as the smaller ones are either not frequently monitored or not monitored at all. Only a few of the water bodies used in this research work are actually monitored (especially the fish ponds). But suffice to say that most of these inland water bodies were being used for various purposes (recreational, fishing, animal habitat) during the time of this research. Therefore the quality of these various water bodies despite their size should be of concern to everyone. Using a remote sensing based method for monitoring the water quality is an option that should be inculcated in dealing with this problem.

Purpose of Research

The general purpose of this research is the use of remote sensing as a tool in monitoring in-land water bodies. The main objective of this research is to help formulate a model with use

of remote sensing as a tool to monitor water quality parameters in in-land water bodies using Landsat 7. Mostly such monitoring is normally done by way of in-situ or on site measurements to know the actual levels of monitored parameters. This research work seeks to investigate and to examine to potential of using remote sensing in this monitoring rather than the use of in-situ measurements. This is also to investigate the effect of smoothing on satellite imagery. This is because of the sizes of the water bodies being monitored. We seek to find out the possible correlation between Chl-a and other water parameters such as water temperature, nitrogen, carbon, organic carbon and water depth using the Secchi disc.

Significance and Scope

Quite a number of the works in this area have mostly centred on larger lakes. This work seeks to bring out the possibility of using remote sensing as a tool in estimating the levels of water quality parameters in smaller inland water bodies. There is also the issue of noise and cloud effect on images. The smoothing of images over small water bodies can be problematic. The effectiveness of water only mask for purposes of smoothing will be investigated. The models are also intended to work independently regardless of the season and inland water body type as at times not the case in this research area. This research is centred on inland water bodies specifically around the Pardubice and Hradec Kralove region.

1 THEORETICAL PART

1.1 Remote Sensing

This chapter takes into consideration the various theories and principles that will be employed in all aspects of this research work. First all the historical basis of remote sensing and what actually constitutes remote sensing. The various fundamental processes involved in the process of remote sensing is also enumerated in this chapter. This consists of resolution, noise and its effect on remote sensing images. The techniques of image processing is also discussed in chapter. This encompasses classification of remotely sensed data, smoothing techniques and atmospheric correction methods. Some specific works on inland water quality monitoring based on R.S are also reviewed. Some explication would be given on some water quality parameters that can be remotely sensed and the importance of monitoring water quality parameters is done at the end of this chapter.

1.1.1 Historical Background

The American Society of Photogrammetry, defines remote sensing as the 'imagery acquired with a sensor other than (or in addition to) a conventional camera through which a scene is recorded, such as by an electronic scanning, using radiations outside the normal visual range'.In general this technology started in the in the 18th century, where people took aerial images using balloons with newly invented cameras. Some historians attribute this' terminology to Evelyn L. Pruitt of the U.S office of Naval Research as the one who first used this word in 1960' [10] [11].There were other further trials and improvements but this processes really did become more useful and enhanced in the 1970s [11]. This was when instruments were flown on Skylab and on the Landsat, which was one of the foremost satellites dedicated to the monitoring of land and ocean surface globally [12].

To delve a bit further it must be noted that this technique emanated from aerial photography. As earlier said balloons were used in the developmental stage of this technique, specifically in 1858 a balloonist called Gaspard-Felix Tournachon (Nadar) was the first to capture aerial photograph Bievre Valley [13]. He further did a lot more of such 'aerial photography that in the year 1859, the French army asked him for aerial photograph for their

campaign in Italy. Other notable people also contributed to the development of this technique. James W. Black and Professor S. King worked on this technique in Boston in the 1860s. They also took photographs from a balloon at an altitude of 1200 feet by holding a cable to the camera from the balloon [11]. It was not only balloons that was used in taking aerial pictures, kites were also employed for the same purposes someone worth mentioning in this regard is Arthur Batut who did so in the 1880s by attaching a camera to a kite to take aerial photographs [13]. Though there were initial problems in the images that were taken further processing was able to correct these defects. Another pioneer of the use of kite in taking aerial photographs was George R. Lawson, who use a kite to take aerial photographs of an earthquake and wild fires in San Francisco in 1906. He developed the use of kites with cameras attached to them unmanned which was called Captive Airship [11] [13] [14].

Another pioneer of Remote Sensing is Julius Neubranner, in 1903 he designed a breast mounted camera and placed it on pigeons who flew around with it taking images from the skies with the cameras taking shots within 30 second intervals [13].

What Is Remote Sensing

With all the above historical background given one would ask what is **Remote sensing?** Many academicians and writers alike have given quite a number of definitions, some of which has been defined in this work. Remote sensing is not the same as Earth Observation, which is a term that is used for remote sensing measurements made using aircrafts and satellites, observations are often collected in two-dimensional arrays of pixels recorded at different wavelengths or bands comprising of digital images, to this extent Earth observation image may contain both spatial and spectral information of the earth surface [15]. Early researchers in Remote sensing came up with different views with respect to its definition. In Colwell [16] the term Remote Sensing is described in its broadest sense merely means reconnaissance from a distance. Landgrebe [17] defines RS as 'the science of deriving information about an object from measurement from a distance from the object, that is without the actually coming in contact with it'. The quantity measured in present- day remote sensing systems is the electromagnetic energy emanating from objects of interest and although there are possibilities such as seismic waves, sonic waves and gravitational force, attention is mostly focused on systems which, measure electromagnetic energy. Remote Sensing includes all methods of obtaining images or other forms of electromagnetic records of the earth surface from a distance

and the treatment and processing of the image data. In a wider sense is concerned with detecting and recording electromagnetic radiation from the target areas in the field of view of the sensor instrument. This radiation may have originated directly from separate components of the target area; it may be solar energy reflected from them; or it may be reflections of energy transmitted to the target area from the sensor itself [18]. It can also be said to be the art and science of reading, measuring, and analysing information about a phenomenon from a distance [19]. Remote Sensing is defined by Jensen [20]'as the technique of obtaining information about objects through the analysis of data collected by special instruments that are not in physical contact with the objects of investigation'. It can also be said to be the measurement of object properties on the earth surface using data acquired from an aircraft or a satellite [21]. We can say is the practice of deriving information about the earth land and water surfaces using images acquired from an overhead perspective, using electromagnetic radiation in one or more regions of electromagnetic spectrum, reflected or emitted from the earth surface [22]. Its therefore something at a distance rather than on the spot. As such, remote sensing can be regarded as reconnaissance from a distance,*"tele detection"* or a form of the common adage *"look but don't touch"*. Remote sensing thus differs from **in situ sensing**, where the instruments are immersed in, or physically touch, the objects of measurement. Furthermore this technique involves the measurement of objects on the earth surface using data acquired from aircraft and satellites with the reason being its attempt to measure objects of interest from afar rather coming in contact with the objects as illustrated in [23]. Liew [24] described remote sensing as 'activities of recording/perceiving/observing objects or events at faraway places and the sensors are not in direct contact with the objects or events being observed'. A common example of an in situ instrument is the soil thermometer. Liu and Mason [25] furthermore puts RS as 'the science and art obtaining information about an object, area, or phenomenon through the analysis of data acquired by a device that is not in contact with the area, object, or phenomenon under investigation'.

Traditionally, the energy collected and measured in remote sensing has been electromagnetic radiation, including visible light and invisible thermal infrared (heat) energy, which is reflected or emitted in varying degrees by all natural and synthetic objects. The scope of remote sensing has been broadened to include acoustical or sound energy, which is propagated under water. With the inclusion of these two different forms of energy, the human eye and ear are examples of remote sensing data collection devices. The instruments used for

this special technology are known as **remote sensors** and include photographic cameras, mechanical scanners, and imaging radar systems. Most of these sensors pick up information by measuring the transmission of energy from the surface of the earth in different portions of electromagnetic spectrum regardless of type of sensor, they are designed to both collect and record specific types of energy that impinges upon them and detect variations in energy in both the visible and non-visible areas of the spectrum [11]. In relation to monitoring water quality remote sensing could be defined as by Campbell [26] to be the practice of deriving information about the earth's land and water surfaces using images acquired from an overhead perspective, using electromagnetic radiation in one or more regions of the electromagnetic spectrum, reflected or emitted from the earth's surface.

Remote sensing devices can be differentiated in terms of whether they are active or passive. Active systems, such as radar and sonar, beam artificially produced energy to a target and record the reflected component. Passive systems, including the photographic camera, detect only energy emanating naturally from an object, such as reflected sunlight or thermal infrared emissions. Today, remote sensors, excluding sonar devices, are typically carried on aircraft and earth-orbiting spacecraft, which has led to the familiar phrase "*eye in the sky*". Sonar systems propagate acoustical energy through water for the reconnaissance of subaqueous features. In remote sensing the atmosphere does play a major role in the capturing of data. The atmosphere separates the earth and the sensors especially on satellites, in this direction it's essential for us to understand the impact of electromagnetic radiation moving from the earth to the sensor through the atmosphere. The effect of this radiation passing through the atmosphere is absorption and scattering of radiation in the atmosphere[24]. To complete the remote sensing process, the data captured and recorded by remote sensing systems must be analysed by interpretive and measurement techniques in order to provide useful information about the subjects of investigation (Figure 1). These techniques are diverse, ranging from traditional methods of visual interpretation to methods using sophisticated computer processing. It cannot be emphasised too strongly that data is not information. Accordingly, the two major components of remote sensing are data capture and data analysis [27].

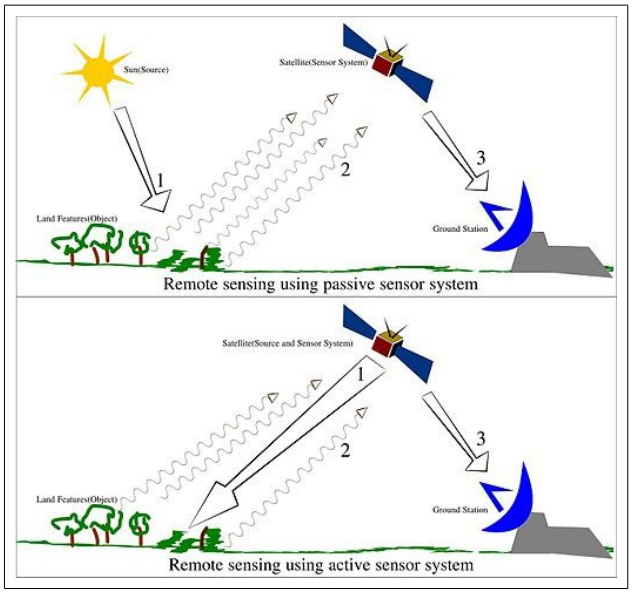

Figure 1: Principle of remote sensing. [23]

1.1.2 Resolution

Remote sensing uses sensors as a tool in its measure of the various parameters being researched on. Sensors of satellites are used to gather information about the object that is of attention. This information about these objects are normally stored as a grid. This grid form of the covered area and this individual image points called pixels. Resolution is very key in understanding exactly how these parameters are remotely sensed. Sensing different aspects of the environment requires different type of resolution. Resolution could be said to be the dimensions and the information content that the pixels of an image contain [28]. The ability of an imaging system (sensor) to record in fine detail a distinguishable manner [29]. Its the maximum separating or discriminating power of measurement and could be high or low [30]. Maini and Agrawal defined resolution as the ability of an entire remote sensing system to be able to render a sharply define image [31]. Generally an image could be of high, medium or low resolution. Image resolution applies to raster digital images, film images, as well as other types of images and its units could be tied physical sizes such lines per mm, lines per inch or to the overall size of the image [32]. In a more inclusive sense resolution would the ability of a remote sensing system (sensor) to record and display fine spatial, temporal, spectral and radiometric detail [22]. Resolution is divided into four types, which are Spatial, Temporal, Spectral and Radiometric resolutions [26].

1.1.2.1 Spatial Resolution

Generally the sizes of pixels are dependent on the sensors being used (Table 2). This determines the resolution of the image. Pixel could be said as defined by Gatrell [33] to be the 'fundamental spatial entity in a GIS based raster'. The size of a pixel is the resolution at which the pixel is displayed. From the NASA handbook for Landsat 7, spatial resolution is defined as the power that revolves an instrument needed for the discrimination of features, based on detector size, focal length, and sensor altitude is referred to as spatial resolution [28].

Table 1: Resolution types and their pixel sizes.

Resolution Type	Pixel Size (m)
Low	Larger than 30
Medium	2-30
High	Less than 2

In other words could be said to be the measure of how closely resolved lines are in an image [32]. The ability to distinguish between two closely placed objects and to an extent the minimum distance between two objects at which the images of the two objects appear distinct and separate [34]. Table 1 summaries the quantitative categories of resolution types and their pixel measurements. Figure 2 Gives example how different spatial resolutions influence shape of an object as seen in remote sensing image. Table 2 shows various satellite sensors and their spatial resolutions.

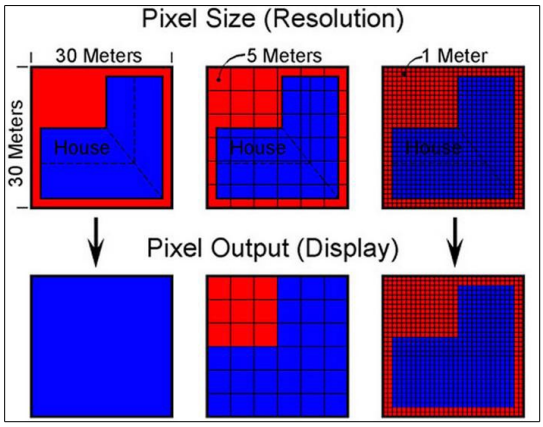

Figure 2: Spatial resolution- pixel size. [134]

Table 2: Satellite sensors and their spatial resolution [243].

Satellite	Orbital Height	Spatial Resolution
Landsat	700	30m MS, 15m pan
SPOT 2.4	832	20m MS, 10m pan
SPOT 5	832	10m MS, 20m SWIR, 25m pan
IRS P5	618	25m pan
CBERS	778	80m MS, 160m thermal
IKONOS	681	MS 4m, pan 1m
Orb View 3	470	MS 4m, pan 1m
Quick Bird 2	450	MS 244m, 0.61m pan

Mather and Koch [35] defines spatial resolution as the measure of the smallest angular or linear separation between two objects that can be resolved by a sensor and is expressed by the size of the specific pixel on the ground in meters. Spatial Resolution also can be said to be the ability to distinguish between two closely spaced objects on an image, taking into consideration the minimum distance between two objects at which the images of the objects appear distinct and separate [36]. It corresponds to the area covered on the earth's surface to compute one measurement (or one picture element 'pixel') of the sensor [37]. Spatial resolution can also be the fineness of detail visible in an image and this corresponds to the ground pixel size [38]. Figure 3 shows how images with various types spatial resolution is seen [39]. For example as stated by Townsend [40], there are four separate criteria on which one can base on. One of such measures which is commonly used is the geometric properties of the imaging

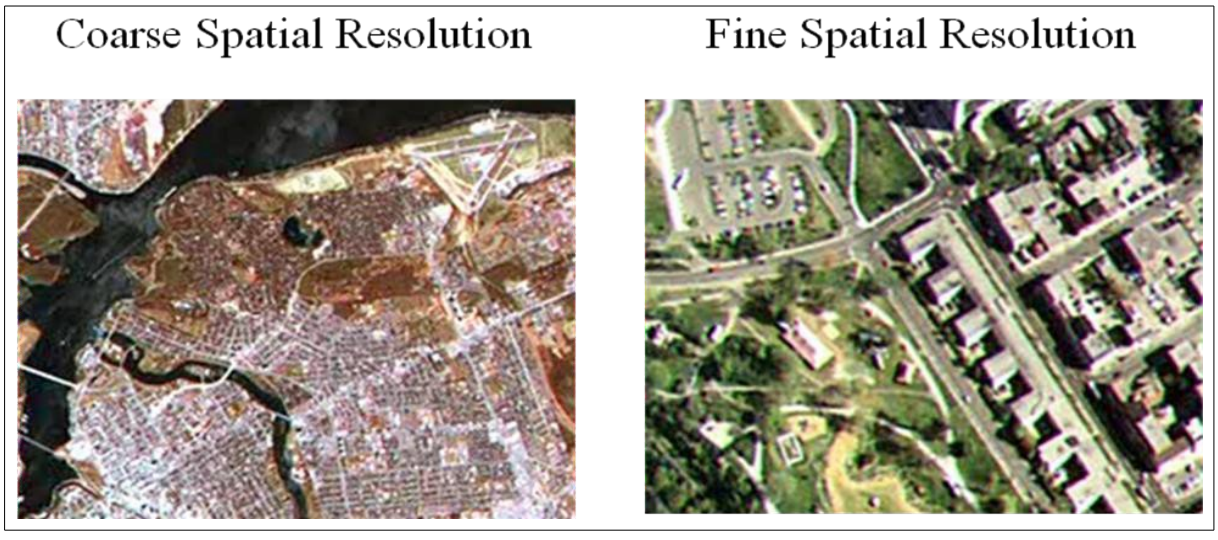

Figure 3: Low and high spatial resolution. [39]

system, based on the instantaneous field of view (IFOV), its the area on the ground, view by an instrument in a given altitude at any given instant of time [35]. An alternative to this measure is the angular field of view of a sensor which is independent of height. It is a relative measure as it an angle and not length [20]. To measure IFOV is normally done in two ways as described by [35], one this can be done as an angle α or the equivalent of the distance XY on the ground as seen in Figure 4. To calculate the actual and distinct from a nominal IFOV depends on a number of factors. With regards to satellite, there is none with a stable orbit therefore its height from the earth will vary. Example Landsat 1 to 3 had a nominal altitude of 913 km and the actual varied between 880 and 940 km [35]. The lower the altitude of the sensor the smaller the IFOV and the higher the altitude, the bigger the IFOV.

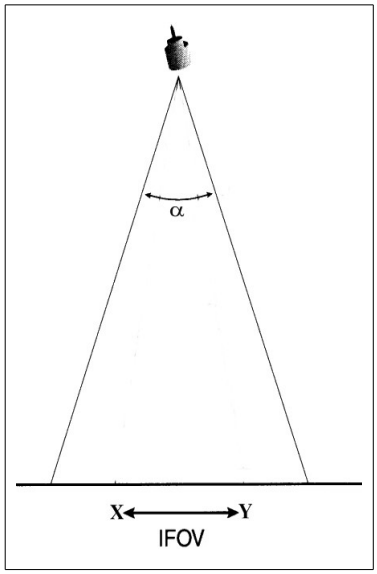

Figure 4: Instantaneous field of view. [35]

The alternative method or measure of IFOV is on point spread function (PSF) as described in [41] [35], [42]. For instance the presence of relatively bright dark objects within an IFOV of a sensor will increase or diminish the PSF to make the observed radiance either high or low with respect to the surrounding areas.

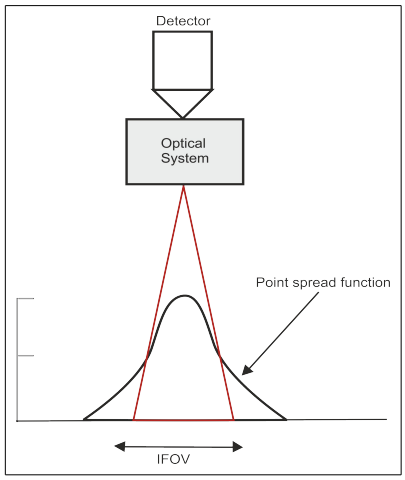

Figure 5: The point spread function as a way of measuring IFOV [35]

This is described in Figure 5 example thats why, objects with features that has high-constrast such narrow rivers and canals are mostly visible on Landsat ETM+. This is the case even though they have a width that is less than the sensor's 30m resolution.

Spatial Resolving Power

The use of these word is sometimes done interchangeably with spatial resolution but these two are not the same. Spatial resolving power is the imaging system or a component of the system [36]. Wassai and Kalyankar defines spatial resolving power as the ability of a particular sensor to render sharply defined image [43]. Some researchers and writers a such based their definition of resolving power on IFOV. Basing our definition solely on the IFOV is more of geometric and we must take into account the radiance that is generated as per the definition of remote sensing, it detects and records the radiance of spectral properties being measure of a specific target. Its worth taking into account effective resolution element (ERE), [35]

1.1.2.2 Temporal Resolution

It could be said to be either the theoretical or operational capabilities for a remote sensing system to repetitively acquire imagery over a time interval [44]. Temporal resolution

refers to repeatedly observe a scene at a regular interval, taking into consideration the temporal frequency with which a given scene can be imaged which could expressed in days [45]. Mather defines temporal resolution as the time that elapses between successive dates a sensor acquires images of a given point on the ground and this revisit time may be measured in minutes [46]. The amount of time it takes for a sensor to return to a previous image location, which is known as the repeat cycle or the time interval thats between acquisitions of two images [47]. This is further elaborated in Table 3. Other researchers and writers alike have defined TR in similar fashion. This can be seen in Jensen [48], Bhatti [49], Yuan [50], Webster and Eren [37]. In respect to the sensor being used, temporal resolution may vary in terms of the time. The platform as earlier mentioned has effect on it as well, specifically whether it's geostationary or not. The location of the sun and its illumination has an impact on temporal resolution of a sensor, that is, sun illumination directs the a sun-synchronous orbit and dictates the time and period of the day that images should be taken at a particular location [50]. The imaging revisit time in general increases at higher latitudes due to significant side lap between consecutive satellite passes [38]. This is relevant as it helps the sensors within the visible to infrared region from taking images especially in the dark or night. This makes most of the images taken usable and thereby maximising the temporal resolution of the sensor being used [38].

Table 3: some satellite sensors and their revisit time or temporal resolution [245]

Name of Sensor	Revisit or Temporal Resolution (days/years)
NOAA AVHRR	1 day
MODIS	1 to 2 days
BuickBird	1 to 3.5 days
IKNOS	16 days
Landsat ETM+	16 days
RADARSAT 1	24 days
SPOT 5	26 days
NAPP	5 years

Actual resolution depends on a variety of factors some being, the sensor or satellite capabilities, the swath overlap as well as the latitude, signal to noise ratio, swath with of the sensor [51]. Its possible to have a shorter revisit time for an area that has overlap in the imaging swaths of adjacent orbits [52]. Figure 6 depicts this phenomena. A typical example is the polar regions as it has more side laps and this is displayed in Figure 7.

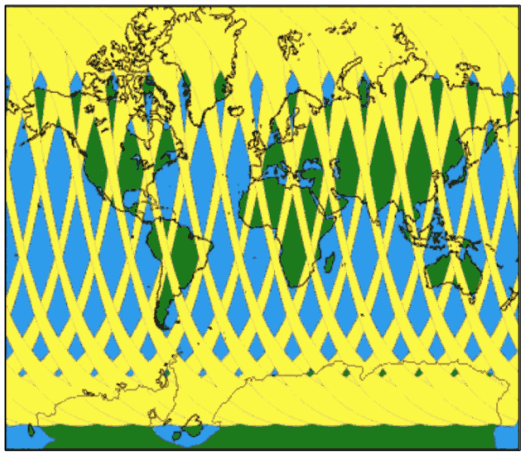

Figure 6: Overlap in adjacent swaths: revisit time. [44]

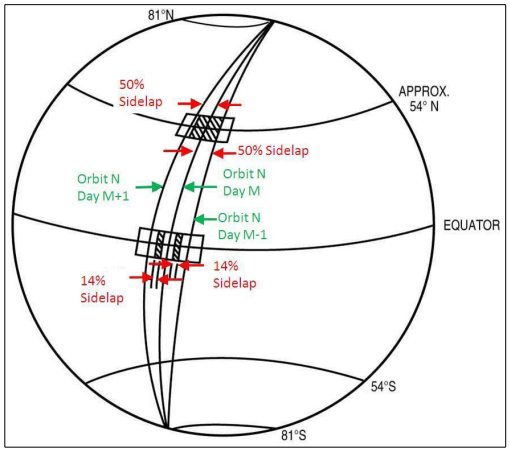

Figure 7: overlap in adjacent swaths. [52]

1.1.2.3 Spectral Resolution

The sensitivity of a sensor to respond to specific frequency range, which often covers not only visible light but also non-visible light as well as electromagnetic radiation. The spectral resolution in R.S denotes the ability of a sensor to define the fine wavelength intervals [22]. Bandwidth at which an electromagnetic radiation is used by a sensor [31]. It reflection of the bands that a sensor is able to acquire within a given electromagnetic spectrum [53]. In other words, its the point of sensitivity of a remote sensing system (sensor) within an electromagnetic spectrum with respect to its width and intervals. The wavelength at which band to which a sensor is sensitive [54]. It could also be said to be the bandwidth utilized in an electromagnetic spectrum [37]. Figure 8 displays electromagnetic spectrum and the respective wavelength. Spectral resolution can be either high or low depending on the bandwidth's width. Furthermore this could be referred to as the width across the electromagnetic spectrum that an

R.S instrument is detecting [38] [55]. The narrower the bandwidth, the higher the spectral resolution and vice versa.

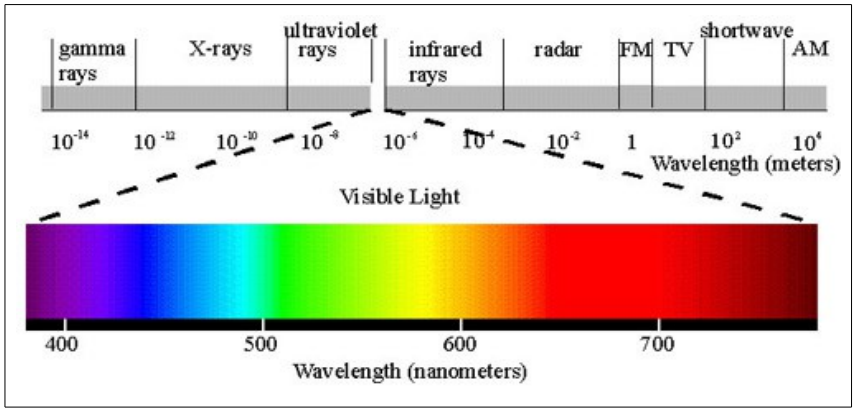

Figure 8: Spectral resolution: electromagnetic spectrum. [55]

The number of bands of a sensor its an important aspect of spectral resolution of every sensor and its electromagnetic spectrum as stated earlier. Sensors could be be grouped into three categories based on their bands as seen in Table 4. Also other factors to be consider in determination of spectral resolution of a sensor are, the spectral response of the function (SRF) of each band and the full-width at half-maximum (FWHM).

Table 4: Spectral Resolution types and the number of bands they contain.

Spectral Resolution	Number of Bands
High	220
Medium	3 to 15
Low	3

Signal to noise ration (SNR), has to do with the ratio between the intensity of received signal containing wanted physical information and the background noise [56]. Furthermore, SNR has to do with the minimum power level required by a sensor to be able to identify an object in the presence of noise [31]. A measure of the purity of a signal [35]. Example Smith

and Curan [57], [58] estimates the SNR for these sensors AVHRR, Landsat TM and SPOT HRV as 38:1, 341:1, 410:1 respectively.

$$N = 2^R \tag{1}$$

where *S* is the signal which is the actual energy reaching the detector of the sensor and *N* is the background Noise (random error in the measurement). *N* can be derived by equation,

$$N = \sqrt{\frac{\sum_{i=1}^{n} (DN_i - m_{DN})^2}{n-1}} \tag{2}$$

Where m_{DN} is the mean value of the *DNs* in the sample. *N* is the number of *DN* values in the sample. Figure 9 displays the spectral response for Landsat 7 ETM+ and landsat 8 OLI.

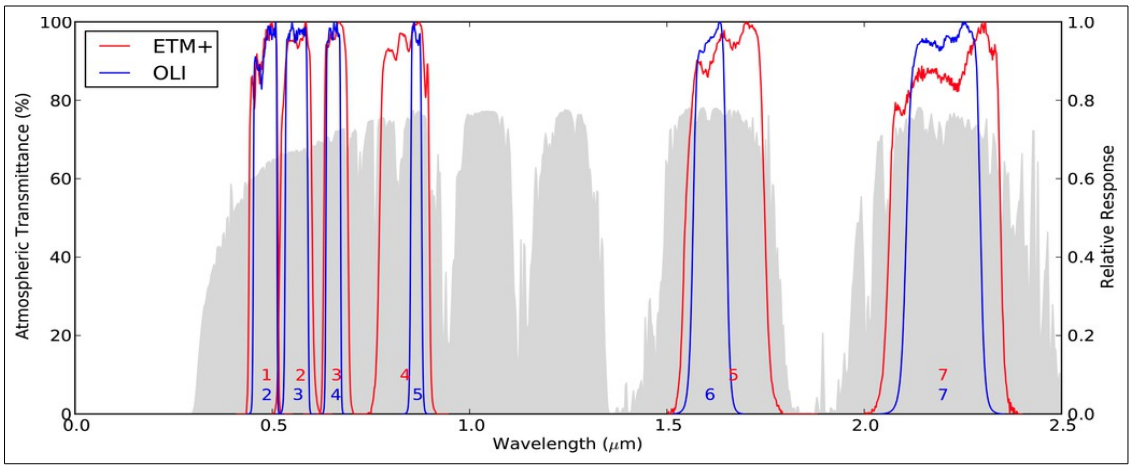

Figure 9: Spectral response for Landsat7 ETM+ and Landsat8 OLI. [247]

It is important to bring a balance between SNR and higher spectral resolutions. As there no perfect image with good resolution as well as a perfect SNR. In other word to deal with this better to adapt multi variate measures so both SNR and spectral resolution are appreciably dealt with. As stated by Mather, it is better to adopt a multivariate approach that significant differences (or similarities) that may remain hidden variables, are considered one at a time and not simultaneously [59].

1.1.2.4 Radiometric Resolution

Radiometric resolution is the number of digital quantization levels thats used to express data collected by a specific sensor [35]. The smallest change in intensity level that a remote sensing system can detect [24]. The specification of differences in brightness of an image that can be perceived [60]. In other words its the level of sensitivity of sensor or detector to be able to differentiate in signal strength as it records the radiant flux reflected or emitted from the coverage area [54]. Radiometric type of resolution is the ability of a remote sensing system to be able to record many levels of values for example, Landsat MSS recorded data in grid cells ranging from 0-63 where as the ETM and ETM+ does record from range of 0-255 [38]. Navulur [61], explains this type of resolution as the number of grey levels that can be recorded for a given pixel. Its measured in bits. The total number of quantization levels used in a sensor [62]. Radiometric resolution, takes into consideration the wavelength as expressed by Webster and Eren [37], it is the number of bits that are used in the recording of a given energy corresponding to a given wavelength. In most cases the higher the radiometric resolution, the better it is for small differences in the reflected or emitted radiation and also the larger its volume the measured data would be. Radiometric resolution mostly depends on the wavelengths and the type of spectrometer of the sensor being used. In monitoring the environment using remote sensing, the reflected signal are captured as analog and then converted to digital numbers (DN) or grey level values. The conversion from analog to DN is referred to as analog to digital conversion (A/D). To find the range of pixel values, one can use the below equation

$$SNR = S/N \tag{3}$$

where N is the range and R is the radiometric depth.

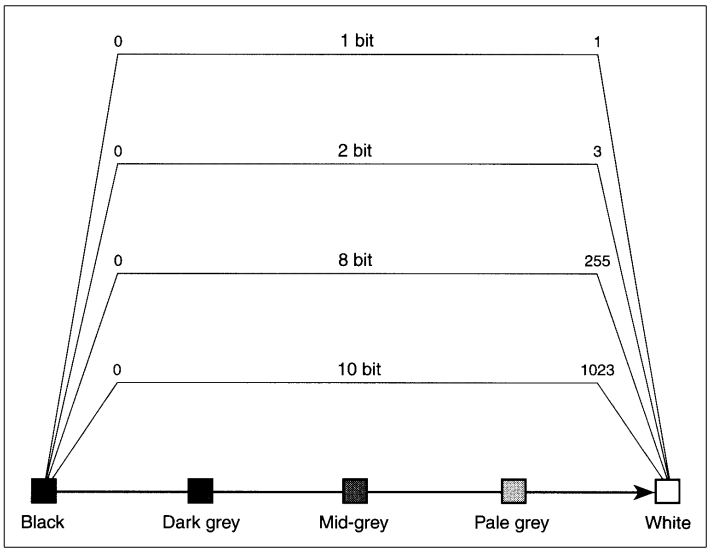

Figure 10: Radiometric range of a sensor. [51]

As earlier stated that the finer the radiometric resolution, the higher the number of grey levels as shown in Figure 10 and 11. This also increases the degree of details, precision that the image will have is as well increased.

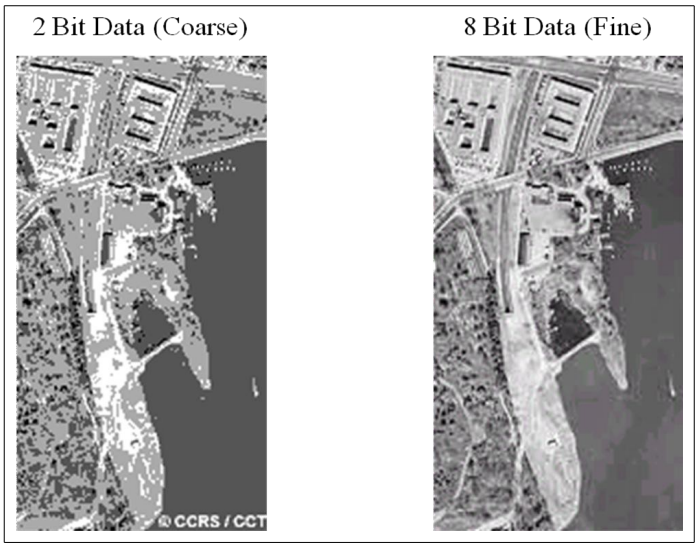

Figure 11: Radiometric resolution of a remotely sensed image. [52]

The SNR has to be taken into consideration in having a higher radiometric resolution. Its important because the step up to the next level can not be less than the noise level if not it would be impossible to say if the change in level is real change in radiance of the target or rather change in the level of noise [35]. Therefore, a low quality remote sensing system with a high noise level will have a lower radiometric resolution compared with a high quality as well as a high SNR instrument [22].

1.1.3 Noise

Remotely sensed systems has an implicit assumption that information can be conveyed to the sensor via electromagnetic energy that has been emitted or reflected from the Earth. This information theoretically dictates whether this assumption is correct or valid. Furthermore the information-bearing attributes of this radiance must be in its variation, be it over time, space, spectrum, or the combination of these [63].

Noise is a considerable problem in R.S sometimes as sensors take images. To this effect noise is an undesirable element which limits the use of an image. When a satellite takes an image the noise content leads to a distorted pixel values and there is the need to limit or reduce the effect of noise on the image. Reflected light which satellite sensors detected coming from the earth's surface can be changed or altered as well as blocked a variety of phenomenon. The

image taken by the satellite which contains noisy signals leads to a distorted pixel values which in turn affects the data captured [64]. This noise effect has to be reduced and this can be done using certain techniques to filter out the noise [65] [66].

1.1.3.1 Types Of Noise

There are a number of noise types that affect images some of which are considered below based on what is espoused in Bhosale and Manza [67], Al-amri et al [64], Corner et al [68], Rani and Kamboj [69], Afrose [70], Chan et al [71]. In general image noise is 'the random variation of brightness or colour information in images produced by the sensor and circuitry' [70].

Random Variation Impulsive Noise (RVIN) / Gaussian

Figure 12: Effect of gaussian noise on an image remotely sensed [67].

This particular of noise can also be termed as Gaussian noise or normal noise and defined as the noise with a Gaussian amplitude distribution [67], [69] [71]. This type of noise is visualised in Figure 12. It normally occurs randomly as white intensity.

Salt and Pepper Noise (SPN)

Its a type of noise that contains random occurrences of both black and white intensity values [67] [71]. This type of noise tends to increase the mean grey level of a local area. Speckle noise is caused by signals from elementary scatterers, the gravity capillary ripples, and manifests as a pedestal image [70]. It is demonstrated in Figure 13. These are often caused by the threshold of noise image. Gaussian and salt and pepper are called impulsive noise.

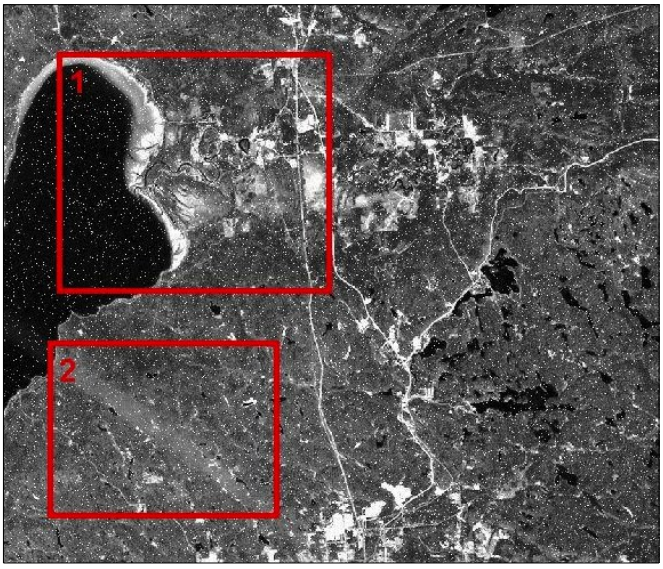

Figure 13: Impact of salt and pepper noise on a remotely sensed image. [239]

Speckle Noise (SPKN)

If the multiplicative noise is added in the image, speckle noise is a ubiquitous artefact that limits the interpretation of optical coherence of remote sensing image. The scattered waves constructively or destructively do interfere with each other causing a speckle appearance on the image [68] and is visualised in Figure 14. This can be expressed as

$$J = I + n \cdot I \tag{4}$$

Where: J is distribution speckle noise image, I is the input image and n is the uniform noise image by mean o and variance v. This particular type of noise is dependent on the reflected signal magnitude [68].

1.1.3.2 Other Forms Of Noise

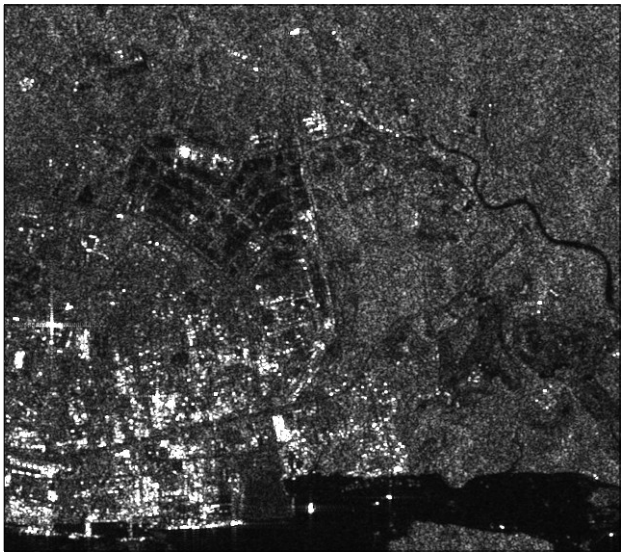

Figure 14: Effects of speckle noise on remotely sensed images. [242]

Thermal Noise

This type of noise is also referred to as the Johnson noise. It's due to a consequence of random motion of electrons in conducting materials because of thermal activity as stated by Landgrebe and Malaret [63] and visualised in.

Quantization Noise

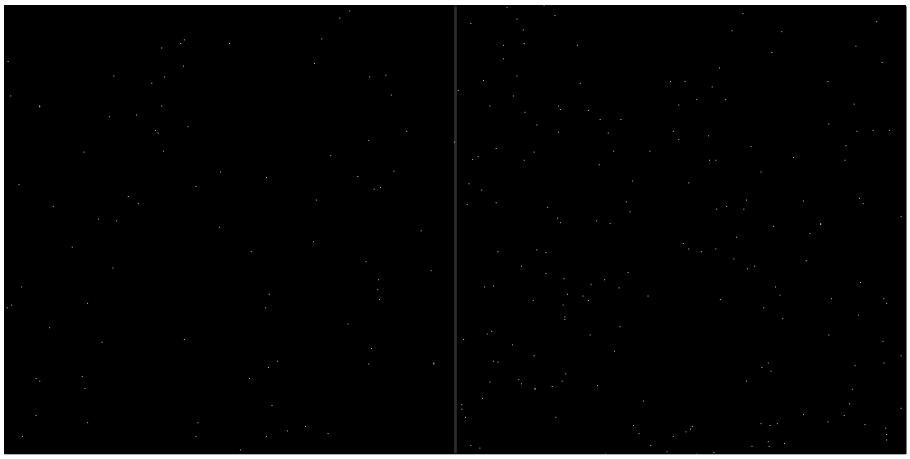

Figure 15: The impact of thermal noise on remotely sensed images. [248]

As expounded by Landgrebe [63], when the suitable preamplification is done, firstly the processing signals from a sensory system is usually A/D conversion. It requires the sampling of the signal at usually uniformed space intervals of time. After this converting of each analog magnitude X to X_q, the nearest of $q=2^n$ levels, where n is the number of bits available. The difference is

$$\epsilon = x - x_q \tag{5}$$

Referred to as quantization noise. In a case where a uniform quantizer is used, the signal to be quantized is assumed to be uniformly distributed over the dynamic range of the quantizer. The noise will have a uniformed distribution over the range Δ, where Δ is the size of a quantization interval $1/q$ and equal to times the dynamic range established for the signal. In most signal distribution and values of q used in practice, the noise mean square value is quite insensitive to the signal distribution, thus the uniform assumption in one commonly used.

Photon Noise

This happens as explained in Young et al [72] when the physical signal observation is based upon light whereby the quantum nature of light plays a significant role. This noise emanates from the fundamental statistical nature of a photon production. Photon production is based on or guided by quantum physics laws and this limits us from inculcating the average number of photons in a given observation window [72]. Therefore the probability with respect to the distribution of photon p in an observation window of length T seconds is referred to as Poisson [72]. This type of noise is illustrated in visualised form as Figure 16

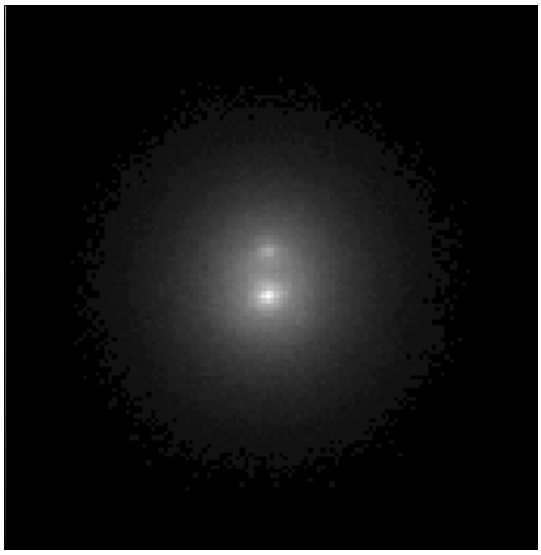

Figure 16: Photon noise and its effect on remotely sensed images. [251]

On-Chip Electronic Noise (READOUT NOISE)

A type of noise originating from the process of reading a signal from a sensor and in a specific case the field effect transistor (FET) of a CCD chip [72]. It's impact on images is visualised in Figure 17.

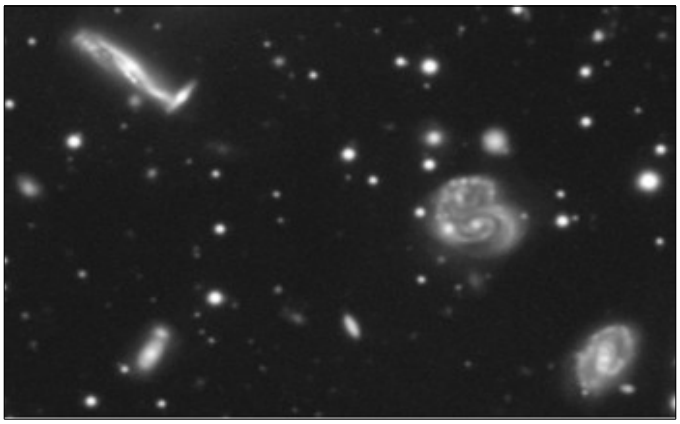

Figure 17: Effects of on-chip electronic noise vis a vis remotely sensed images. [252]

Amplifier Noise

As discussed by Young et al [72] the standard model for this type of noise is additive, Gaussian and independent of the signal. In most modern sensors especially cameras, this is limited but an exception to this is in colour cameras where more amplification is used in the blue colour channel than the green or red channel which leads to noise in the blue channel.

1.2 Image Processing Techniques

1.2.1 Classification

This is where remotely sensed data is used to assign corresponding levels with respect to groups with homogenous characteristics, with the aim of specifically identifying multiple objects from each other within an image. When RS system records an image, radiation reflected from a scene in a number of spectral bands which generates spectral classes which in essence can be thought of as clouds of data points, concentrated around cluster centres in an n-dimensional, Cartesian spectral space [65] [66]. Classification is done to make sense of the specific objects we are considering in our environment by basically grouping them or categorizing them. Pixels in remotely sensed images can either be categorised by their multi variable statistical properties or by the segmentation which based on both statistical and spatial relationship [25]. The process of categorizing all pixels in a digital image into different land themes and this is mostly done by using multi-spectral images based on the spectral pattern present within the data for each of the pixel used as the numerical basis for categorization [73]. Where the overall objective is to automatically categorize all pixels in an image into specific classes based on their spectral patterns, nature of surface materials which have similarities [74]. Classification follows two stages. The first stage has to do with the categorization of real-world object. These real objects could be for example water bodies, wood lands, grasslands as well as other land cover types [35]. The second stage of classification, is the labelling of the categorized land cover types. These classification of categories are mostly numerically (***priori***) done [35]. These afore mentioned steps or stages are sometimes referred to classification and identification [75], [35], [25]. Classification which deals with the categorization, is based on predetermined numbers of classes as well as, those observed on ground at the chosen spatial scale. Clustering which is part of the classification process, deals with classes that are more spectrally distinct referred to as spectral classes [75]. Clustering which deals with data analysis

determines the number of land cover categories that could be separated in the area the image covers and allocating pixels to these categories [35]. This process is divided into two, hierarchical and non-hierarchical clustering. Identification of categories in the nature of the land cover type is the step that follows after clustering [76]. It is important to note that in all this the properties of the pixel that is used in labelling a specific pixel as stated by [77]. Set of grey scale values for a specific pixel which is measured in a number of spectral bands is called a **pattern**. Therefore classification could be said to be part of or a form of pattern identification as pattern identification is associated with each pixel of a specific image with respect to objects or materials that corresponds to the specific point on the earth surface [35]. Thus it can be said to be a set of measurements of the specific pixel(Object) that has to be classified. Spectral bands for example the seven bands of Landsat 7 ETM+ and other derived properties of a specific pixel such as its context and texture are known as **features**. Texture is the measure of how homogenous neighbourhood of a pixel is whereas context is the relationship of an object to other objects nearby [77], [78].

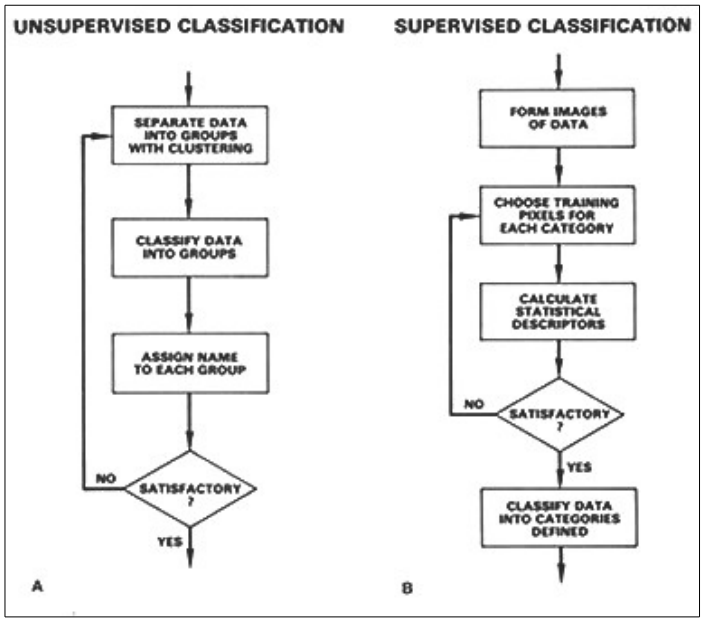

Figure 18: The types of classification: unsupervised and supervised. [79]

Generally classification can be categorized into two, unsupervised and supervised [35], [25]. This is schematically described in Figure 18.

1.2.1.1 Unsupervised and Supervised Classification

In some situations we might not have sufficient or the necessary land cover types thats present or available for a geographical area covered by a remotely sensed image. In such situations estimating of classes mean becomes is very difficult. The only way is to fish for the needed data and therefore, the need for unsupervised classification [35].

It is a method of classification thats based on entirely the statistical data distribution of the image and this is mostly referred to as clustering [25]. This method also examines a large number unknown pixels by dividing them into class base depending on their natural groupings present in an image's values. In that the values within a given cover type are mostly close together in a measurement space Lillesand and Kiefer [30], Sabins [79].

Whereas Supervised classification is the process of using samples of known identity (pixels already assigned to informational classes)to classify pixels of unknown identity(to assign unclassified pixels to one of several informational classes), [22]. Kanellopoulos terms classification as a technique which aims at allocating each pixel in an image to the class with which it has the highest probability of membership [80]. This process is pictorially depicted in Figure 19.

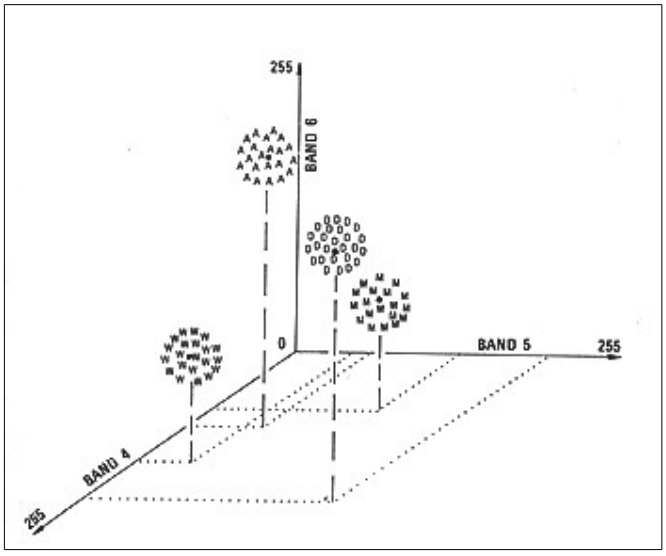

Figure 19: Process of unsupervised classification. [79]

1.2.2 Smoothing Techniques (Algorithms)

Light waves that are reflected that are detected by satellite sensors emanating from the earth's surface can be impeded by a variety of occurrences. This might be due to clouds in the atmosphere or aerosols. Such occurrences, at times, introduces noise into the satellite data. In limiting the effect of noise on remotely sensed images there are a number of techniques that have been suggested by various researches. These techniques are normally to filter out and in most cases estimate the standard deviation of noise [68].

Data Filtering Techniques

One of the methods of reducing the effect of noise on remotely sensed images is data masking. Filtering the image spatially can be done by convolving the image with a small moving window or mask as this implements a desired characteristic frequency [68]. In this procedure, each pixel with the original image is replaced by a weighted average of the product of the window and the neighbouring pixels [81] [68]. It is important to note that from practise most analyst estimate the standard deviation of imagery so as to come out with the most suitable filter to remove or limit the effect of noise in an image [68]. The process of using average window is referred to as discrete convolution filtering or data masking [81]. As stated in [81] if a 3×3 window or mask given by

$$\begin{matrix} Z_1 & Z_2 & Z_3 \\ Z_4 & Z_5 & Z_6 \\ Z_7 & Z_8 & Z_9 \end{matrix} \tag{6}$$

where the new pixel values of the image are

$$DN_{new} = \sum_{i=1}^{9} Z_i DN_{i_{orig}} \tag{7}$$

where the DN represents the brightness values of the pixels. The specific data mask is moved one pixel at a time normally with the pixel being filtered directly in the centre of the mask as well as the neighbouring pixels having the equation (7) applied subsequently until every pixel has been filtered.

Linear Filters

There are number of linear filters for image smoothing of which some are elaborated on in this section based on Young et al [72]. It is further elaborated in Tamim [82], Pratt[83] [84]Kuan et al[85], Rani and Kamboj [69].

- *Uniform Filter*

This type of filter, the input image is usually based on the local average of the input filter. All the values within the filter support have the same weight [72]. In respect of the continuous spatial domain (*x, y*) the point spread function and transfer function are used. Example for a discrete spatial domain (*m, n*) values for filtering are the samples of the continuous domain case [72]. In a case of a rectangular case, *(J=K=5)* and a circular case *(R=2.5)* are expressed below based on Young et al [72] as formulas (8) and (9), respectively:

$$h_{rect}[j,k]=\frac{1}{25}\begin{bmatrix}1&1&1&1&1\\1&1&1&1&1\\1&1&1&1&1\\1&1&1&1&1\\1&1&1&1&1\end{bmatrix} \tag{8}$$

$$h_{o}[j,k]=\frac{1}{21}\begin{bmatrix}0&1&1&1&0\\1&1&1&1&1\\1&1&1&1&1\\1&1&1&1&1\\0&1&1&1&0\end{bmatrix} \tag{9}$$

In each case the filter is normalised so that $\sum h[j, k]=1$. Furthermore this is done so that if input is a constant then the output image will show the same value $a=[m, n]$.

- *Triangular Filter*

As espoused by Young et al, it is the output image is based on a local averaging of the input filter where the values within the filter support differing weights. In this situation the filter can be seen as the convolution of two uniform filters as in rectangular or circular. This invariably has a direct consequence for computational complexity [72].

- *Gaussian Filter*

This type of filter employs the Gaussian kernel for smoothing and employs certain properties such as central limit theorem, minimum space-bandwith product of the Gaussian as well as application of edge finding and scale space analysis [72].

Non-Linear Filters

There a number of smoothing filters that are non-linear, though these type filters can not be analysed by Fourier analysis, they are still used extensively [72]. These non-linear filters discussed below are based on Young et al [72], Tamim [82] He et al [86], Mancuso [87], Rani and Kamboj [69].

- *Median Filter*

  This type of filter is based on moving a window over an image as in a convolution as well as computing the output pixel as the median value of brightness within the input window [72] [82] [88]. It also involves a simple and powerful non-linear filter which is based on order statistics and reduces the amount of intensity between one pixel and the other pixel[69] [89]. The filter works by moving through an image pixel by pixel and replace each value with a median value of neighbouring pixels. This pattern of neighbour is called the window and slides pixels by pixels over the entire image [90].

  This expressed below as described in Sivasundari et al [88].

$$M(P_1 \ldots\ldots\ P_n) = Median\ (\|P_1\|^2 \ldots\ldots\ \|P_n\|^2) \tag{10}$$

The above is an optimum which help limit the effect of noise on the image and it causes no changes in the shift boundaries and no reduction in contrast and proved to be more robust in the presence of noise [88].

- *Wiener Filter*

  Its a filter that incorporates an optimal tradeoff between inverse filtering and noise smoothing, this removes additive noise as well as deblurring concurrently [88] [91] [92] [93]. This form of filter involves two processes, one of the process is inverse filtering and the other is noise smoothing [88].

- *Relax Median Filter*

As expounded by Afrose [70] Hamza et al [94] this type of filter is normally obtained by relaxing the order of statistic for pixel substitution. Furthermore the 'noise attenuation as well as the edge and line preservation are analysed statistically. The trade-off between noise elimination and detail preservation is analysed'[70] [94].

- *Centred Median Weighted Filter(CWM)*

Ko and Lee [95] expresses CWM as a type of filter which has a weighted median filter giving more weight only to the central value of each window. In the use of CWM, its always important to consider median and weighted median filters in arriving at your centre weighted median filter. It is worth noting that a CWM with a larger CWM performs better in detail preservation but worse in noise suppression than one with a smaller CWM.

1.2.3 Atmospheric Correction

When remotely sensed images are taken, the prevailing atmospheric conditions have enormous effect on the images. Mather and Koch states that a value recorded at a given pixel location on a remotely sensed image is not a record of the true ground-leaving radiance at that point, for the magnitude of the ground-leaving signal is attenuated due to atmospheric absorption and its directional properties are altered due to scattering [35]. Large amounts of imagery collected by satellites are largely contaminated by the effects of atmospheric particles through absorption and scattering of radiation from the earth surface Jaja [96], Fallah-Adl et al [97]. This process is described in Figure 20.

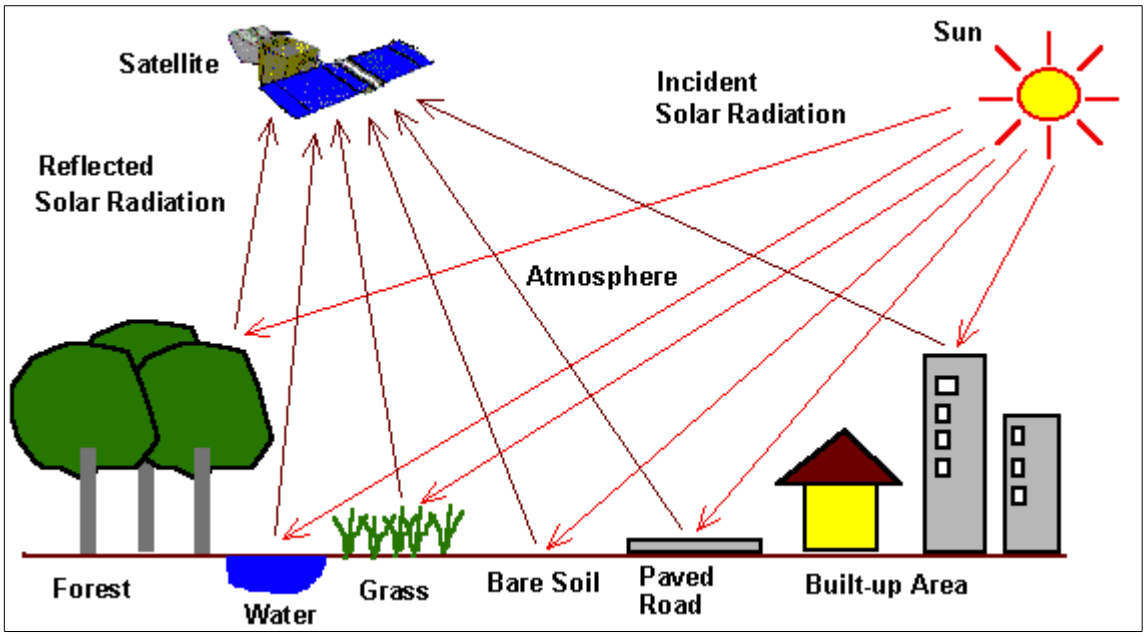

Figure 20 Components of signal received by an air-borne or satellite-mounted sensor. [242]

From Figure 20, some of the signal from water would have that of grass been scattered into the signal path of water thereby giving a wrong representation to the satellite sensor that is collecting the information. This phenomenon will make the signal seem to emanate from the water surface but in fact that would not be the case. A signal may appear to be originating from a specific point on the ground whereas, in fact, scattering from another point redirects some of of the incoming electromagnetic energy within the atmosphere into field of view of the sensor (atmospheric path radiance) and the scattered energy is referred to **Environmental Radiance** [35]. Additional difficulties are caused by variations in the illumination geometry (the geometrical relationship between the sun's elevation and azimuth angles, the slope of the ground and the disposition of topographic features) [35]. Figures 21 and 22 show the effect of atmosphere on a remotely sensed image before and after atmospheric correction.

Hadjimitsis et al describes atmospheric correction as radiation from the Earth's surface which undergoes significant interaction with the atmosphere before it reaches the satellite sensor. This interaction with the atmosphere is stronger when the target surfaces consist of non-bright objects, such as water bodies or vegetation [98].

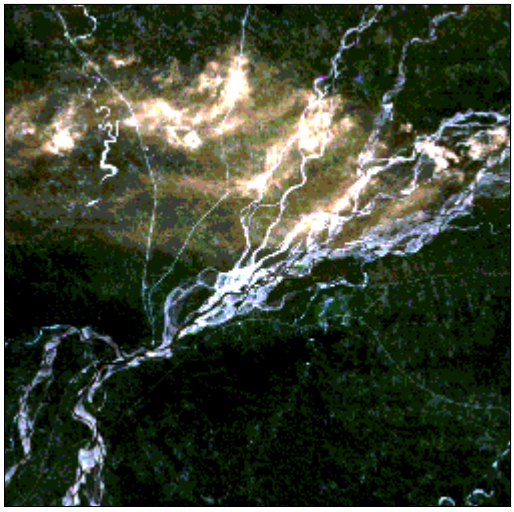

Figure 22: Image affected by atmospheric conditions. [250]

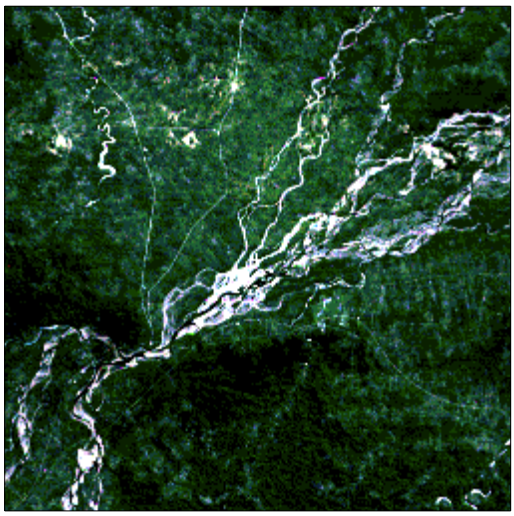

Figure 21: Image corrected limiting the effect on atmospheric effect on the image. [250]

Based of the above described causes for the need of atmospheric correction, the main effects of atmospheric scattering on remotely sensed data are upwelling atmospheric radiance or path radiance and atmospheric absorption with multiplicative characteristics [99] [100]. In general infrared TM bands are affected by air molecule and aerosol particle scattering which are additive and create haze [100]. Air molecules are mostly stable and obey Raleigh's scattering rule, nonetheless the character of aerosol particles are often variables and their influence are difficult to estimate [100]. In the visible bands, the absorption caused by water vapour or other gases are very weak and can be disregarded, consequently the impact of short wavelengths is predominantly from Rayleigh scattering [100]. Nevertheless, in near infrared and middle infrared wavelengths, the effect of air molecules and aerosol particle scattering can be insignificant, the main crash is from the atmospheric absorption which is caused by water vapour, carbon dioxide, methane and other gases [100]. Usually, the contents of carbon dioxide, carbon oxide and methane are stable, however water vapour is variable and therefore a good model should be able to simulate the above phenomena and to correct the influences caused by scattering and absorption [100].

Atmospheric correction may be necessarily in three situations. The first is where there is the need to compute a ratio of the values in two bands of a multi-spectral image. The scattering increases inversely with the wavelength and therefore the shorter wavelengths experience more

scattering then the longer wavelength data. Secondly, where there is the need to relate upwelling radiance from a surface to some property of that surface in terms of a physically based model. This situation requires that the atmospheric component present in the signal recorded by the sensor must be estimated and removed. Third case is when the ground measurements made at one time are to be compared with a results of a later date. In this case prevailing atmospheric conditions will not be the same [35].

There are a number of techniques adopted in dealing with atmospheric effects on remotely sensed images. The main objective of atmospheric correction is to retrieve the surface reflectance (Characterises the surface properties) from remotely sensed imagery by removing the atmospheric effects [97] [96]. Many works has proven that atmospheric correction greatly helps and can significantly improve image classification Fallah-Adl [97], Fraser and Kaufman [101], Fraser et al [102].

1.2.3.1 Image Based Techniques

There many methods used in atmospheric correction and the first to be considered is the image based methods. These methods are discussed based on Mather and Koch [35].

The Histogram Minimum Method (Dark Pixel Method)

The histogram minimum method, histogram of pixels values in all bands are computed for the full image and this generally contains some areas of low reflectance (clear water, deep shadows, exposures of dark coloured rocks). These pixels will have values very close to zero in near-infrared bands (Examples Landsat TM band 4, SPOT HRV band 3) also other bands may have near-zero values in their spectral region [35]. This is further expounded by Hadjimitsis et a1 [98] [103], this approach states that most of signal reaching a satellite sensor from a dark object was contributed by the atmosphere at visible wavelengths. The pixels from dark targets indicates the amount of upwelling path radiance in the band. The atmospheric path radiance adds to the surface radiance of the dark target and thus gives the target radiance at the sensor. expresses the DP algorithm below [104].

$$L_{ts} = L_{tg} + L_p \tag{11}$$

Where

L_{ts} is the target radiance at the sensor's

L_{tg} is the target radiance at the ground level

L_p is the atmospheric path radiance

By selecting a dark object, such as a water body, and by assuming the radiance from the dark target at ground level (L_{dg}) to be zero, the path radiance is equal with at-satellite (at the sensor) radiance of the dark object.

$$L_{ds} = L_{dg} + L_p \tag{12}$$

Where

L_{ds} is the dark object radiance at the sensor

L_{dg} is the dark object radiance at the ground level

Assuming the $L_{dg}=0$

$$L_p = L_{ds} - L_{dg} = L_{ds} \tag{13}$$

Otherwise, where a known spectral radiance or reflectance value is known (or assumed)

in advance for specific dark target L_{dg} has a value. In the case, the recorded at– satellite radiance for the dark target is assumed to be the sum of radiance of the dark target at the ground level and the atmospheric path radiance. It is worth noting that the path radiance is much reduced in mid-infrared bands such as Landsat-TM bands 5 and 7 [35]. This method of atmospheric correction is further expounded in detail by Chavez [105].

Regression Method

Mather and Koch [35] expressed the regression method as applicable to the areas that were described in the DP method. With respect to Landsat ETM+ sensor, pixel values in the near infra-red band are plotted against the values in the other bands in turn and a best-fit straight line is computed for each using standard regression methods.

Empirical Line Method (EL)

In general remotely sensed image DN are difficult to interpret as buttressed by Baugh and Groeneveld, remotely sensed DN of image cannot be assumed to represent the actual

surface conditions because of a variety of atmospheric reasons [106] [107].The empirical line method therefore one of the commonly used methods of correcting multispectral and hyper spectral data from raw DNs as well as radiance and reflectance [106]. This method assumes a linear relationship between DNs and ground measured reflectances surface with a range of differing albedo [108] [35]. This is described visually in Figure 23. Different researchers have tried to use this method with different sensors to limit the effect of atmospheric conditions on remotely sensed images such as Karpouzli and Malthus [107] used the empirical line method of atmospheric correction on IKONOS data, Smith and Milton [108] used empirical line method on CASI data, Moran et al [109] used the empirical method on both Landsat TM and ETM+ data, whilst Vaudour et al [110] used this method on SPOT data.

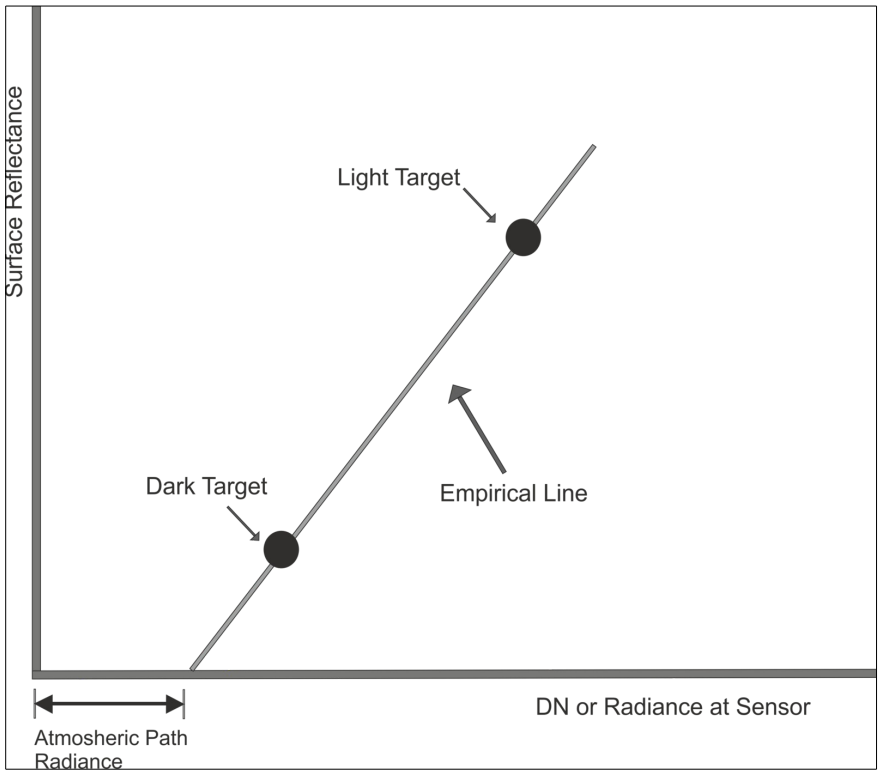

Figure 23: Example of empirical line method using two targets of contrasting albedo. [106]

1.2.3.2 Physically Based Models

These are methods that involve complex models that are also very accurate in converting digital numbers to into surface reflectances [100]. These particular methods convert remotely

sensed digital numbers to surface reflectance or radiance by removing the effects that are caused by atmospheric attenuation, topographic conditions and other parameters Lu et al [100]. Also, these methods depend on information from the image itself to in order to estimate the path radiance for each spectral band [35]. Furthermore it is imperative to focus on the extraction of subtle differences in reflectance to be able to estimate biological properties such as biomass and forest volume, which needed when creating relationships between ground truth data and those that are remotely sensed (measured) [100]. Based of this principle a number of models have being created by researchers and some these models commonly used are [35] [100], 5S (Simulation of Satellite Signal in Solar Spectrum) 6S (Second Simulation of Satellite Signal in Solar Spectrum), MODTRAN (Moderate Resolution Atmospheric Subtraction), LOWTRAN, ATREM, DOS (Dark Object Subtraction) [111] [112] [113] [114] [115] [116] [100]. Some of these models have been fused into GIS and RS softwares such as 6S is used in GRASS GIS for the purposes of atmospheric correction.. The model 6 S for instance, predicts reflectances of objects at the top of atmosphere by using information vis a vis the surface reflectance and the atmospheric conditions [116]. Masek et al [117] developed the 6S physically based model for atmospheric correction used in the LEDAPS project by NASA for processing images into atmospherically corrected images into atmospherically corrected images. The 6S algorithm is explained further based of the following expression described below.

$$\rho TOA = T_g(O_3 O_2 C O_2 N O_2 C H_4) \times [\rho R + A + T_{R+A} T_g(H_2O) \frac{\rho_s}{1 - s_{s+A\rho_s}}] \quad (14)$$

where ρ_s is the surface reflectance

T_g is the gaseous transmission due the gases $O_3, O_2, CO_2, NO_2, CH_4$

T_{R+A} is the Rayleigh and aerosol transmission

$\rho R + A$ is the Raleigh and aerosols atmospheric intrinsic reflectance

S_{R+A} is the Raleigh and aerosols spherical albedo

The computation of the transmission, intrinsic reflectance and spherical albedo was done based on 6S radiative transfer code [117].

1.3 Works on Inland Water Monitoring Based of Remote Sensing

Quite a number of researchers in one way or the other have tried to use remote sensing as a tool in the analysis and water monitoring. Ritchie et al [118] came out with an approach that estimates suspended sediments in water

$$Y = A + B.X \qquad (15)$$

or

$$Y = A.B^{x} \qquad (16)$$

In the equations, Y is the remote sensed measurement example radiance and X is the water quality parameter being measured example chlorophyll. In this approach A and B are empirically derived factors. In empirical approaches, statistical relationships are determined by measuring the spectral or thermal properties and water quality parameters. The limitation of this approach is that such empirical models could only be used to estimate water quality parameters for water bodies with similar conditions.

Another approach that can be used in estimating water quality parameters is the analytical approach, Schiebe et al. [119] based this approach on optical properties of water and water quality parameters to develop a physical based model. He based this model on reflectance and statically determined coefficients which were used in estimating suspended sediment concentrations. Their model had the form

$$R_i = B_i[1 - \exp(c / S_i)] \qquad (17)$$

where R_i is the reflectance i, c is the suspended sediment concentrations, B_i represents the reflectance saturation level at suspended sediment concentrations in wave band i and Si is the concentration parameter equal to the concentration.

Harding et al [120] using measurements from aircrafts created an algorithm in determining the seasonal patterns of chlorophyll content in the Chesapeake Bay:

$$\log_{10}[chlorophyll] = a + b(-\log_{10}(G)) \qquad (18)$$

where a and b are empirical constant derived from in situ measurements and

$$G = (R2)^2 / (R1 * R3) \qquad (19)$$

where $R1$ is radiance at 460 nm, $R2$ is radiance at 490 nm, and $R3$ is radiance at 520 nm.

Lesht et al developed a model of using satellite measurements to estimate the level of chlorophyll in the Great Lakes Region. They used MODIS to develop an algorithm for estimating chlorophyll concentration in the Great Lakes [121].

Rundquist et al [122], estimated Chl-a by using, remote measurement of algal chlorophyll in surface waters looked at hyper spectral signatures, in the visible and near-infrared, associated with two experiments conducted outdoors in large water tanks; one involving relatively low amounts of chlorophyll over a narrow range and a second involving relatively high amounts over a wide range. The principal finding was that the commonly used near-infra red ratio is best for estimating pigment amounts when the concentration of chlorophyll is relatively low, and the first derivative of reflectance around 690 nm is best when the concentration is relatively high.

S.Novoa et al [123] estimated chlorophyll-a concentration in waters by developing a regional algorithm to retrieve Chl-a in surface water using in situ, for a subsequent application to Medium Resolution Imaging Spectrometer (MERIS) satellite images.

Yu et al [124] used a NIR-red based algorithm based on the SAMO-LUT (Semi-Analytical Model Optimisation and Look-Up Tables). They used this method on five Asian lakes in Japan and China. With this model of chlorophyll estimation, rather than relying on in situ data, a comprehensive synthetic data set is used for model calibration. This model involves the use of imagery of case II water body where only one of the constituents changes and the other two remaining are controlled as constants.

He et al [125] used water quality retrieval models to analyse water variables in Guangting reservoir based on Landsat data. Other researchers have also used Landsat data in the monitoring of water quality parameters, Hellweger et al [126], Sudheer et al [127], Papoutsa et al [128], Liu et al [129], Wang et al [130], Brezonik et al [131], Braga et al [132].

1.4 Water Quality Monitoring

Water quality monitoring is a systematic collection of samples as well as in situ analysis with the aim of providing information and knowledge about a water body [15]. It is a term used to express the suitability of water to sustain various uses or processes [133]. Bukata et al [134] described water quality monitoring as a descriptive term that refers to the state or condition of a water body in relation to a set of criteria established for its designated use'.

The term water quality is defined by U.S. EPA [135] as the sampling and analysis of water constituents and conditions for the purpose of identifying whether waters are meeting designated uses, identify specific pollutants, determine trends and screen impairment. It can also be termed as the making of observations and taking measurement that are analysed and reported to provide information and knowledge about the catchments of the particular water body [136]. The European Commission [137] terms water quality monitoring as the studies conducted to estimate the quantity and quality of pollutants, nutrients and suspended solids contained in water bodies and to assess sources and factors associated with agricultural practices, industrial activities or other human activities. It could also be defined as the sampling and analysis of water constituents and conditions which may include introduced pollutants such as pesticides, metals and oils as well as constituents found naturally in water which can be affected by human sources. Examples are oxygen, bacteria and nutrients [138].

The actual collection of information at set locations and at regular intervals in order to provide the data which may be used to define conditions, establish trends etc [139]. Water quality monitoring can be used for many purposes some of which are as follows: To identify if the various inland water bodies are meeting the designated uses as each water body has a specific use. Examples, reservoir, lakes, fish ponds, recreational purposes. Identifying specific pollutants and their sources, this helps to link sources of water body pollution to the specific pollutants. To determine trends, these are some of the many factors why water quality monitoring is important. Its also of importance to understand what monitoring really entails. As per the definition in [140] and [135], monitoring is the programmed process of sampling, measurement and subsequent recording or signalling, or both of water characteristics, often the aim of assessing conformity to specified objectives. In water quality monitoring it is important to take into consideration, ***monitoring***, ***surveys*** and ***surveillance*** [1].

1.4.1 General Water Quality Methods

General methods for water quality monitoring can be classified into three groups. These are biological, chemical, physical [141] [134].

Biological method of water quality monitoring involves sample collection, processing and counting, identification of aquatic organisms [142]. It's also the evaluations of the condition of water bodies using surveys and other direct measurements of resident biological organisms [139]. Most of the biological methods are used depending on the specific need and this are normally divided into five categories; Ecological methods, Physiological and

biochemical methods, Controlled bio tests, Contaminants in biological tissues and, Historical and morphological methods [139].

Chemical methods of water quality monitoring, has to with the measurement of various elements and molecules dissolved or suspended in water. Example water pH levels, nitrogen levels.

Physical methods of water quality monitoring, involves methods used to determine physical characteristics of inland water. Example temperature, water transparency, velocity etc [139].

1.4.2 Importance of Water Quality Monitoring

Water quality is very relevant as water resource is in scarce supply [143]. Water quality monitoring becomes a necessity due to:

- Identify possible human impact on waterbodies
- Identifying possible pollutant and their sources [144].
- Eutrophication process in inland waterbodies are caused by increase in nutrient inputs and sometimes introduced toxins and odour to these inland waters. Its important to monitor their levels [144].
- Some of these waterbodies serve as a source for drinking water and costs for purification is higher if these water bodies are polluted [145].
- Inland waterbodies also serve as an economic source (fishing) and recreational source (swimming) as well. The condition of these waterbodies are very crucial [145] [134].

1.4.3 Problems Affecting Inland Water Quality Monitoring

There are a number of issues affecting inland water quality monitoring, water quality issues or problem could be defined as an impairment or problem that adversely affect the quality of the water body preventing the use of the water for the specific purposes that they are meant for [139]. For example if a lake located in an industrialised region like Great Lakes in North America has faced a lot of water quality problems due to urban and social development issues [146].

1.4.4 Advantages and Disadvantages of Remote Sensing in Inland Water Quality Monitoring

Relying on remote sensing methods rather than in situ method for inland water quality monitoring has a number of advantages which makes it worthwhile pursuing. Remote sensing provides both temporal and spatial information for inland waterbodies whereas the traditional methods of water monitoring do not [147]. A variety of inland water quality parameters can be observed or monitored concurrently within a specific period of time based on remote sensing whereas its not the case with traditional methods of monitoring [148]. It is relatively less costly to use remote sensing methods in inland water quality monitoring which allows one to adequately manage various inland water bodies [9] [149]. In situ measurements are restricted to the specific sampling points but that of remote sensing gives rather a synoptic view of a water body [141] [150] [151] [152] [153]. There is also the reason to minimizing human error as these are some streamlined and automated processes [154]. In as much as there are merits in the use of remote sensing in inland water quality monitoring, it comes with some demerits. Its not all water quality parameters that can be remotely sensed and therefore can not fully replace traditional way of field surveying as well as sampling [154]. Heavy cloud cover and hazy conditions makes the use of images taken for remote sensing of inland water quality monitoring impossible [155]. Shallow inland water bodies sometimes have the potential to interfere with sensoring of these water bodies. Additionally spatial and temporal resolution of inland water bodies can be insufficient as well as controllable [126].

1.4.5 Some Water Quality Parameters that can be Remotely Sensed

There are various variables that are used in determining inland water quality, due to the fact that some water quality parameters are monitored by the use of in situ methods. These parameters could be determined based on remote sensing methods [156] [157] [158]. The substance usually found on the surfaces of water bodies do change the backscattering of the surface of the water body [159] [160]. Based on remote sensing techniques one is able to measure these changes within the spectral signature that emanates (backscattered) from the surface of the water body. These techniques measuring the changes could be linked empirical or analytical depending on the water quality being measured[160]. These water quality parameter could be chlorophyll, turbidity, secchi disk depth, total phosphorus, temperature,

Coloured dissolved organic matter, total nitrogen and many others. Table 5 summarises a number of remotely sensed water quality parameters and the sensors that were used.

Table 5: Some water quality parameters remotely sensed using different sensors

References	Locations	Sensors	Water Quality Parameters
Wang et al, 2006	Reelfoot Lake, Tennessee, USA	Landsat TM	Chlorophyll-a, Turbidity, Secchi Depth, Total Suspended Sediments
Cox et al, 1998	Catawba River, North Carolina,USA	Landsat TM	Turbidity, Secchi Depth, Chlorophyll, Temperature
Koponen et al, 2002	Finland Lakes	AISA, MERIS	Secchi Depth, Turbidity, Chlorophyll-a
Mancino et al, 2009	Monticchio Lakes, Italy	Landsat TM	Secchi Depth, Chlorophyll concentration
Ostlund et al, 2001	Lake Erken, Sweden	CASI, Landsat TM	Chlorophyll and Turbidity
Aparslan et al, 2007	Omerli Dam, Istanbul City, Turkey	Landsat ETM	Chlorophyll-a, Suspended Solid Matter, Secchi Depth, Total Phosphate
Vignolo et al, 2006	Medano Creek, Argentina	Landsat ETM	Water Quality Index
Lillesand et al, 1998	Lakes in Minnesota, USA	Landsat TM, MSS	Secchi Depth, Chlorophyll, Turbidity
Verdin, 1985	Flamin Gorge Reservoir,Wyoming, USA	Landsat MSS	Secchi Depth, Chlorophyll
Baruah et al, 2002	Kasumigura, Japan	Landsat TM	Total Suspended Solids, Chlorophyll
Schiebe et al, 1992	Lake Chicot, Arkansas, USA	Landsat MSS	Total Suspended Solids
Giardino et al, 2001	Lake Isco, Lombardy, Italy	Landsat TM	Total Suspended Solids and Chlorophyll
Fraser, 1998	Lakes in Nebraska, USA	Landsat TM	Turbidity
Dekker et al, 2001	Frisian Lakes, Netherlands	Landsat TM, HRV	Total Suspended Solids
Brivio et al, 2001	Lake Garda, Italy	Landsat TM	Chlorophyll
Mayo et al, 1995	Lake Kinneret, Israel	Landsat TM	Chlorophyll
Barale et al, 2002	Black Sea	CZCS, MOS	Chlorophyll
Lathrop, 1992	Lakes:Green, Bay, Michigan, USA	Landsat TM	Secchi Depth, Chlorophyll, Turbidity, Total Suspended Solids

Chlorophyll

Normally pigments of phytoplankton consist of chlorophyll a, b, c and d with chlorophyll-a being the most commonly remotely sensed and used as an indicator of phytoplankton [161]. The pronounced scattering/absorption features of chlorophyll-a are: strong absorption between 400–500 nm (blue) and at 680 nm (red), and reflectance maximums at 550 nm (green) and 700 nm (near-infrared (NIR)) [162].

In inland water bodies the greater the chlorophyll concentration the lower their reflectance in the short wavelengths (blue) and the higher in the middle wavelengths (green) of visible light [163]. Weissel [126] used the ratio between the green band and the red band to estimate the levels of chlorophyll-a. Han and Jordan, also did use the ratio between the green band and the blue band to measure the levels of chlorophyll-a [164].

Secchi Disk Depth

Clarity of water is essential for water quality evaluations, as it helps to identify how polluted a water body is or the possibility of algae growth. It is also said to be the optical property of water and is often associated with constituents present in these water bodies [164]. Secchi depth can be defined as the measure of light penetration into a water body and is a function of the absorption and scattering of light in water [165]. Therefore it is depth at which a white disc is distinguishable from the surrounding water, or black and white quadrants of a black and white disc are distinguishable from each other when lowered in a water body [165]. Secchi disk depth can be remotely sensed based on the visual spectral bands as shown in Wang et al [156] where individual bands (red) and ratio between bands (green and red) were used in quantifying Secchi disk depth.

Total Phosphorus

Total phosphorus (TP) is defined as the sum of all phosphorus compounds that occur in various forms [166], the sum of all phosphorus components in a water body [167], it is the measure of both organic and inorganic forms of phosphorus [168]. Griesbach [167] defined TP 'as the basis on how much phosphorus in its various forms will be oxidized into orthophosphate by a specific oxidant'. Inorganic phosphorus is the form which most readily available for uptake during photosynthesis and this aids algal blooms [168]. This can be indirectly related to water clarity as well due to biomass of phytoplankton [169]. TP is normally analysed in the laboratory spectrophotometrically, It is important to have an appropriately defined phosphorus detection limit. Limiting TP & TN has been suggested to reduce or help in controlling eutrophication [170] [171] [172].

Through the use of MODIS Total Phosphorus can be remotely sensed at its levels known [150]. Integrating the green and red bands showed visible relationship with total phosphorus. TP is known to be the most analysed as a fraction of phosphorus for its in a variety of empirical models with respect to phosphorus in a wide variety of limnological variables [173]**.** TP has been remotely sensed based on a number of methods one of such is the integral colour index [174] derived from resolutions ranges of 415-445nm, 655-685nm and 405-605 nm.

Turbidity

Turbidity is the measure of relative clarity of a liquid [175]. It can also be said to the amount of cloudiness in water [139]. Its one of the physical inland water parameters, which tries to measure the penetration capacity of light to the depth of the water body [176]. Turbidity is defined by US EPA [135] as the measure of clarity of how much the material suspended in water decreases the light through the water. These suspended materials could be sand or clay and these materials do affect the colour of the water [177]. Moderately low turbid waters may show a well functioning water body but a water body with high levels of turbidity poses a lot of problems within the water. This can lead to low levels of dissolved oxygen as well as sediment bearing run off or nutrient inputs that causes plankton blooms [178]. The knowledge of turbidity levels of a water body gives a quantitative information with respect to the state of that particular water [179]. Wang et al, Khoram et al and Forsythe et al [156] [180] [181] have all shown that it is possible to quantify turbidity based on visual spectral bands such as red, green and blue.

Temperature

Water temperature could be defined as the measure of average energy of water molecules and is a very critical parameter in water quality monitoring and assessment. It exerts a major influence on biological activities in the water. Water temperature also affects or influences water chemistry. The more the chemical reaction the more the temperature in the water rises. The warmer the water the less oxygen content the water has and more oxygen when its cool which directly affect aquatic life in the water [182]. It also influences other activities in water bodies such as, rate of photosynthesis by algae and sensitivity of organisms to toxic waste, parasites and aestivation of aquatic organisms. With the current change in the temperature, it is very important that temperature in inland waters are monitored [183]. Studies have shown that the world's surface air temperature has increased 0.7 °C ±2, globally during the 20th century this definitely has an effect on inland water bodies [184].

The infra red thermal band measures the amount of infrared radiant flux which is emitted from the surface of water bodies [9]. This is supported in literature as stated in [181], [185].

Coloured Dissolved Organic Matter

Coloured Dissolved Organic Matter can be said to be a major part of dissolved natural organic matter which is found in natural water bodies. It has bearing on the aquatic ecology as well as the chemistry and suitability of water use for human beings. It can be divided into two sources: allochthonous which is normally derived from decomposition of woody plants in terrestrial environment and autochthonous which is from decomposing algae and aquatic vegetation within a water body [186].

This refers to the organic matter in water that absorbs strongly in ultraviolet spectrum which is also known as chromophoric dissolved organic matter and also as gelbstoff or yellow substances [187]. It contains the largest store of organic carbon and contributes to light absorption in water [188]. Furthermore CDOM is comprised of a number of molecules with different sizes which are strongly not only in the ultraviolet region but the blue region as well and their exact chemical composition are difficult to ascertain [189]. It should be noted that at first CDOM was seen as a disturbance in the formulations of algorithms for Chl-a. Its a bio-optical parameter representing part of the whole amount of dissolved organic carbon in water bodies [190]. It is the optically measurable part of dissolved organic matter in water bodies. This (CDOM) affects productivity as it modifies availability of nutrients as well as light in the water body [191], [192]. Coloured Dissolved Organic Matter originates naturally in water environment basically from tannins that are released from decaying Detritus. It strongly absorbs short wavelength light that comes from blue to ultraviolet as stated earlier but pure water (with less CDOM) normally absorbs longer wavelength red light [193].

Total Carbon

Total carbon includes both inorganic and organic sample constituents [194]. In other words could be said to be the organic and inorganic carbon in water which includes elemental carbon. This also shows the level of carbon in an organic compound and plays a role in water purity [195].

Total Organic Carbon

This is the sum of the concentration of all carbon atom covalently bonded in the organic molecules of a given sample of water body or water. The sum of this does not really identify all the specific organic contaminants but at the same time it helps detect the presence of organic molecules in water. Total Organic Carbon when high in water bodies can affect the level of oxygen in these water bodies and can be very harmful to the aquatic life in them. Low levels or concentrations can also have some adverse effect on the water body, as they positively affect the growth of anaerobic bacteria [196].

Total Nitrogen

Nitrogen is one of the main nutrient for plant growth. Some plants, example blue-green algae have the ability to directly access nitrogen from the atmosphere [197]. Excess of nitrogen in inland water bodies will cause eutrophication and limit the amount of oxygen in these water bodies [198], [199]. In order to control eutrophication it is essential for total nitrogen being one of the major causes to be controlled [200], [201]. But it has also been recently suggested that reducing nitrogen in inland water bodies does not necessarily control eutrophication [202].

Total Suspended Matter

Not all materials are able to dissolve or mix up completely in water bodies. Some of these materials have bigger molecules which makes it difficult to mix with that of water which are smaller thus forming whats referred as particulate matter. Suspended matter with its total, represents the living organic matter as well the inorganic suspended solids which are referred to as phytoplankton and tripton respectively [203]. Tripton as a section of total suspended matter mostly contribute to light scattering with low absorption. Suspended matter serves as a medium for the transportation of certain elements of pollutants such as heavy metals [204] [205]. High concentrations of TSM creates a degradation problem for inland water quality [206], [207].

Trophic State

When water is over rich in nutrients or have nutrients (nitrogen, phosphorus) in excess, which leads to excessive growth of plants and algae, this called eutrophication [208] as seen in Figure 25. This causes the water quality to deteriorate and has significant side effect over the over all usage of the water.

Eutrophication may be caused by a number factors, algal bloom can be caused by natural occurrences [209]. But there are also the human caused factors: land clearing, discharge of sewage into water bodies etc. It is worth noting that higher levels of nitrogen and phosphorus have been ending in inland waters [208]. From the algae blooms the blue-green blooms are most dangerous to inland water bodies as (certain species) they produce a toxins that are very harmful. These toxins can cause irritation of the skin, gastrointestinal disorder and its know that in some extreme cases they can cause permanent human organ damage or death [210]. Eutrophication can as well be caused by human activities such as the increase in the amount of nitrogen and phosphorus in the biosphere [211], [212], [213], [214] [215] [216]. To control eutrophication in itself is quite expensive [215]. As suggested by some writers that it is best when nutrients such as nitrogen and phosphorus are controlled would help reduce eutrophication [170] [171] [172] [217].

There are different trophic states of lakes. These oligotrophic, mesotrophic, eutrophic, hypereutrophic [9] [218], as can be seen in Figure 24. Water bodies in the Czech Republic are classified as follows, class1:unpolluted, class 2: slightly polluted, class 3: polluted, class 4: heavily polluted, class 5: very heavily polluted [219].

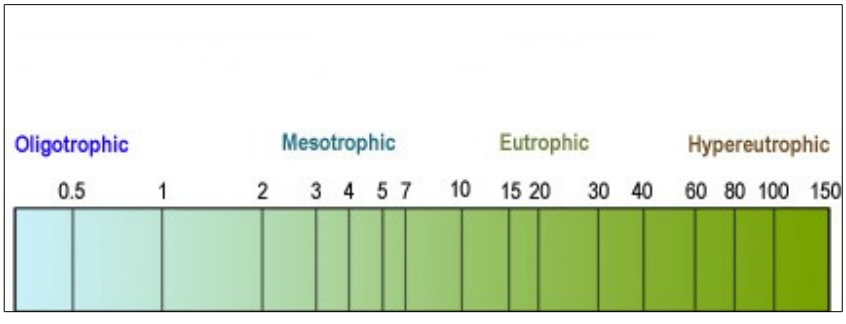

Figure 24: Trophic states of lake as some of the water bodies samples fell within this range [238]

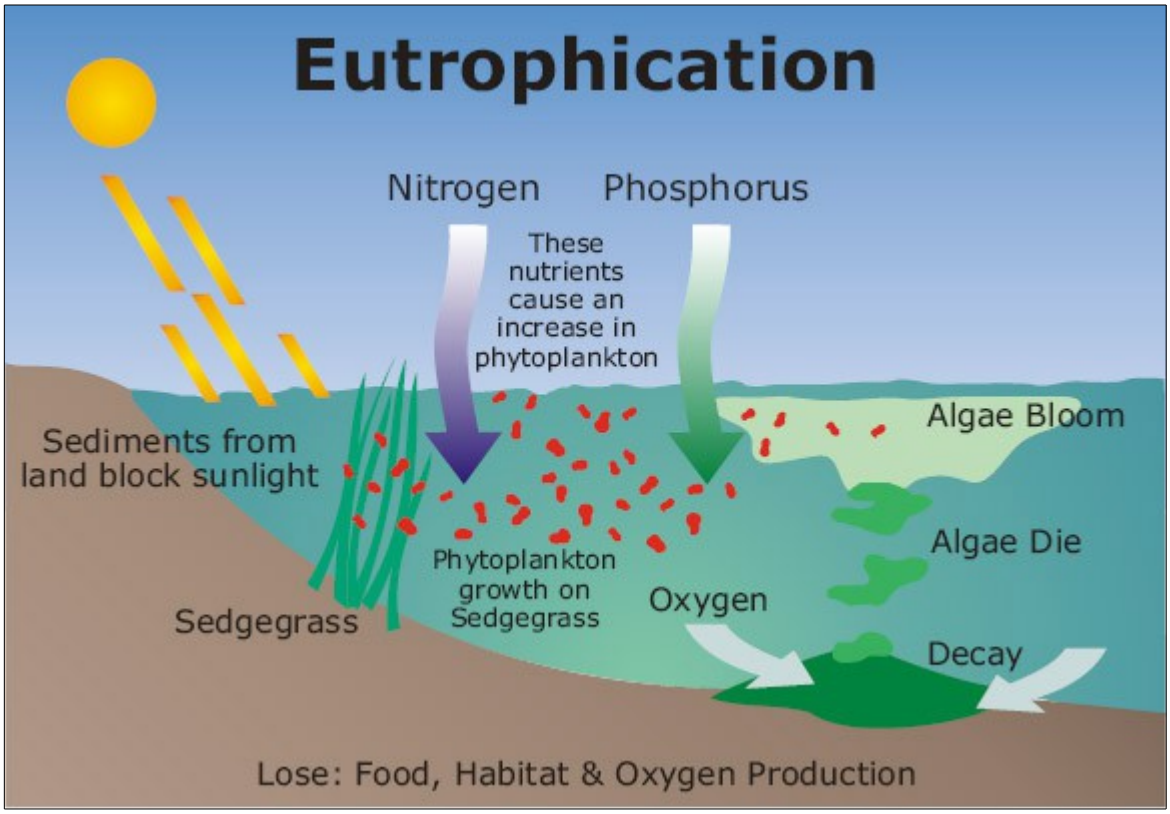

Figure 25: Eutrophication, [240]

Summary of Chapter One

In summary, this chapter discussed the historical antecedents of remote sensing. That is how remote sensing started, some of the various definitions given by various researchers and authors alike. Furthermore the current trends in remote sensing. Resolution which is the dimensions and the information content of pixels of an image [28] as well as the types of resolution (Spatial, Temporal, Spectral and Radiometric) was also expounded on. Some of the noise types that impact remotely sensed images were looked at. A couple of these noise types are gaussian, salt and pepper, speckle, thermal and quantization noise. Image processing techniques in remote sensing was discussed. These techniques included classification, smoothing techniques (data filtering techniques) used in remote sensing. Atmospheric correction which is needed in remote sensing due to the effect of atmospheric conditions on remotely sensed data. Some of the techniques discussed are image based technique and

physical technique. reviewed some works that particularly used remote sensing for monitoring inland water quality parameters. Some of the works that used remote sensing to monitor inland water quality parameters reviewed were, Ritchie et al [118], Schiebe et al [119], Harding et al [120], Bisun Datt [220], Rundquist et al [122], Novoa et al [123], Yu et al [124], He et al [125] as well as others. The final part of this chapter dealt with various inland water quality parameters that can be remotely sensed and how important it is to monitor these parameters.

2 EXPERIMENTAL PART

In trying to achieve the set objectives for this research work, various tasks will be undertaken based on the theories and principles propounded in chapter two. This chapter describes the exact steps that was taken in arriving at the set out goals for this research. This includes in situ measurements for water quality parameters under study, laboratory analysis of these sampled parameters and processing remotely sensed data from Landsat ETM+.

2.1 Study Area

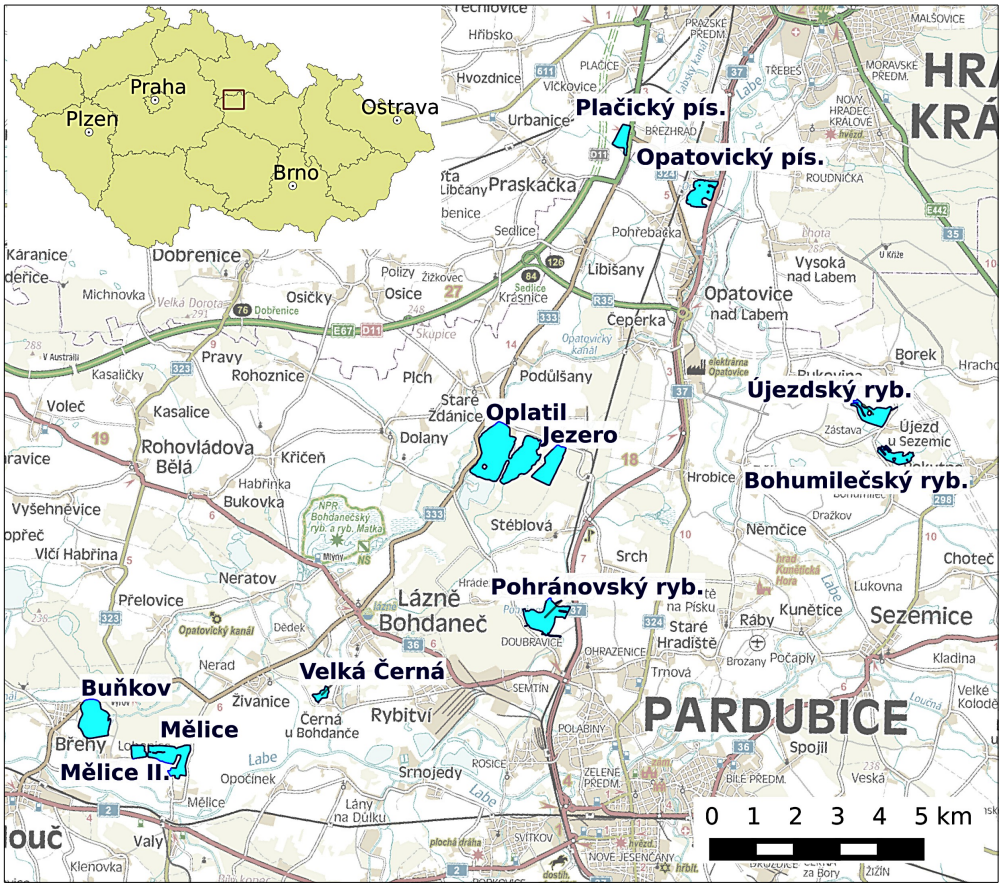

Figure 26: Water bodies that were sampled and their location.

This work concentrates on water bodies near town Pardubice 50°02′19″N 15°46′45″E and Hradec Kralove 50°12′34″N 15°50′00″E. Water bodies in this area are mainly fishponds

and lakes created by sand mining. The water bodies in the area of study are shown in Figure 26. All the water bodies are relatively small, those sampled in this work range from 8 to 90 hectares, approximately. The fish ponds were established in middle ages and have inlets and outlets [221]. Water bodies originating from sand wining are relatively new, the wining on some of the water bodies stopped few years ago, and do not have surface inlet or outlet. They are located in quite flat landscaped areas and the depth of the water bodies were taken into consideration. Most of water bodies of both types are used for fishing and swimming. The lakes that were monitored are at different states within these categories mostly specifically between oligotrophic and eutrophic [214]. The water bodies sampled for this research work are Bunkov, Melice, Jezero, Oplatil, Pohranovsky rybnik, Velka Cerna, Opatovicky pisnik, Ujezdsky rybnik, Bohumilecky rybnik, Spravcicky pisnik, pisnik Hradek, Bohdanecsky rybnik.

2.2 In Situ Sampling and Laboratory Analysis

2.2.1 In Situ Measurement

In situ measurement was started in autumn of 2011 until spring of 2015. Sampling took place on 12 water bodies in all as earlier stated. The measurements were made on the day of Landsat 7 (ETM+) overpasses. Some times they were taken a day before or a day after when overpass was a weekend coupled with other activities such teaching. An inflatable boat as seen i n Figure 27 was used for all our sample taking. A Trimble Juno SB GPS was used to geographically locate all the points at which samples were specifically taken as seen in Figure 28. We used a Testo 110 digital thermometer to take or record the temperature of water at each sampling point as seen in Figure 29.

Figure 27: Inflatable boat with equipment to take samples and measurements in situ.

Figure 28: Trimble Juno SB GPS.

The water samples were taken using plastic bottles and were lowered around about 5 to 15 cm to collect the samples. The boat was made static as much as possible is order to make sure the GPS location and point of sampling are the same. Up to 1.5 litres of water sample was taken at each sampling point. Samples taken were immediately placed into an ice chest in order to keep the original properties and prevailing sample conditions intact. Visibility was checked at all times that sampling took place. This was done by setting up a thread to meteorological facilities near to the areas of sampling to record visibility conditions at the time of taking the samples.

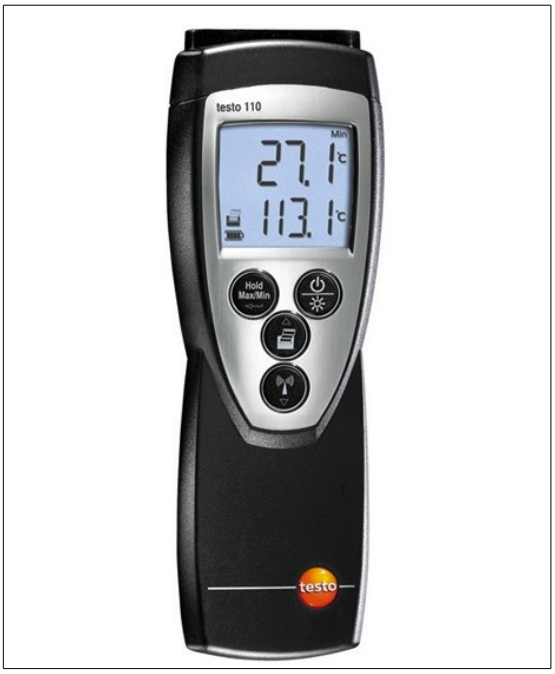

Figure 29: Testo 110 digital thermometer. [241]

They were then placed in a laboratory fridge before they are analysed. Table 6 shows the summary of the measurements made. The blank cells show where the said water quality parameter was not measured.

Table 6: Measured parameters and water bodies

Date	Sample No.	Water Body	Chl [ug/l]	TC [mg/l]	TOC [mg/l]	TN [mg/l]	T [°C]	Secchi [cm]
2011.09.15	1	Melice	2.2				20.2	
2011.09.15	2	Melice	2.2				20.3	
2011.09.15	3	Melice	1.5				20.6	
2011.09.15	4	Bunkov	71				19.7	
2011.09.15	5	Bunkov	65				19.5	
2011.09.15	6	Melice	3.7				20.9	
2011.09.15	7	Pohranovsky	6.7				20	
2011.09.15	8	Pohranovsky	6.7				20	
2011.09.15	9	Pohranovsky	5.2				20	
2011.09.26	1	Melice	4.4					
2011.09.26	2	Melice	0.2					
2011.09.26	3	Melice	2.2					
2011.09.26	4	Bunkov	17.4					
2011.09.26	5	Oplatil	2.2					
2011.09.26	6	Hradek	29					

2011.09.26	7	Hradek	29					
2011.09.26	8	Oplatil	2.2					
2011.09.26	9	Oplatil	0.2					
2012.05.29	1	Pohranovsky	17.4	58.2	18.07	0.18	22.6	110
2012.05.29	2	Pohranovsky	11.6	58.9	17.7	0.16	22.3	185
2012.05.29	3	Oplatil	3.6				21.5	480
2012.05.29	4	Oplatil	3.6				21	480
2012.05.29	5	Oplatil	2.2				21	400
2012.05.29	7	Oplatil	2.2				21	480
2012.05.29	8	Bunkov	31.9	53.31	16.03	0.16	23.4	21.5
2012.05.29	9	Bunkov	20.3	53.9	15.27	0.16	23	21.3
2012.06.22	1	Pohranovsky	36.3	65.96	20.23	0.16	26.3	62
2012.06.22	2	Pohranovsky	24.7	71.5	21.31	0.14	26.1	74
2012.06.22	3	Oplatil	18.9	34.2	8.75	0.11	24.6	179
2012.06.22	4	Oplatil	2.9	35.52	8.48	0.1	24.2	186
2012.07.31 to 01.08	1	Spravcicky	2.9					
2012.07.31 to 01.08	2	Spravcicky	3.6					
2012.07.31 to 01.08	3	Spravcicky	3.6					
2012.07.31 to 01.08	4	Pohranovsky	4.8				29.5	42.5
2012.07.31 to 01.08	5	Pohranovsky	9.7				28.4	44.5
2012.07.31 to 01.08	6	Oplatil	0.7				26.3	201
2012.07.31 to 01.08	7	Oplatil	1.5				26.3	194
2012.07.31 to 01.08	8	Oplatil	1.5				26.7	228
2012.09.11	1	Pohranovsky	28	89.52	32.92	0.19	21.6	15
2012.09.11	2	Pohranovsky	3				22.2	25
2012.09.11	3	Oplatil	4.3	31.2	6.15	0.1	22.9	220
2012.09.18	1	Pohranovsky	26	84.11	30.63	0.13	19.5	24
2012.09.18	2	Pohranovsky	24.5				20.3	25.5
2012.09.18	3	Oplatil	11.6	32.92	6.97	0.13	21.7	223
2012.09.18	4	Oplatil	14.6				21.6	210
2012.09.18	5	Bunkov	68.9	37.35	14.65	0.15	21.3	29
2012.09.18	6	Bunkov	7.3				21.7	33
2012.11.14	1	Oplatil	8		6.86		9.2	240
2012.11.14	2	Oplatil	6.5		5.45		9.1	268
2012.11.14	3	Oplatil	7.3		6.09		8.3	269
2012.11.14	4	Jezero	7.3		4.16		8.4	514
2012.11.14	5	Jezero	3.6		4.4		8.5	635
2012.11.14	6	Jezero	2.2		4.79		8.5	614

Date	Sample No.	Water Body	Chl [ug/l]	TC [mg/l]	TOC [mg/l]	TN [mg/l]	T [°C]	Secchi [cm]
2013.04.23	1	Spravcicky	4.1	43.16	9.53	0.11	11.9	125
2013.04.23	2	Spravcicky	7.3	38.45	4.55	0.11	11.5	123
2013.04.23	3	Placicky	4.9	41.09	7.73	0.15	13.4	184
2013.04.23	4	Placicky	3.9	38.16	5.21	0.15	13.8	176
2013.05.09	1	Jezero	0.4	35.01	7.06	0.33	18.9	530
2013.05.09	2	Jezero	0.4	33.68	6	0.31	18.7	620
2013.05.09	3	Bunkov	4.6	39.76	8.77	0.94	22.7	140
2013.05.09	4	Bunkov	6.1	38.96	7.96	0.81	22.1	170
2013.05.09	5	Melice	0.2	32.46	8.16	0.45	21	334
2013.05.09	6	Melice	0.7	31.36	7.41	0.43	20.6	324
2013.05.09	7	Pohranovsky	17.3	59.57	18.39	1.52	21.5	57
2013.05.09	8	Pohranovsky	20.9	59.29	18.59	1.3	20.5	54
2013.05.09	9	Pohranovsky	15.3	60.81	19.09	1.68	20.8	52
2013.05.09	10	Pohranovsky	17.4	60.81	19.09	1.68	20.8	52
2013.06.19	1	Placicky	3.4	44.3	15.75	1.02	25.8	190
2013.06.19	2	Placicky	2.8	39.56	11.51	1	25.7	218

Date	Sample No.	Water Body	Chl [ug/l]	TC [mg/l]	TOC [mg/l]	TN [mg/l]	T [°C]	Secchi [cm]
2013.06.19	3	Opatovicky	0.2	39.66	7.7	0.38	25.1	363
2013.06.19	4	Opatovicky	1.8	39.19	8.91	0.36	28.3	364
2013.06.19	5	Ujezdsky	29.6	68.19	31.66	2.02	28.4	26
2013.06.19	6	Ujezdsky	47.2	70.65	32.2	2.16	28.4	29
2013.06.19	7	Bohumilecsky	65.7	70.65	34.2	3.19	29.7	19
2013.06.19	8	Bohumilecsky	58.6	71.44	34.72	2.65	29.4	23
2013.06.19	9	Bohumilecsky	59	72.23	34.85	2.69	29.9	21
2013.07.29	1	Placicky	4.736	29.18	10.16	0.64	27.5	166
2013.07.29	2	Placicky	2.4	28.53	9.49	0.64	27.5	164
2013.07.29	3	Opatovicky	1	36.2	5.41	0.55	26.8	448
2013.07.29	4	Opatovicky	0.5	36.46	5.69	0.36	26.6	479
2013.07.29	5	Oplatil	1.5	29.95	6.45	0.46	27.2	485
2013.07.29	6	Oplatil	2.5	26.8	6.49	0.49	27.1	325
2013.07.29	7	Pohranovsky	49.5	95.83	39.96	2.86	29.4	22
2013.07.29	8	Pohranovsky	39.7	99.55	43.86	3.52	29.3	30
2013.08.12	1	Placicky	3.8	32.76	10.56	0.64	24.7	135
2013.08.12	2	Placicky	2.1	30.5	8.64	0.6	24.8	148
2013.08.12	3	Opatovicky	1.2	35.59	4.97	0.35	25	467
2013.08.12	4	Opatovicky	2.5	35.58	4.63	0.5	25	499
2013.08.12	5	Oplatil	4.7	26.47	6.31	0.36	25.2	226
2013.08.12	6	Oplatil	4	26.8	6.75	0.47	52.2	233
2013.08.12	7	Velka Cerna	0.4	45.48	12.2	1.23	25.7	65
2013.08.12	8	Velka Cerna	0.4	44.57	12.16	0.91	25.7	72
2014.05.21	1	Melice	3	31.57	8.68	0.64	18.8	240
2014.05.21	2	Melice	2.2	31	8.87	0.62	18.9	220
2014.05.21	3	Melice	1.5	31.59	9.2	0.66	19	275
2014.05.21	4	Bunkov	0.7	43.88	8.16	1.4	20.9	125
2014.05.21	5	Bunkov	1.5	43.48	8.18	1.39	19.8	200
2014.05.21	6	Pohranovsky	8.1	52.81	14.96	1.27	21.6	140
2014.05.21	7	Pohranovsky	4.4	52.29	14.04	1.15	21	170
2014.07.23	1	Pohranovsky	22.9	83.35	29.73	2.4	25.1	26
2014.07.23	2	Pohranovsky	34.9	95.58	42.17	3.35	24.9	23
2014.07.23	3	Pohranovsky	25.7	82.72	29.15	2.3	25.8	23
2014.07.23	4	Oplatil	0.2	35.7	6.49	0.59	24.6	325
2014.07.23	5	Oplatil	0.8	35.84	6.55	0.59	24.6	305
2014.07.23	6	Oplatil	2.4	36.04	6.4	0.59	24.7	325

Date	Sample No.	Water Body	Chl [ug/l]	TC [mg/l]	TOC [mg/l]	TN [mg/l]	T [°C]	Secchi [cm]
2014.09.16	1	Pohranovsky	34.3	85.22	30.92	2.54	20.8	24
2014.09.16	2	Pohranovsky	39.1	82.3	27.39	2.01	20.3	26
2014.09.16	3	Pohranovsky	33.5	80.55	27.34	1.97	20.3	28
2014.09.16	4	Oplatil	5.8	37.34	5.8	0.6	20.8	486
2014.09.16	5	Oplatil	2.4	37.2	6.09	0.59	20.4	490
2014.09.16	6	Oplatil	4.4	37.91	6.24	0.63	20.4	465
2014.09.16	7	Melice	1.9	33.96	9.21	0.64	21	310
2014.09.16	8	Melice	3.4	34.98	10.04	0.66	20.9	368
2015.04.21	1	Pohranovsky	12.9	43.75	13.04	1.21	14.3	80
2015.04.21	2	Pohranovsky	9.6	46.24	15.51	1.39	14.2	66
2015.04.21	3	Oplatil	8.9	38.42	7.91	0.8	11.9	117
2015.04.21	4	Oplatil	9.2	38	7.41	0.78	12.3	114
2015.04.21	5	Oplatil	11.1	37.58	7.08	0.84	12.4	127
2015.04.21	6	Bunkov	35.6	44.36	15.45	1.57	15.1	227
2015.04.21	7	Melice	7	34.63	9.36	0.66	13.4	255
2015.04.21	8	Melice	5.1	34.49	8.96	0.64	12.6	255

2.2.2 Laboratory Analysis

Chlorophyll-a

Chlorophyll-a (Figure 30) is an indicator of the abundance of phytoplankton in the water. The pronounced scattering/absorption features of chlorophyll-a are: strong absorption between 400–500 nm (blue) and at 680 nm (red), and reflectance maximums at 550 nm (green) and 700 nm (near-infrared (NIR)) [223] as visualised in Figure 31. Chlorophyll-a is one of the parameters recommended for water quality analysis as suggested by Jones and Lee [224].

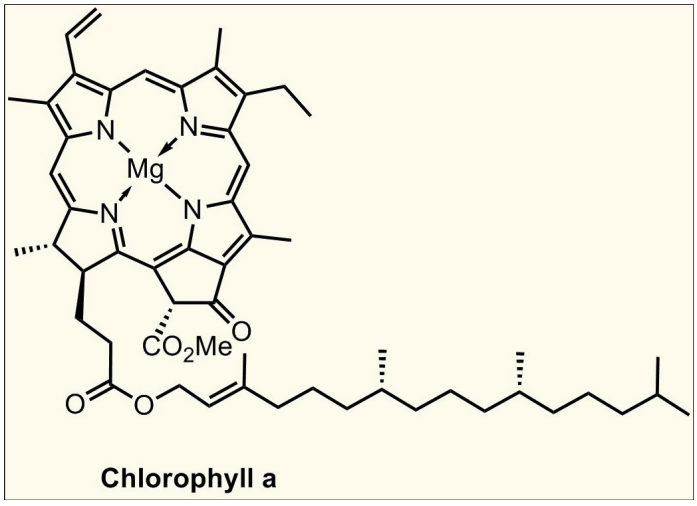

Figure 30: Structure of chlorophyll-a [244]

Chlorophyll-a determination was carried according to ISO-10260 standard [225].Samples collected were kept in cool dark container and refrigerated. None of the samples were frozen though some researchers have suggested it's possible to freeze samples. The analysis of chlorophyll-a were done within 24 hours of collection. A glass fibre filter (Fisher F263) was used in filtering the samples collected.

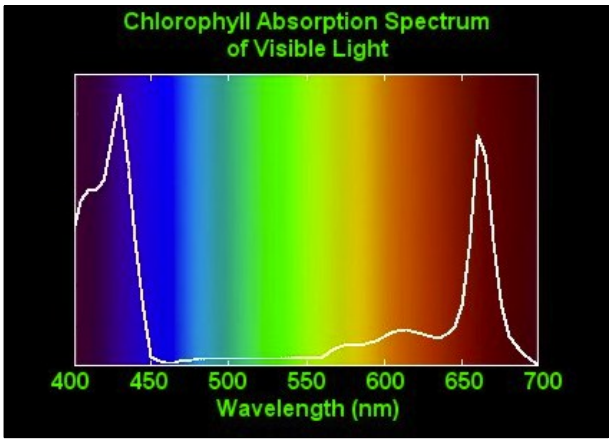

Figure 31: Chlorophyll absorption spectrum of visible light [246]

The filter used in filtering water samples taken had the following specifications, a low hygroscopicity with a retention efficiency of fine particles (<3μm in size). It also had a maximum temperature of 500 °C, a fast flow rate and with a chemical and biological inert which has no organic binders. In most cases 250 to 1000 ml of the samples were filtered depending on the thickness of the impurities (algae) within the water. The bottles containing the collected water samples were well shaken to ensure that the contents were thoroughly mixed before filtration. The filter was then carefully dropped into 25 millilitres of 90% ethanol [225].

The filter was mashed in the ethanol and then hot water bathed the extract for 5 minutes at a constant temperature of 75 °C (Figure 32). A glass container meant for this purpose was used. It had a tight cap to check evaporation.

Figure 32: Memmert hot water bath

This was then left to cool for 15 minutes after which it was put into a refrigerator for 30 minutes. It was then filtered again using the same type of micro fibre filter. The filtrate was then put in a refrigerator before spectrophotometric determination (Figure 33) using a range of 400 to 760 nm. A glass cuvette with optical path of 1 cm was used.

Figure 33: Biochrom Libra 22 spectrophotometer [249]

Total Organic Carbon (TOC) and Total Carbon (TC)

TC is all the carbon in a sample which includes organic, inorganic and volatile. It is represented as the total mass of carbon per amount of sample.

$$TC = TOC + IC \tag{20}$$

Where *TC* is the total amount of carbon, *TOC* total organic carbon and *IC* inorganic carbon. Samples were analysed using FormacsHT TOC/TN analyser (Figure 34) which is based on ISO 8245, EU 2.2.44, USP<643> [226]. To determine the level of TC, the sample was injected by means of an automated septum-less rotary port into the high-temperature reactor. In the reactor, at a temperature of 950 °C all organic and inorganic carbon were oxidized into gaseous carbon dioxide (CO_2).

Figure 34: FormacsTH TOC/TN analyser [227]

TOC is the organic carbon that is converted into carbon dioxide after oxidation [227] [228]. In directly measuring TOC, the measurement was done after acidification of the sample. In water samples it should preferably include carbon in volatile materials. Though most a times they are removed before analysis were done [227].

$$TOC = TC - IC \tag{21}$$

Total Nitrogen (TN)

This is all the nitrogen in a given sample and this includes organic and inorganic nitrogen. This is normally represented as the total mass of nitrogen per amount of sample [227]

$$TN = (TKN + NN) \tag{22}$$

Where *TN* is total nitrogen, *TKN* total Kjedahl nitrogen and *NN* nitrate and nitrite. The sample was added by manual means into a high temperature combustion reactor with an oxidative catalyst. The reactor at a temperature of 850 °C all the carbons were oxidized to carbon dioxide and all chemically bound nitrogen were converted to nitric oxide NO [227]. Flow of oxygen, which was used as a carrier gas and as a source of oxygen, then transported these products into the detector. Firstly, the products were led into the infrared detector where the carbon dioxide was determined then into the ND25 detector (on the right in Figure 34) where the nitric oxide was determined.

In the chemiluminescent detector sample gas was mixed with ozone in the reaction chamber which was then heated at 50 °C to form excited nitrogen dioxide NO_2 [227].

$$NO + O_3 \rightarrow NO_2^* + O_2 \rightarrow NO_2 + O_2 + h\nu \tag{23}$$

The fast decomposition of the NO_2^* produces light, this was measured by a photo multiplier tube (PMT) and was cooled to a temperature of 10 °C. The electric signal from the PMT was amplified and then transported into the controlling computer and was calculated [227].

2.2.3 Data Processing

Images from Landsat 7 ETM+ data with a spatial resolution of 30 m were used. The study area is fully covered by both Landsat scenes of WRS-2, path and row 191/25 and 190/25 respectively, which gives average satellite revisit time of 8 days. The Landsat ETM+ images were downloaded from earth explorer site (http://earthexplorer.usgs.gov) run by the USGS (United States Geological Survey). The images were downloaded in tif file format. The files were then loaded into Grass GIS and Quantum GIS as visualized in figure 35. The projection for the images was in UTM zone 33N, Ellipsoid being WGS84. The images had gaps in them

which were caused by Scan Line Corrector (SLC). Since 21st of May 2003 Landsat 7 ETM+ has developed this fault as the SLC is to ensure that all scans are well aligned parallel to each other which compensates for the motion (forward) of the satellite [229].

Figure 35: Band combination 7,5,3 of Landsat ETM+ with points of sampling loaded unto it.

Due to the above issue all sampling points that fell within the gaps were completely removed. To check for points that fell within hazy, cloudy and shady areas, RGB colour combination was used. This visually enhanced the areas that were affected by the above mention phenomena. All such points that were within cloudy, hazy and shady areas were removed. Bands combination 1,6,6 was used for highlighting haze and clouds whereas 4,2,1 was used for highlighting green vegetation [230]. The gps points were then transformed into vector files and were loaded onto the images and data from the point sampling were extracted (Figure 35). The extracted values were further analysed using various tools.

Conversion of raw Digital Numbers (DN) numbers to Spectral radiance at sensor

The data extracted from the from the TIFF were calibrated as DN numbers and had to be converted to spectral radiance based on the recorded signal. The conversion of DN was based

on the equation as espoused by Chander et al [231], Landsat 7 science data users handbook [28] and this is seen in equation 24 below,

$$L_\lambda = [\frac{LMAX_\lambda - LMIN_\lambda}{Qcal\,max - Qcal\,min}](Qcal - Qcal\,min) + LMIN_\lambda \quad (24)$$

where

L_λ is the Spectral radiance at sensor's aperture [$w/(m^2\ sr\ \mu m)$]

$Qcal$ is the Quantised calibrated value in DN

$Qcal\,min$ is the Minimum quantised calibrated value corresponding $LMIN_\lambda$ in DN

$Qcalmax$ is the Maximum quantised calibrated value corresponding $LMAX_\lambda$ in DN

$LMIN_\lambda$ is the Spectral radiance at sensor scale $Qcalmin$ [$w/(m^2\ sr\ \mu m)$]

$LMAX_\lambda$ is the Spectral radiance at sensor scale $Qcalmax$ [$w/(m^2\ sr\ \mu m)$]

Conversion of DN numbers to Top of Atmosphere Reflectance

By using this formula the output was then processed into TOAR by relying the formulas below also based on Landsat 7 science data users handbook [28] and Chander et al [231]. This converted the radiance recorded at sensors to reflectance.

$$\rho_\lambda = \frac{\pi * L_\lambda * d^2}{ESUN_\lambda * \cos(\theta o)} \quad (25)$$

Where

ρ_λ is Planetary TOA reflectance

π is determined constant

L_λ is the spectral radiance at the sensor's aperture

d is the Earth Sun distance

$ESUN_\lambda$ is the Mean exoatmospheric Solar irradiance

θo is the Solar Zenith angle.

Each of the images downloaded were processed based on the above equations by the use of Grass GIS and Quantum GIS software. This particular process was embedded in the i.landsat.toar command in Grass GIS.

Atmospheric Correction

The conditions pertaining to the exact time that images are taken do have considerable effects on them. Therefore the best data to be derived from the acquired satellite data, these effects of the atmosphere needs to limited. A number of methods for reducing the effect of atmospheric conditions on remotely sensed images have been deliberated on in chapter1.2.3. Atmospherically corrected images (Landsat Surface Reflectance product) were downloaded from USGS website (http://earthexplorer.usgs.gov). The input material was TOAR and based on the method proposed by Masek et al [117] and the output landsat surface reflectance product. Masek et al used the following steps described below [117]. These steps are embedded in LEDAPS.

$$\rho TOA = T_g(O_3 O_2 CO_2 NO_2 CH_4)\,\mathrm{X}[¿\rho R + A + T_{R+A} T_g(H_2 O)\frac{\rho_s}{1 - S_{S+A\rho_s}}] \qquad (26)$$

where ρ_s is the surface reflectance

T_g is the gaseous transmission due the gases O_3,O_2,CO_2,NO_2,CH_4

T_{R+A} is the Rayleigh and aerosol transmission

$\rho R + A$ is the Raleigh and aerosols atmospheric intrinsic reflectance

S_{R+A} is the Raleigh and aerosols spherical albedo

The computation of the transmission, intrinsic reflectance and spherical albedo were done based on 6S radiative transfer code [117].

Smoothing

When the images are being taken by the satellite the noise as a property of the sensor affects the images taken. The noise prevents some important data from standing out and also contributing to some data being missing. To check this phenomenon we first created a water only image based on a map of water bodies in the Czech Republic (Figure 36).

Based on the map a water only mask was created by classifying water and non water areas. Classification of water and non water areas were considered but this method did not give a favourable result. Normalised difference water index [232] was tried where the green (band 2) and shot wave infra-red 1 (band 5) of Landsat 7 ETM+ were used in creating the NDWI. The mask was used during the smoothing of data to limit the effect of noise and to avoid non water areas such as vegetation along the banks of the water bodies.

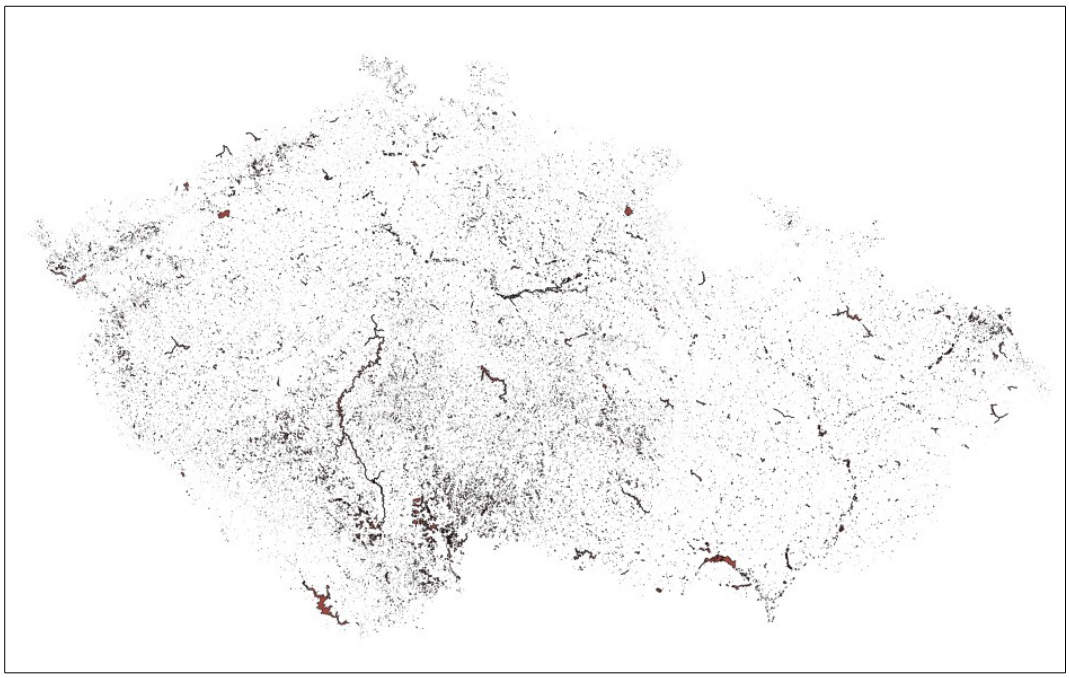

Figure 36: Map of water areas in the Czech Republic

The images were spatially filtered by convolving the image with a small moving window [68]. Each pixel in the original image was replaced by a weighted average of the product from the window as well as the neighbouring pixels [81].

```
Title: 3x3 average, non-null data only
Matrix 3
1 1 1
1 1 1
1 1 1
Divisor: 0
Type: P
```

Figure 37: 3x3 averaging window definition

The discrete convolution filtering was adopted where the 3×3 averaging window (Figure 37) was used.

The resultant pixel values in the new image were expressed based on equation (7).

In achieving the above the following steps were followed

Step 1. Using r.mask command in Grass GIS, a mask was created based on the water only map of Czech Republic. Non water areas were classified and masked out

Step 2. Using map calculator in Grass GIS, a water only mask was created based on an expression (27) using band 7 short-wave infrared (SWIR) of atmospherically corrected images.

$$Band\ 7 < 210 \tag{27}$$

Step 3. Using the r.mfilter in Grass GIS a filter (Figure 37) was ran to smooth the data using the 3×3 average window.

The shortwave infra-red 2 band (band 7) was chosen because it has limited cloud penetration, which provides good contrast between different vegetation also helps to differentiate between clouds and snow[28].

2.3 Regression Analysis, Model Creation and Testing performance of models

2.3.1 Regression Analysis

The sample points were loaded unto the Landsat ETM+ images using the v.what module in Quantum GIS, the values was extracted from the images through the use of the attribute table. The attribute table is then exported to a spread sheet for the regression analysis.

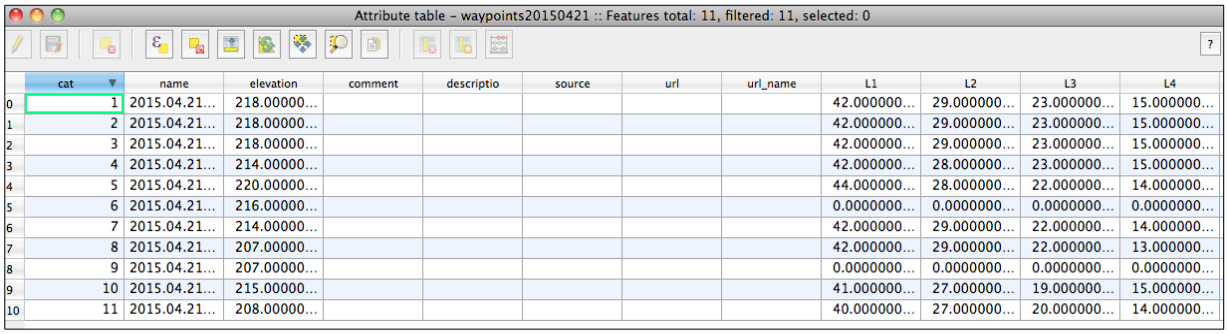

	cat	name	elevation	comment	descriptio	source	url	url_name	L1	L2	L3	L4
0	1	2015.04.21...	218.00000...						42.000000...	29.000000...	23.000000...	15.000000...
1	2	2015.04.21...	218.00000...						42.000000...	29.000000...	23.000000...	15.000000...
2	3	2015.04.21...	218.00000...						42.000000...	29.000000...	23.000000...	15.000000...
3	4	2015.04.21...	214.00000...						42.000000...	28.000000...	23.000000...	15.000000...
4	5	2015.04.21...	220.00000...						44.000000...	28.000000...	22.000000...	14.000000...
5	6	2015.04.21...	216.00000...						0.0000000...	0.0000000...	0.0000000...	0.0000000...
6	7	2015.04.21...	214.00000...						42.000000...	29.000000...	22.000000...	14.000000...
7	8	2015.04.21...	207.00000...						42.000000...	29.000000...	22.000000...	13.000000...
8	9	2015.04.21...	207.00000...						0.0000000...	0.0000000...	0.0000000...	0.0000000...
9	10	2015.04.21...	215.00000...						41.000000...	27.000000...	19.000000...	15.000000...
10	11	2015.04.21...	208.00000...						40.000000...	27.000000...	20.000000...	14.000000...

Figure 38: Attribute table with data from uploaded sampling points in QuantumGIS

This statistical analysis was done to check the relation between two variables being spectral data and the various water quality parameters [233]. Coefficient of determination (r^2), was used in the analysis. The selected spectral data and the water quality parameters that had good correlation were then further analysed.

2.3.2 Regression models and Validation

To build the various models for each inland water quality parameter, these parameters were measured or analysed, bands or combination of bands with high correlations were used. The data with the best fit were used to create a calibration model in this work. With dependent variable y as against x independent variable base on least squares regression $(y-y')^2$ [234]. This process was repeated for all the chosen bands and band combination with high correlation. It must be noted that a good regression should have a prediction of r^2 values that are close to 1. The slope intercepts of actual measured water quality parameters was then used in predicting possible levels. The predicted values were then drawn against the actual values from which the best correlation r^2 was used in creating the model for the specific water quality parameter.

Some critical indicators such as root mean square error (RMSE) and normalised root mean square error (NRMSE) were used to evaluate the level of accuracy of the models. They are defined below.

$$RMSE = \sqrt{\frac{\sum_{i=1}^{n} \left(X_{obs,i} - X_{mo\ del,i} \right)^2}{n}} \tag{28}$$

$$NRMSE = \frac{RMSE}{X_{obs,\max} - X_{obs,\min}} \tag{29}$$

Where $X_{obs,\ i}$ are estimated or measured parameter, $X_{model,\ i,}$ values from the model created, n is the number of samples and NRMSE $X_{obs,\ max}$- $X_{obs,\ min}$ is the difference between the maximum of measured parameter and the minimum of measured parameter.

Summary of chapter Two

In summary, the water bodies around the Pardubice and Hradec Kralove region that were sampled for water quality parameters were Bunkov, Melice, Jezero, Oplatil, Pohranovsky rybnik, Velka Cerna, Opatovicky pisnik, Ujezdsky rybnik, Bohumilecky rybnik, Spravcicky pisnik, pisnik Hradek. In situ measurements were made from autumn 2011 to spring of 2015. The samples were analysed in the laboratory for the Chl-a, TC, TOC, TN. SDD and T were measured during sampling. Data remotely sourced were processed as TOAR and atmospherically corrected images based on LEDAPS from from which the values were extracted. Sampled points that were found in gaps created by SLC (chapter 2.2.3), covered by cloud and cloud shadow were removed. TOAR image values and atmospherically corrected image values were both smoothed to limit the effect of noise. Both smoothed, non-smoothed TOAR and atmospherically corrected data were statistically analysed. Models were developed based on smoothed TOAR image and atmospherically corrected image values. Bands or band combinations with good r^2 values were used in developing the models for the various parameters. Smoothed atmospherically corrected image values were used for model creation. The developed models were validated using r^2, RMSE and NRMSE.

3 RESULTS AND DISCUSSION

The current chapter outlines the various resultant outcomes of the various steps that were taken. A critical look is also taken vis a vis the results from the preceding chapter whether it meets the various expectations that were set in undertaking the various outlined steps in the previous chapter.

3.1 Sampled Water Quality Parameters

Table 7: Summary of Water Quality Parameters measured and number of samples taken

Date	Samples	Chl-a [ug/l]	TC [mg/l]	TOC [mg/l]	TN [mg/l]	T [°C]	Secchi [cm]
2011.09.15	9	1.5-71				19.5-20.9	
2011.09.26	9	0.2-29					
2012.05.29	9	2.2-31.9	53.31-58.9	16.03-18.07	0.16-0.18	21-23.4	21.5-480
2012.06.22	4	2.9-36.3	34.2-71.5	8.48-21.31	0.1-0.16	24.2-26.3	62-186
2012.07.31 to 01.08	8	0.7-9.7				26.3-28.4	44.5-228
2012.09.18	3	3-68.9	31.2-84.11	6.15-30.63	0.1-0.19	19.5-22.2	15-220
2012.11.14	6	2.2-8		4.16-6.86		8.3-9.2	240-635
2013.04.23	6	3.9-7.3	38.16-43.16	4.55-9.53	0.11-0.15	11.5-13.8	123-184
2013.05.09	4	0.4-20.9	35.01-60.81	6-19.06	0.31-1.68	18.7-22.7	52-620
2013.06.19	10	0.2-65.7	39.19-72.23	7.7-34.85	0.36-3.19	25.1-29.9	19-364
2013.07.29	9	0.5-49.5	26.8-99.55	5.41-43.86	0.36-3.52	26.6-29.9	22-485
2013.08.12	8	0.4-4.7	26.8-45.48	4.63-12.2	0.5-1.23	24.7-52.2	65-499
2014.05.21	8	0.7-8.1	31-52.81	8.18-14.96	0.62-1.4	18.8-21.6	125-275
2014.07.23	7	0.2-34.9	35.7-95.58	6.4-42.17	0.59-3.35	24.6-25.8	23-325
2014.09.16	6	1.9-39.1	33.96-85.22	5.8-30.92	0.59-2.54	20.3-21	24-490
2015.04.21	8	5.1-35.6	34.49-46.24	7.08-15.51	0.78-1.57	11.9-15.1	66-255
Mean		**12.42**	**48.12**	**13.82**	**0.94**	**21.65**	**207.26**
Std Dev		**16.53**	**19.18**	**10.1**	**0.85**	**6.08**	**168.02**

In taking water samples, 198 samples were generally analysed taking into consideration the various water quality parameters (chlorophyll-a, Total Carbon, Total Organic Carbon, Total Nitrogen, Temperature, Secchi Depth).

The mean and standard deviations were also calculated for each of the measured water quality parameters. 121 samples (Table 7) were analysed for the various parameters under consideration was due to the fact that some of the data was retained for application and validation purposes. Those used for the model validation was not used at all in the model creation.

RGB band combinations 1,6,6 (Figure 39) and 4,2,1 (Figure 40) which were employed to check both haze and cloud, as well as green vegetation [230]. When images are in grey, identifying clouds and haze was difficult. Some of the clouds caused shades which also affected the data that was being analysed. This phenomenon gave wrong reflectance values which had to be either removed or corrected.

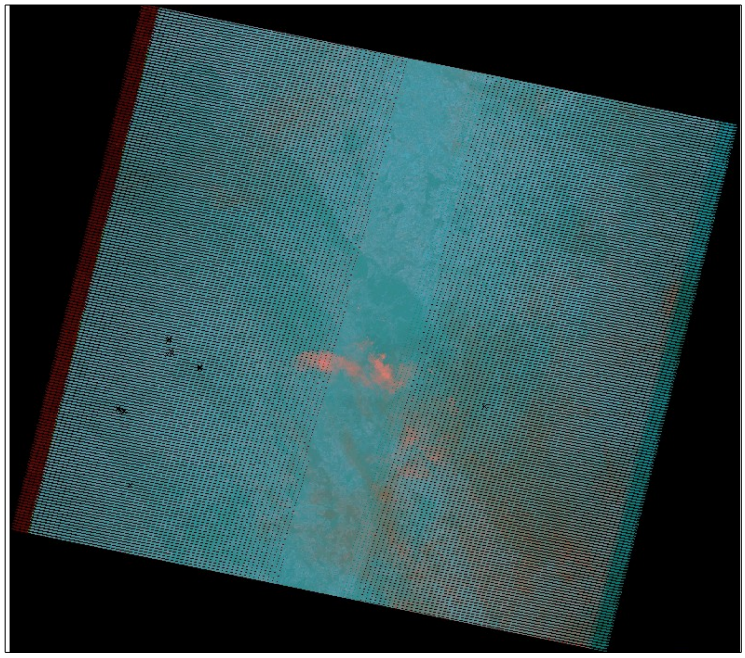

Figure 39: RGB band combination1,6,6

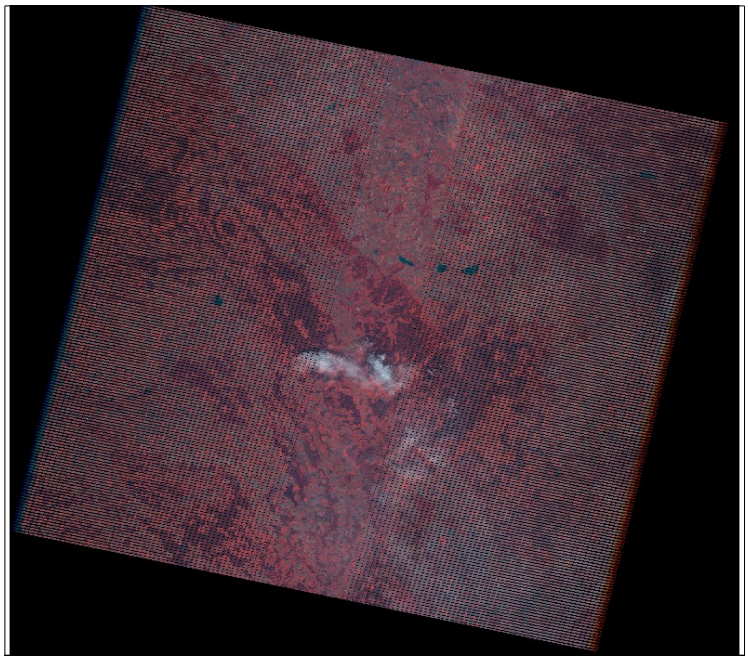

Figure 40: RGB band combination 4,2,1

3.2 Top of Atmosphere Reflectance

All the DNs from the 121 sample points that had been extracted were turned into TOAR values. The regression relationship between the reflectance values (bands and combination of bands) and that of the measured parameters showed varied levels of correlation based on measured Pearson coefficient squared (r^2). Linear correlation varied vis a vis the measured water quality parameters and TOAR values. Band combination of visible bands (from blue to near infra-red) band 1, 2, 3, 4, (450nm to 900nm) with the other bands (Shortwave infra-red 1 to Shortwave infra-red 2) 5, 6, 7 (1550 to 2350). Panchromatic band (band 8) which is 15 m

Table 8: r^2 values of band and combinations based on smoothed TOAR values

(part 1)

Parameter	L61	L62	L1/L2	L1/L3	L1/L4	L1/L6	L1/L8	L2/L1
R^2 chl-a [ug/l]	0.0926	0.0936	***0.4742***	0.3948	0.1554	0.0595	***0.4181***	0.1720
R^2 log chl-a [ug/l]	0.0146	0.0136	0.3550	***0.5184***	0.0634	0.0342	0.3008	0.1678
TC [mg/l]	0.1775	0.1747	0.2179	***0.4717***	0.2566	0.0014	***0.4032***	0.1073
Log TC	0.1481	0.1461	0.2198	***0.4707***	0.2673	0.0090	***0.4153***	0.1203
TOC [mg/l]	0.2791	0.2797	***0.5273***	***0.5331***	***0.4382***	0.1795	***0.6887***	***0.4755***
LogTOC	0.3228	0.3259	***0.6534***	***0.5785***	***0.4185***	0.2951	***0.6446***	***0.4585***
TN [mg/l]	0.0779	0.0745	0.1455	0.2543	0.1906	0.1327	0.2802	0.0564
LogTN [mg/l]	0.0007	0.0003	0.0499	0.1137	0.0479	0.1347	0.0840	0.0117
T [°C]	***0.9032***	***0.9062***	0.2156	0.0581	0.3505	0.3471	0.2406	0.1408
Log T	***0.8932***	***0.9010***	0.2328	0.0556	0.3480	***0.4063***	0.2307	0.1401
Secchi [cm]	0.1737	0.1711	***0.5703***	***0.6217***	0.1073	0.2737	0.3142	0.1975
Log Secchi	0.1859	0.1798	***0.6445***	***0.7648***	0.1774	0.1303	***0.5003***	0.2026

(part 2)

Parameter	L2/L3	L2/L8	L3/L1	L3/L2	L4/L1	L8/L1	L8/L2
R^2 chl-a [ug/l]	0.1992	0.2059	***0.4071***	0.1870	0.2289	***0.4221***	0.2124
R^2 log chl-a [ug/l]	0.3917	0.1376	***0.4919***	0.3570	0.0937	0.2748	0.1296
TC [mg/l]	***0.4662***	0.3536	***0.5206***	***0.5149***	0.2026	0.3475	0.2996
Log TC	***0.4619***	0.3676	***0.5123***	***0.5033***	0.2155	0.3612	0.3139
TOC [mg/l]	0.3142	***0.5139***	***0.5864***	0.3445	***0.4385***	***0.6480***	***0.4824***
LogTOC	0.3192	***0.4076***	***0.6223***	0.3534	0.3565	***0.5652***	0.3718
TN [mg/l]	0.2342	0.2617	0.2885	0.2651	0.2710	0.3076	0.2751
LogTN [mg/l]	0.1131	0.0757	0.1229	0.1260	0.1039	0.1049	0.0930
T [°C]	0.0009	0.1284	0.0717	0.0043	0.2356	0.2262	0.1322
Log T	0.0001	0.1063	0.0672	0.0019	0.2028	0.2007	0.1042
Secchi [cm]	0.3915	0.0739	***0.6119***	***0.4015***	0.0706	0.2590	0.0722
Log Secchi	***0.5461***	0.2045	***0.7917***	***0.5620***	0.1595	***0.4468***	0.1938

was also included. These combinations and single bands had varied r^2 values (table 3.2 part 1 and 2). Values of r^2 that were >0.4 were considered in the regression analysis.

The combination of blue band (band 1) and the panchromatic band (band 8) showed varied correlation levels. In some cases though quite low, generally there seem to be some appreciable level of correlation (Table 8) vis a vis the water quality parameters with the parameter most prominent being Temperature.

The r^2 values for each parameter with the best fit was also identified based on the analysis made. SDD had r^2 value of 0.79 based on band combination L3/L1 and Log of SDD (Figure 41), Chl-a had r^2 value of 0.52 based on L1/L3 (fit was not developed). TOC (Figure 42) had r^2 value of 0.62 from band combination of band 8 (panchromatic), band 1 (blue). TC had the best fit from L3/L1 with r^2 value of 0.52 (Figure 43). Thermal band 62 (1040nm) with temperature had r^2 value of 0.91 (Figure 44). TN had very low r^2 values and therefore no fit was developed. In this regard only smoothed TOAR values were considered in the analysis. This was because the smoothed values limited the effect of noise on them as compared to the non-smoothed TOAR values (see Table 8 and Appendix 6.5). Smoothing was done by using the 3×3 averaging window on the data to limit the effect of noise on the data.

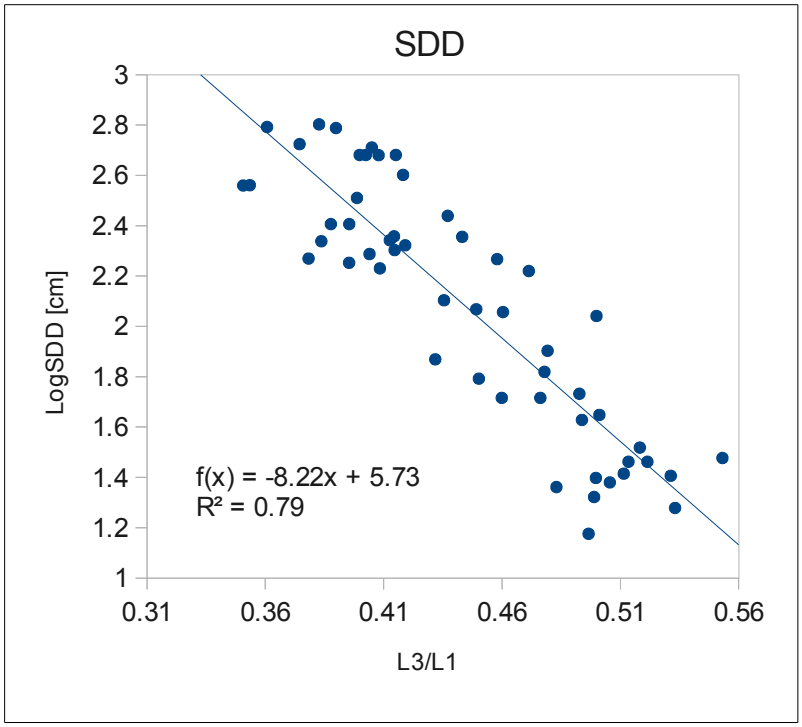

Figure 41: Band combination with the best fit based on TOAR

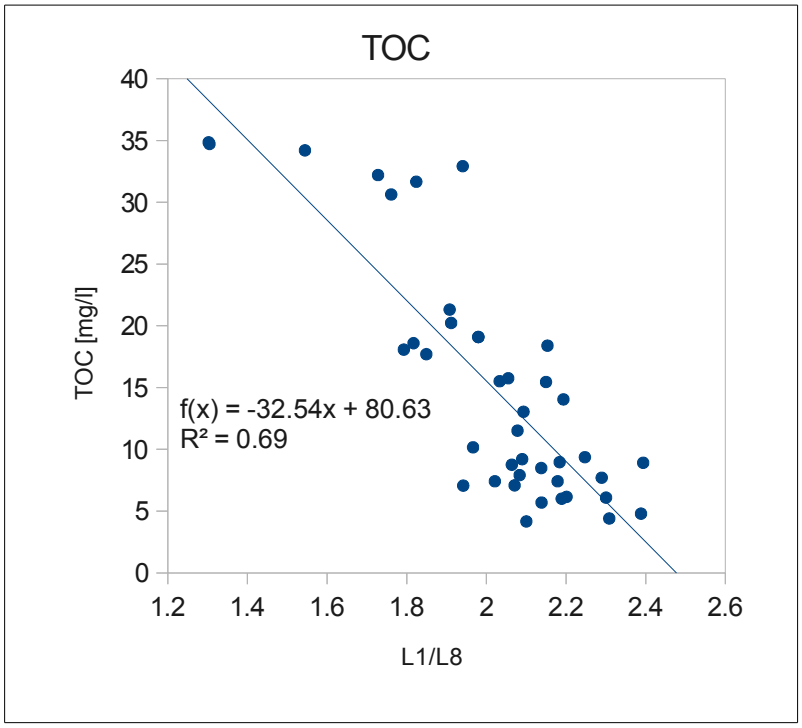

Figure 42: Band combination with the best fit based on TOAR

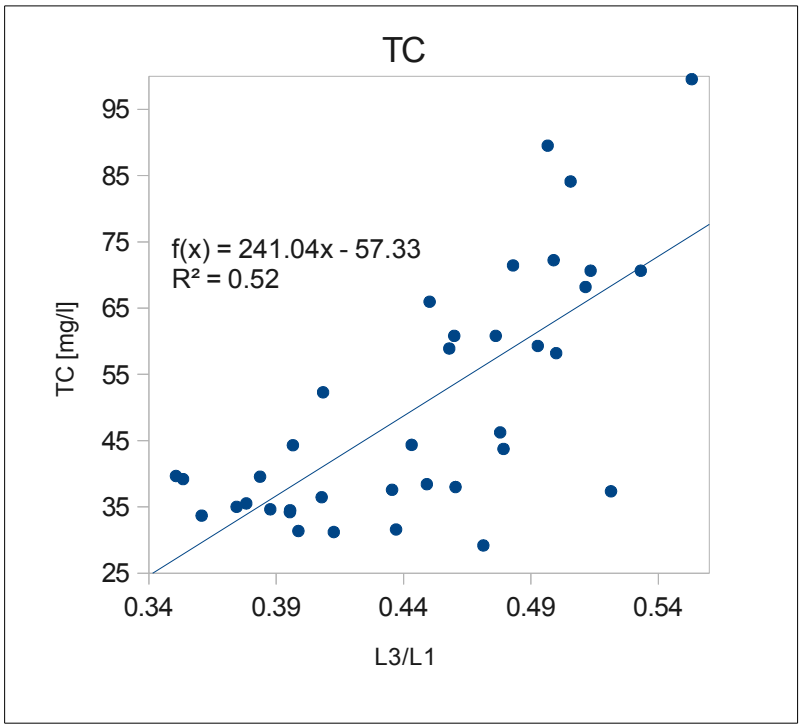

Figure 43: Band combination with the best fit based on TOAR

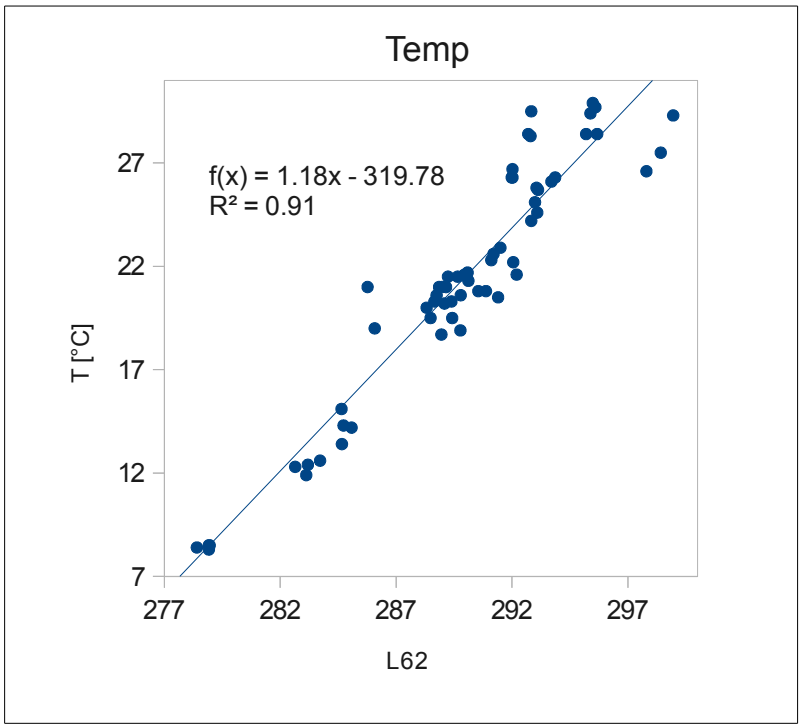

Figure 44: Band combination with the best fit based on TOAR

3.3 Atmospherically Corrected Data

All 121 sample points were considered based on atmospherically corrected images. The RGB band combination (1,6,6) [230] highlighted the issue of sampling points that were affected by clouds or in general atmospheric conditions. It was identified that some of the points were in cloud shade, gaps from SLC as well as those completely covered by cloud. In all 49 sampling points were identified and removed as seen in Table 9. There was general improvement in smoothed data as it limited the general effect of noise on the data. But there was no improvement and no substantial change was observed for TC and LogTOC parameters.

Table 9: Sampling points after removal of problematic points

(part1)

Date	Sample No	Water Body	Chl	TC [mg/l]	TOC [mg/l]	TN [mg/l]	T [°C]	Secchi [cm]
2011.09.15	1	Melice	2.2				20.2	
2011.09.15	2	Melice	2.2				20.3	
2011.09.15	3	Melice	1.5				20.6	
2011.09.15	4	Bunkov	71				19.7	
2011.09.15	5	Bunkov	65				19.5	
2011.09.15	8	Pohranovsky	6.7				20	
2011.09.15	9	Pohranovsky	5.2				20	
2011.09.26	1	Melice	4.4					
2011.09.26	2	Melice	0.2					
2011.09.26	5	Oplatil	2.2					
2011.09.26	8	Oplatil	2.2					
2012.05.29	1	Pohranovsky	17.4	58.2	18.07	0.18	22.6	110
2012.05.29	2	Pohranovsky	11.6	58.9	17.7	0.16	22.3	185
2012.05.29	3	Oplatil	3.6				21.5	480
2012.05.29	4	Oplatil	3.6				21	480
2012.05.29	5	Oplatil	2.2				21	400
2012.05.29	7	Oplatil	2.2				21	480
2012.09.16	2	Melice	3.2				21.2	
2012.09.16	3	Melice	3.2				21.3	
2012.09.16	4	Melice	2.5				21.6	
2012.09.16	5	Bunkov	72				20.7	

(part 2)

Date	Sample No	Water Body	Chl	TC [mg/l]	TOC [mg/l]	TN [mg/l]	T [°C]	Secchi [cm]
2012.07.31 to 01.08	1	Spravcicky	2.9					
2012.07.31 to 01.08	2	Spravcicky	3.6					
2012.07.31 to 01.08	3	Spravcicky	3.6					
2012.07.31 to 01.08	4	Pohranovsky	4.8				29.5	42.5
2012.07.31 to 01.08	5	Pohranovsky	9.7				28.4	44.5
2012.07.31 to 01.08	6	Oplatil	0.7				26.3	201
2012.07.31 to 01.08	7	Oplatil	1.5				26.3	194
2012.07.31 to 01.08	8	Oplatil	1.5				26.7	228
2012.09.11	1	Pohranovsky	28	89.52	32.92	0.19	21.6	15
2012.09.11	2	Pohranovsky	3				22.2	25
2012.09.11	3	Oplatil	4.3	31.2	6.15	0.1	22.9	220
2012.09.18	1	Pohranovsky	26	84.11	30.63	0.13	19.5	24
2012.09.18	2	Pohranovsky	24.5				20.3	25.5
2012.09.18	4	Oplatil	14.6				21.6	210
2012.09.18	5	Bunkov	68.9	37.35		0.15	21.3	29
2012.09.18	6	Bunkov	7.3				21.7	33
2012.11.14	3	Oplatil	7.3		6.09		8.3	
2012.11.14	4	Jezero	7.3		4.16		8.4	514
2012.11.14	5	Jezero	3.6		4.4		8.5	635
2012.11.14	6	Jezero	2.2		4.79		8.5	614
2013.05.09	1	Jezero	0.4	35.01	7.06	0.33	18.9	530
2013.05.09	2	Jezero	0.4	33.68	6	0.31	18.7	620
2013.05.09	6	Melice	0.7	31.36	7.41	0.43	20.6	324
2013.05.09	7	Pohranovsky	17.3		18.39	1.52	21.5	
2013.05.09	8	Pohranovsky	20.9	59.29	18.59	1.3	20.5	54
2013.05.09	9	Pohranovsky	15.3	60.81	19.09	1.68	20.8	52
2013.05.09	10	Pohranovsky	17.4	60.81	19.09	1.68	20.8	52

(part 3)

Date	Sample No	Water Body	Chl	TC [mg/l]	TOC [mg/l]	TN [mg/l]	T [°C]	Secchi [cm]
2013.06.19	1	Placicky	3.4	44.3	15.75	1.02	25.8	190
2013.06.19	2	Placicky	2.8	39.56	11.51	1	25.7	218
2013.06.19	3	Opatovicky	0.2	39.66	7.7	0.38	25.1	363
2013.06.19	4	Opatovicky	1.8	39.19	8.91	0.36	28.3	364
2013.06.19	5	Ujezdsky	29.6	68.19	31.66	2.02	28.4	26
2013.06.19	6	Ujezdsky	47.2	70.65	32.2	2.16	28.4	29
2013.06.19	7	Bohumilecky	65.7	70.65	34.2	3.19	29.7	19
2013.06.19	8	Bohumilecky	58.6	71.44	34.72	2.65	29.4	23
2013.06.19	9	Bohumilecky	59	72.23	34.85	2.69	29.9	21
2013.07.29	1	Placicky	4.74	29.18	10.16	0.64	27.5	166
2013.07.29	4	Opatovicky	0.5	36.46	5.69	0.36	26.6	479
2013.07.29	5	Oplatil	1.5	29.95	6.45	0.46	27.2	
2013.07.29	7	Pohranovsky	49.5	95.83	39.96	2.86	29.4	22
2013.07.29	8	Pohranovsky	39.7	99.55		3.52	29.3	30
2014.05.21	3	Melice	1.5	31.59	9.2	0.66	19	275
2014.05.21	8	Pohranovsky	4.4	52.29	14.04	1.15	21	170
2015.04.21	1	Pohranovsky	12.9	43.75	13.04	1.21	14.3	80
2015.04.21	2	Pohranovsky	9.6	46.24	15.51	1.39	14.2	66
2015.04.21	3	Oplatil	8.9	38.42	7.91	0.8	11.9	117
2015.04.21	4	Oplatil	9.2	38	7.41	0.78	12.3	114
2015.04.21	5	Oplatil	11.1	37.58	7.08	0.84	12.4	127
2015.04.21	6	Bunkov	35.6	44.36	15.45	1.57	15.1	227
2015.04.21	7	Melice	7	34.63	9.36	0.66	13.4	255
2015.04.21	8	Melice	5.1	34.49	8.96	0.64	12.6	255

Figure 45: water only mask showing the southern part of the research area

Water only mask (Figure 45) was used to mask out all the non-water areas specifically in the area of study before smoothing process. The atmospherically corrected image values were smoothed using the 3×3 averaging window. Statistically this improved the values of r^2. Only considered r^2 where values of $r^2 > 0.4$. Without the smoothing of atmospherically corrected values, r^2 values for $r^2 > 0.4$ vis a vis all measured water quality parameters were less. Smoothing generally improved correlation between the measured water quality and the atmospherically corrected data values, thus only results from smoothed imagery are presented here.

Table 1: Change in r^2 due to atmospherically corrected data.

Parameter	**Toar** r^2	**Atcorr** r^2
Chl-a	0.47	0.55
LogChl-a	0.51	0.71
TC	0.52	0.44
LogTC	0.51	0.48
TOC	0.61	0.6
LogTOC	0.65	0.66
T	0.91	
LogT	0.9	
SDD	0.62	0.75
LogSDD	0.79	0.84

Atmospheric correction generally improved the correlations, but there was no improvement for TC and LogTOC parameters in linear r^2 (Table 1).

Model Creation and Verification

Although based on the literature reviewed, it came out that correlation should be expected only with the visible bands and with thermal bands for temperature, all available Landsat ETM+ bands were considered. These are blue (band1), green (band2), red (band3), near-infrared (band4), short-wave infra-red 1 (band5) and thermal infra-red (band6), short-wave infra-red 2 (band7) of Landsat ETM+ gave the necessary range for which we could rely on to create the various models for the water quality parameters being analysed. Band 6 was used for temperature models whereas the rest was considered for all the other water quality

parameters. In all 44 models were created for all the water quality parameters that were analysed. All the models were developed using atmospherically corrected and smoothed data turned into units of reflectance. The model for temperature was developed based on smoothed TOA brightness temperature values in Kelvin [28] as current atmospherically corrected imagery for Landsat ETM+ does not contain thermal bands.

Table 11: Bands used in model creation and their r^2 values based on linear function

Parameter	**Bands**	r^2	**Parameter**	**Bands**	r^2
Chl-a	L2/L1	0.51	T	L61	0.9
Chl-a	L3/L1	0.52	T	L62	0.91
LogChl-a	L3	0.5	LogT	L61	0.82
LogChl-a	L1/L3	0.66	LogT	L62	0.83
LogChl-a	L2/L1	0.45	SDD	L3	0.49
LogChl-a	L3/L1	0.66	SDD	L1/L2	0.66
LogChl-a	L3/L2	0.47	SDD	L1/L3	0.75
TC	L3/L1	0.44	SDD	L2/L1	0.64
LogTC	L3/L1	0.48	SDD	L3/L1	0.7
TOC	L1/L3	0.41	SDD	L3/L2	0.41
TOC	L2/L1	0.53	LogSDD	L3	0.64
TOC	L3/L1	0.5	LogSDD	L1/L2	0.59
TOC	L4/L1	0.42	LogSDD	L1/L3	0.72
LogTOC	L2	0.45	LogSDD	L2/L1	0.69
LogTOC	L3	0.42	LogSDD	L2/L3	0.41
LogTOC	L1/L2	0.55	LogSDD	L3/L1	0.84
LogTOC	L1/L3	0.52	LogSDD	L3/L5	0.45
LogTOC	L1/L4	0.42			
LogTOC	L2/L1	0.64			
LogTOC	L3/L1	0.66			

Models were developed based on not only linear functions but also exponential, power and logarithmic functions. In most of the cases we realised the linear functions worked better as basis for developing the models (see appendix 6.1). Out of the 44 models created 37 (Table 11) of them were based on liner functions and the rest being exponential, power and logarithmic. The model charts with the best fits were chosen to develop the models and model performance charts created (figures 46 to 57). The red line in model performance charts is ideal model line, where estimated and measured values would be equal.

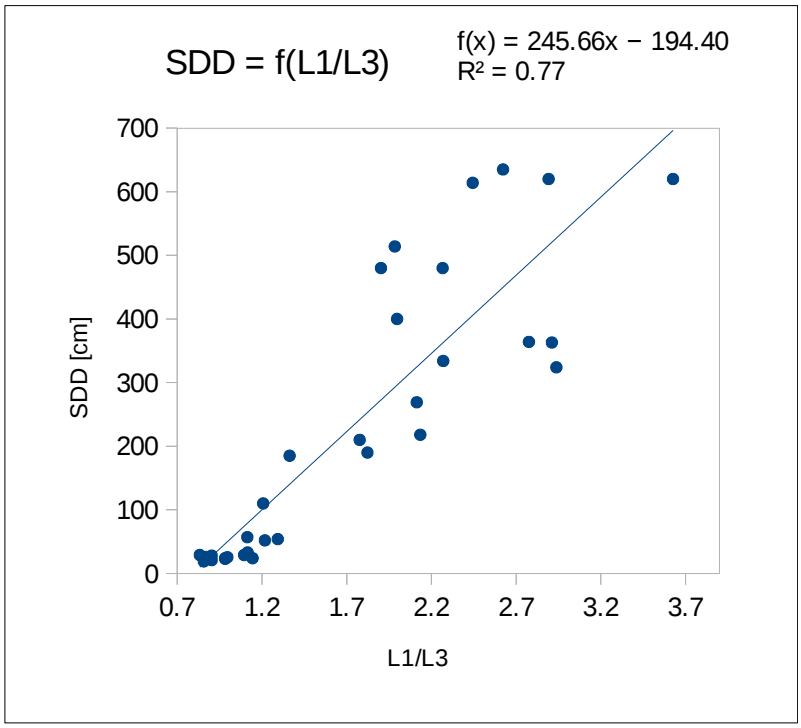

Figure 46: Model fit for SDD

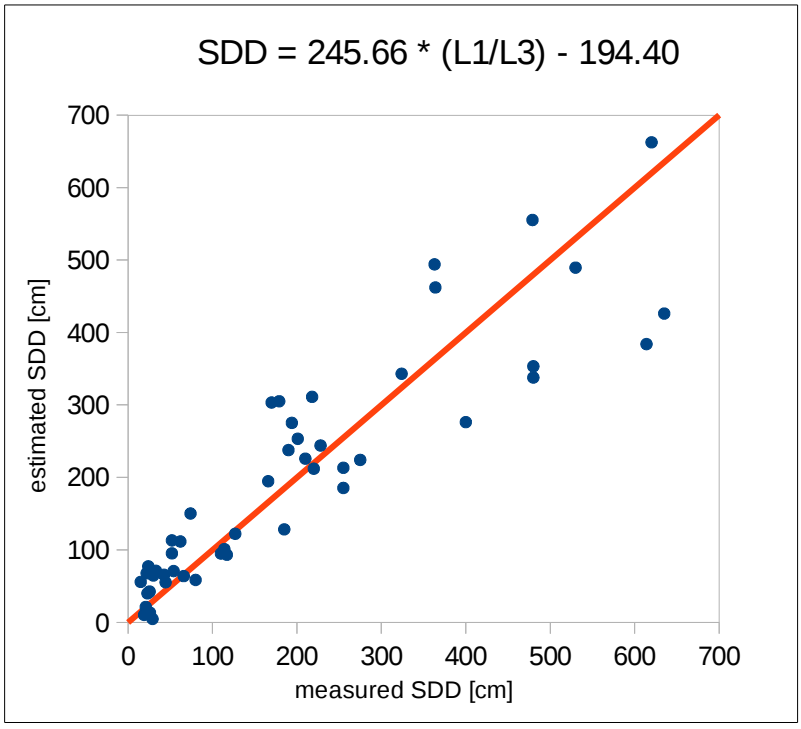

Figure 47: Scatter plot for Model Performance of SDD

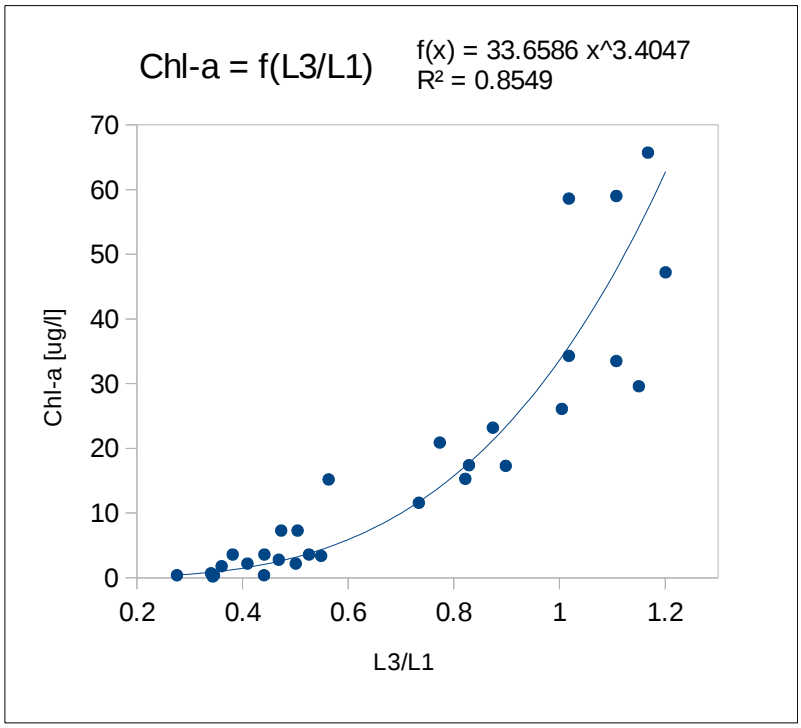

Figure 48: Model fit for Chl-a

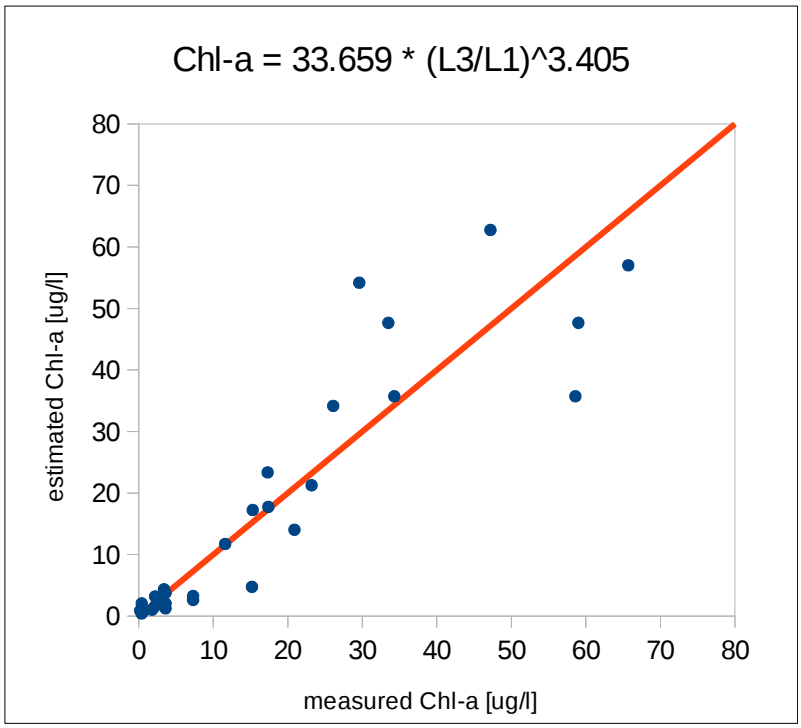

Figure 49: Scatter plot for Model performance of Chl-a

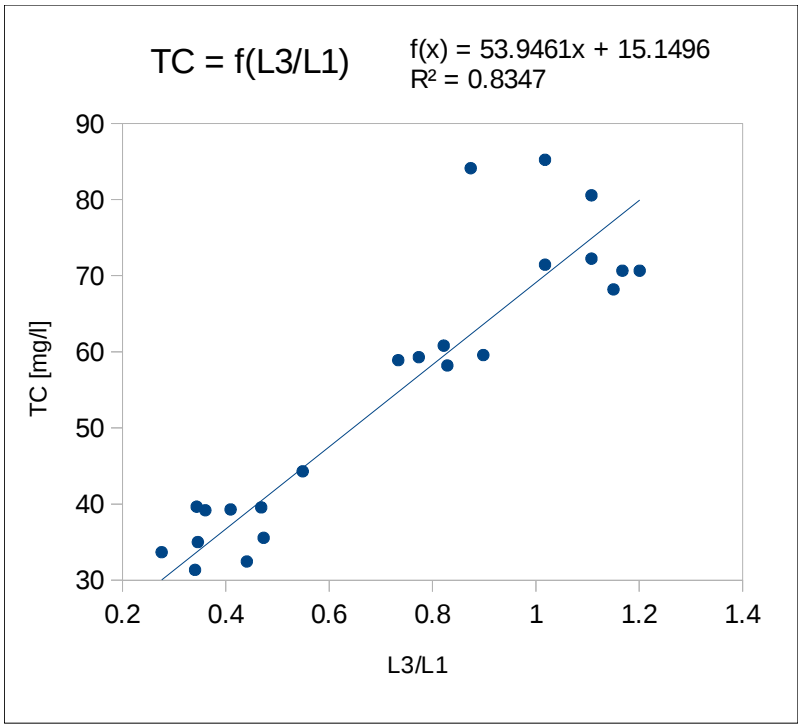

Figure 50: Model fit for TC

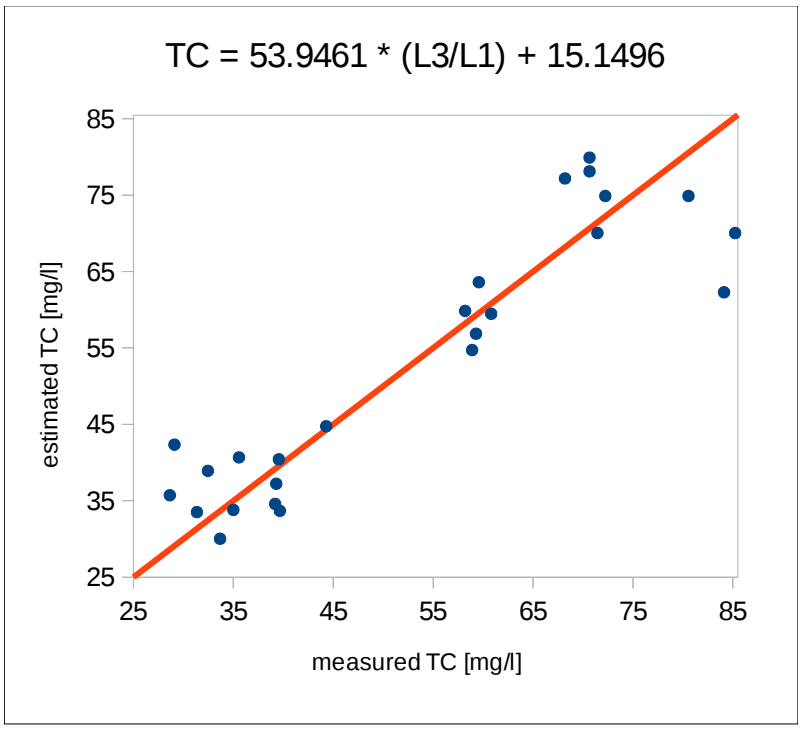

Figure 51: Scatter plot for Model performance of TC

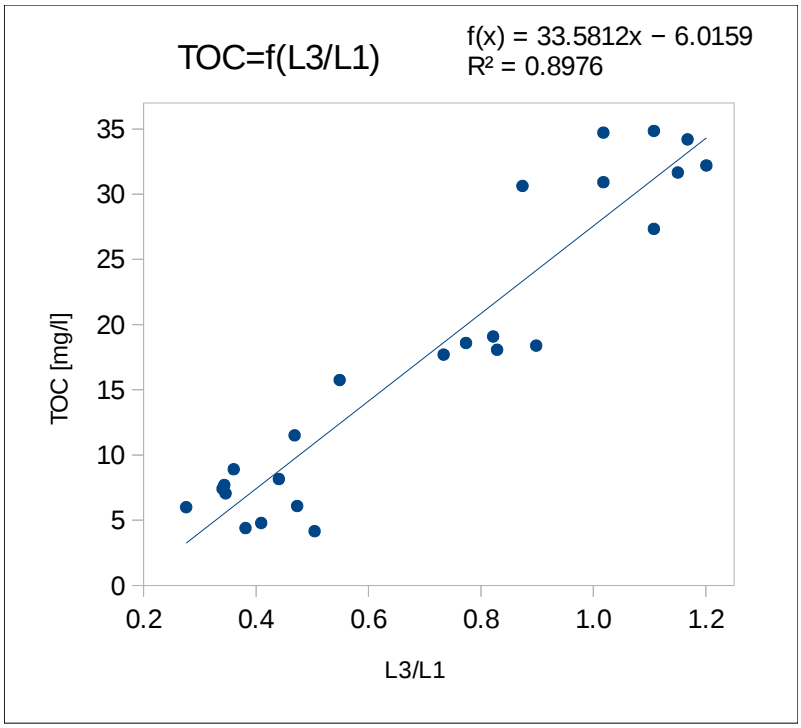

Figure 52: Model fit for TOC

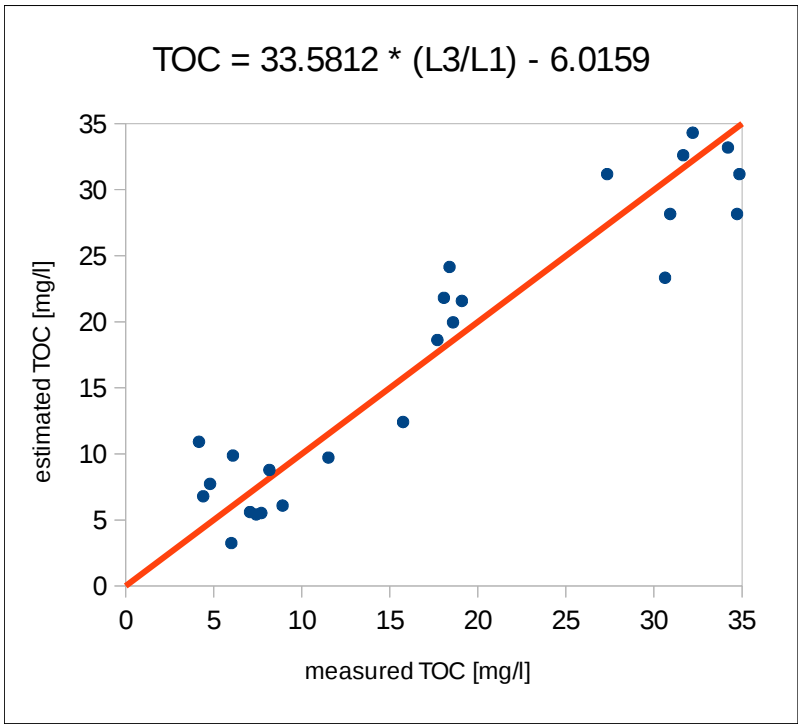

Figure 53: Scatter plot for Model performance of TOC

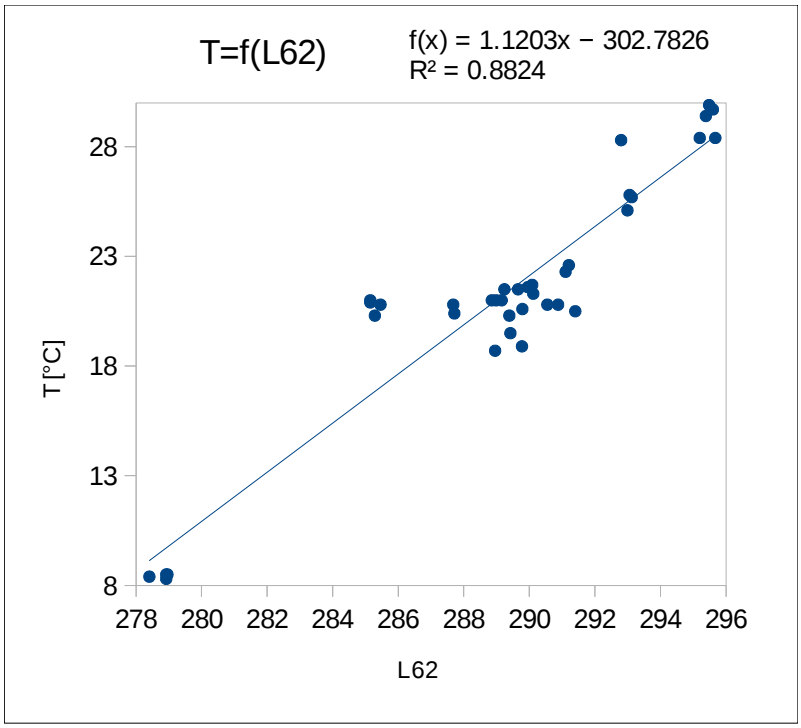

Figure 54: Model fit for T

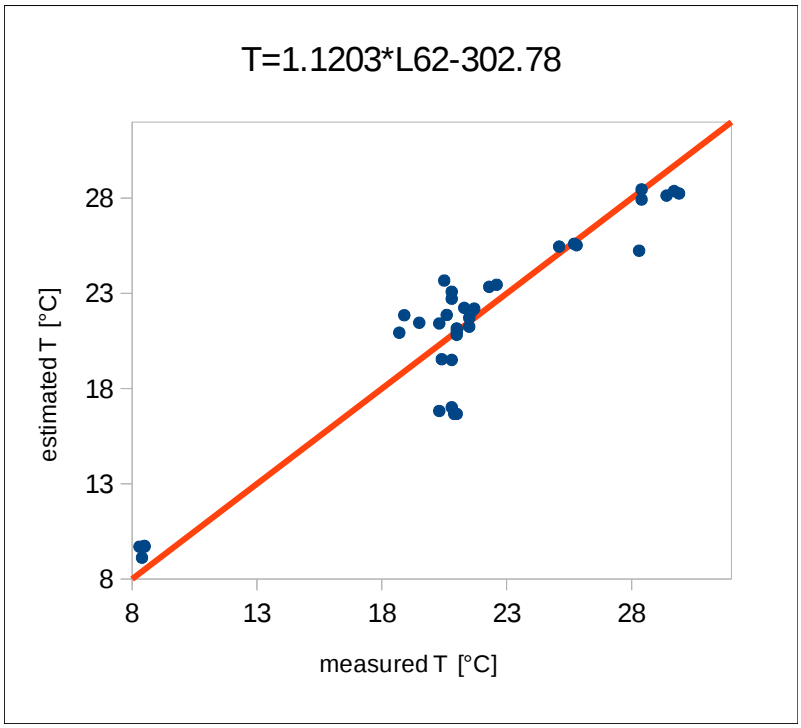

Figure 55: Scatter plot for Model performance of T

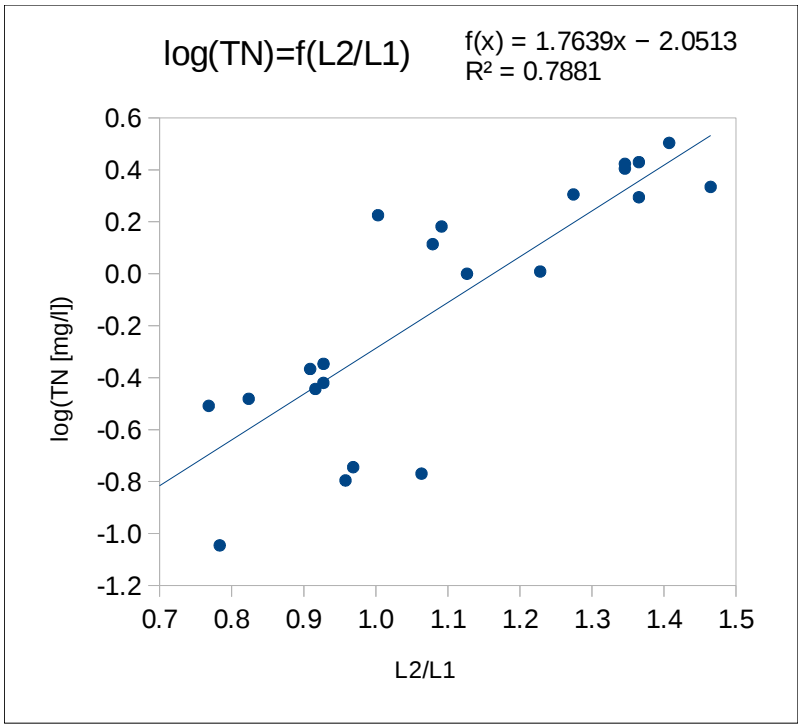

Figure 56: Model fit for TN

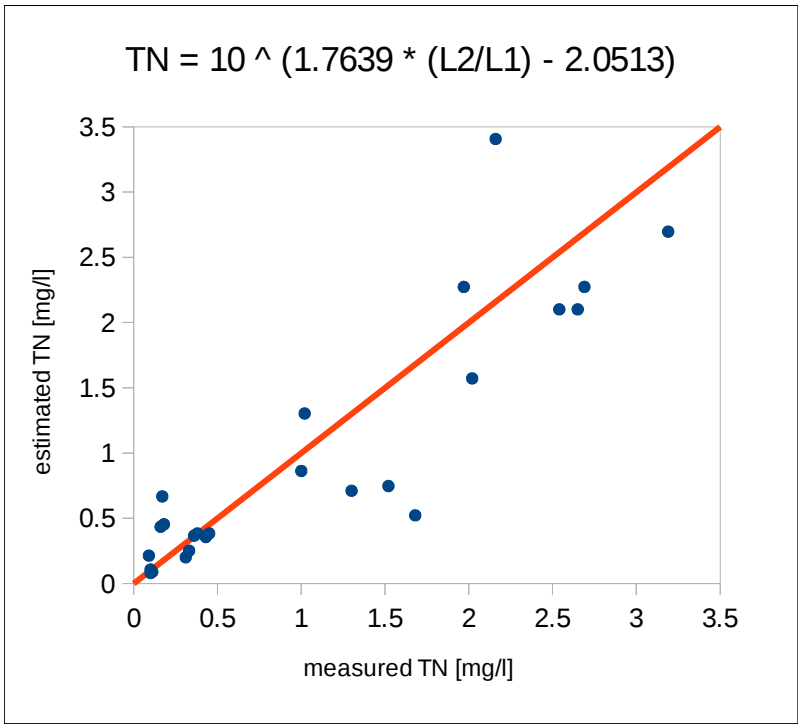

Figure 57: Scatter plot for Model performance of TN

The models developed from model charts showed varied correlations between the measured values vis a vis the estimated values based on the models for validation purposes. The model performances based on scatter plots from which the r^2, RMSE, NRMSE of the created models were measured and a summary of the models of each water quality parameter is seen in Table 12. Figure 47 shows the model fit on which the model for SDD was developed showing fit r^2 value of 0.77. Figure 49 shows the model fit for Chl-a showing a r^2 value of 0.82 and Figure 48 the performance chart of the model. Figure 50 illustrates model fit for TC with r^2 value of 0.83 and Figure 51 shows the model performance. TOC model fit is illustrated in Figure 52 showing r^2 value of 0.87 and Figure 53 shows the model performance chart. Figure 54 shows the model fit for T indicating r^2 value of 0.91 followed by the performance chart of the model (Figure 55). Based on model performance, model maps were built for the two best performing models of each parameter for each of the water quality parameter. The models were developed based on individual water quality parameters (variables) similarly as done by Olmanson et al [235], Hellweger et al [126] and Wu et al [236]. See appendix 6.3 for further performance charts for the models developed.

Table 12: Best Models developed based on water quality parameters

Parameter	Models	r2	RMSE	NRMSE	Range(min,max)	n
SDD [cm]	245.7(L1/L3)-194.4	0.77	102	0.17	19-635	32
SDD [cm]	10^(-1.819(L3/L1)+3.347)	0.77	105	0.17	19-635	32
Chl-a [ug/l]	33.66*(L3/L1)^3.405	0.82	8.4	0.13	0.2-65.7	30
Chl-a [ug/l]	10^(-0.8330(L1/L3)+2.331)	0.82	8.5	0.13	0.2-65.7	30
TC [mg/l]	53.946*(L3/L1)+15.150	0.83	7.5	0.13	29.1- 85.2	25
TC [mg/l]	10^(-0.1640*(L1/L3)+1.988)	0.81	8.1	0.14	29.1- 85.2	25
TOC [mg/l]	33.58*(L3/L1)-6.0159	0.9	3.5	0.12	4.2-34.8	25
TOC [mg/l]	10^(0.9279*(L3/L1)+0.4906)	0.87	4.2	0.14	4.2-34.8	25
TN [mg/l]	10^(1.764*(L2/L1)-2.051)	0.78	0.47	0.15	0.09-3.19	25
TN [mg/l]	3.257*(L2/L1)-2.294	0.75	0.49	0.16	0.09-3.19	25
TEMP [°C]	0.0154*(L62/L1)-27.05	0.9	1.7	0.08	8.3-29.9	36
TEMP [°C]	1.1203*L62-302.78	0.88	1.9	0.09	8.3-29.9	36

The best two models for each water quality parameter with highest correlation as well as good RMSE and NRMSE were used in creating the model maps (Figure 56 to Figure 65). From

Table 12, all the best correlations are based on visible bands 1,2,3 as espoused in the reviewed literature. Models with the best r^2 fit, RMSE and NRMSE are summarised in Table 12.

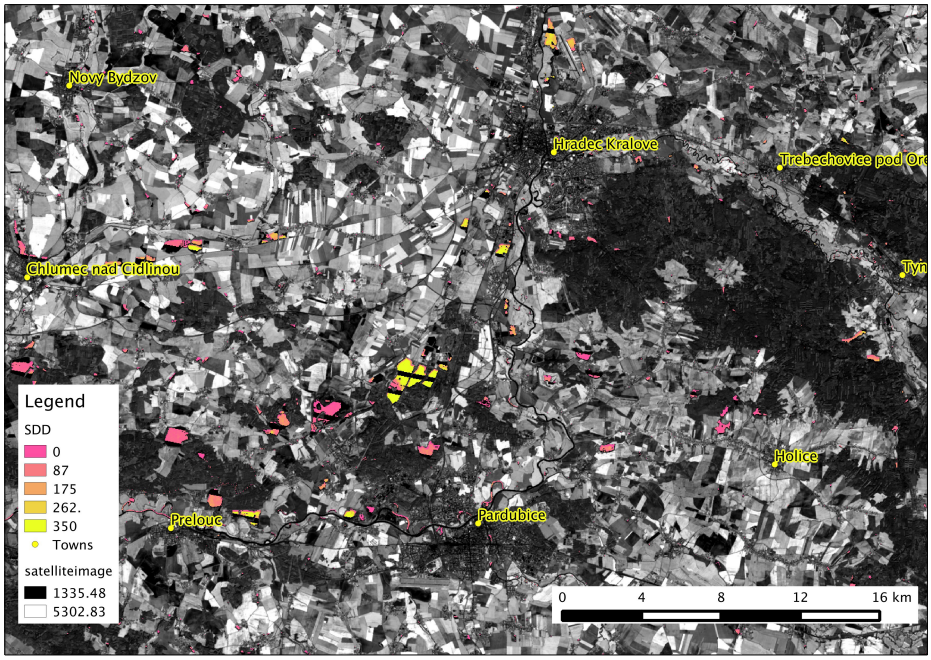

*Figure 56: Model (245.7*L1/L3-194.4) map of SDD levels for 2013.05.09.*

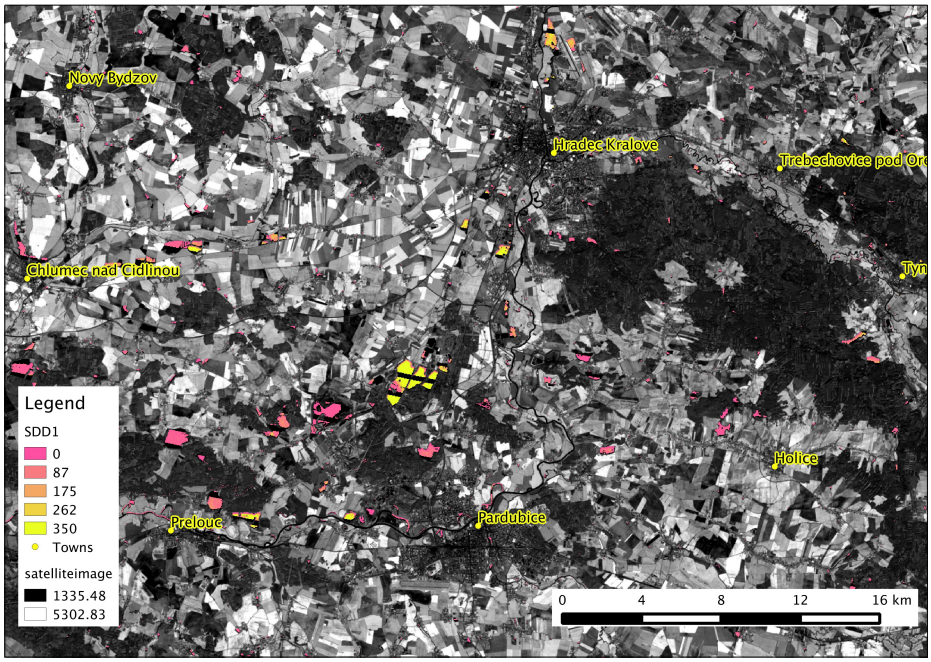

Figure 57: Model 10^(-1.819(L3/L1)+3.347) map of SDD levels for 2013.05.09

The model maps show the various levels of water quality parameters (SDD, Chl-a, TC, TOC, TEMP) on some of the water bodies sampled as well as those that were not sampled. They are depicting the levels for these water quality parameters for the date 2013.05.09 (figures 56, 57). The maps depicts the spatial distribution of the concentrations of the water quality parameters in relation to the area the map covers.

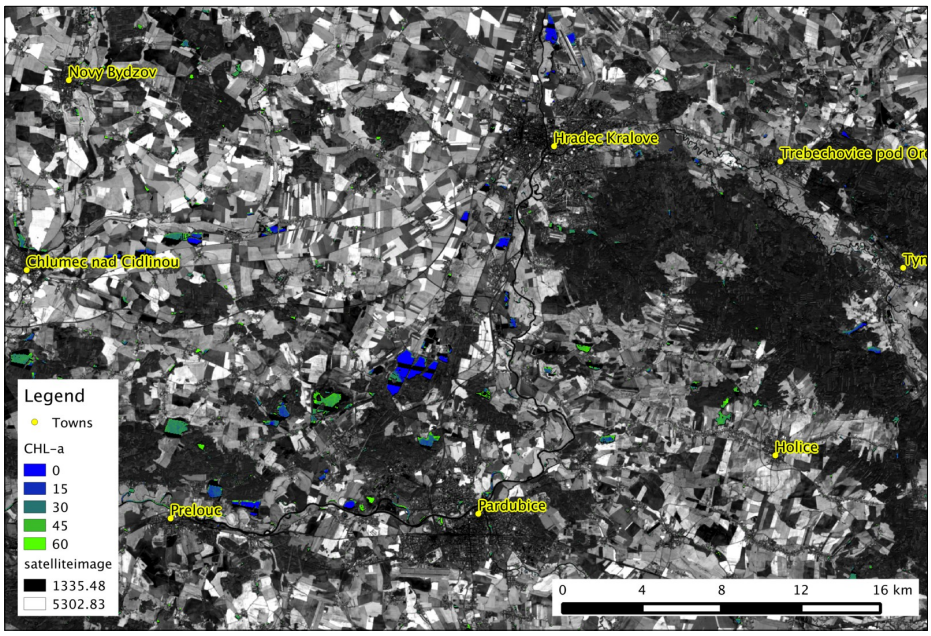

Figure 58: Model 33.66(L3/L1)^3.405 map showing the levels of Chl-a for 2013.05.09*

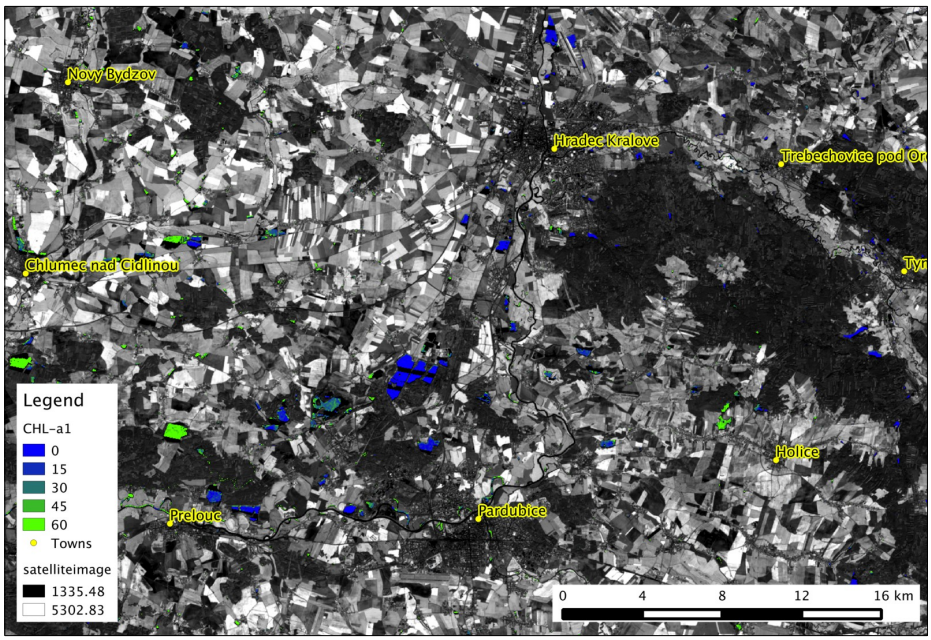

*Figure 59: Model (10^(-0.8330*L1/L3)+2.331) map showing the levels of Chl-a for 2013.05.09*

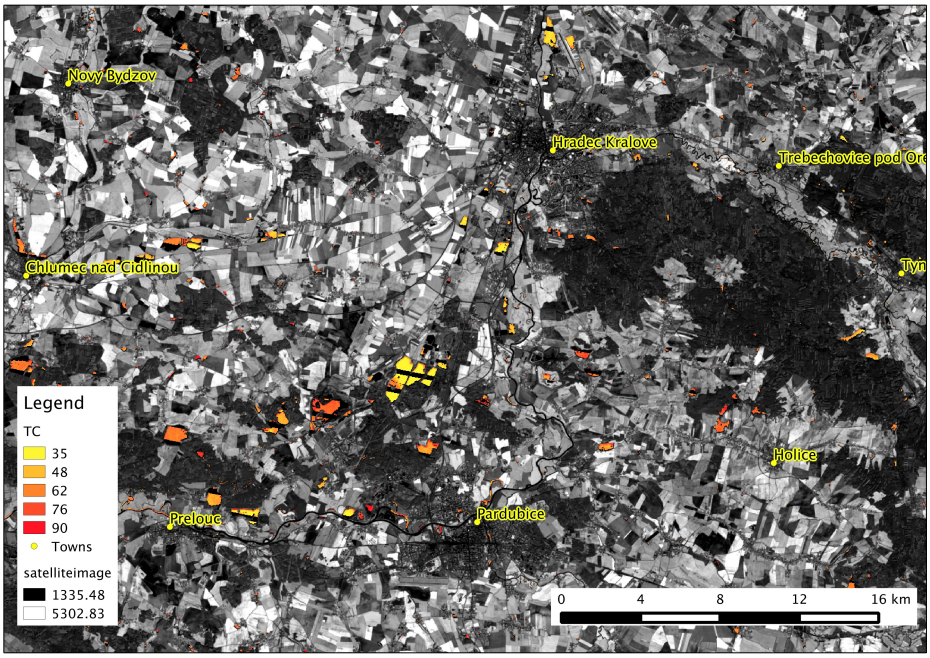

Figure 60: Model (53.946(L3/L1)+15.150) map showing the levels of TC for 2013.05.09*

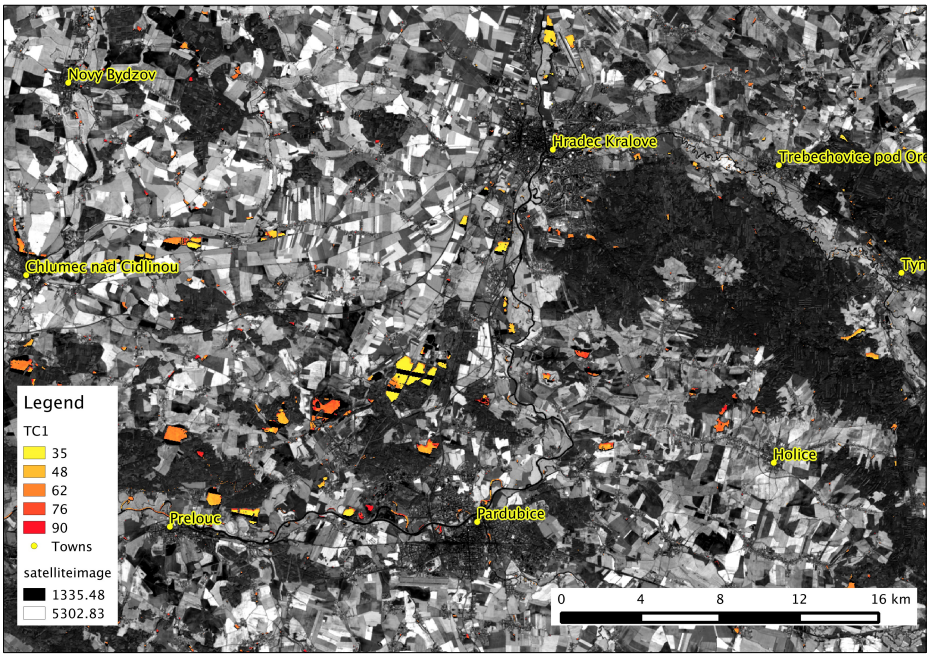

Figure 61: Model (10^(-0.1640(L1/L3)+1.988)) map showing the levels of TC for 2013.05.09*

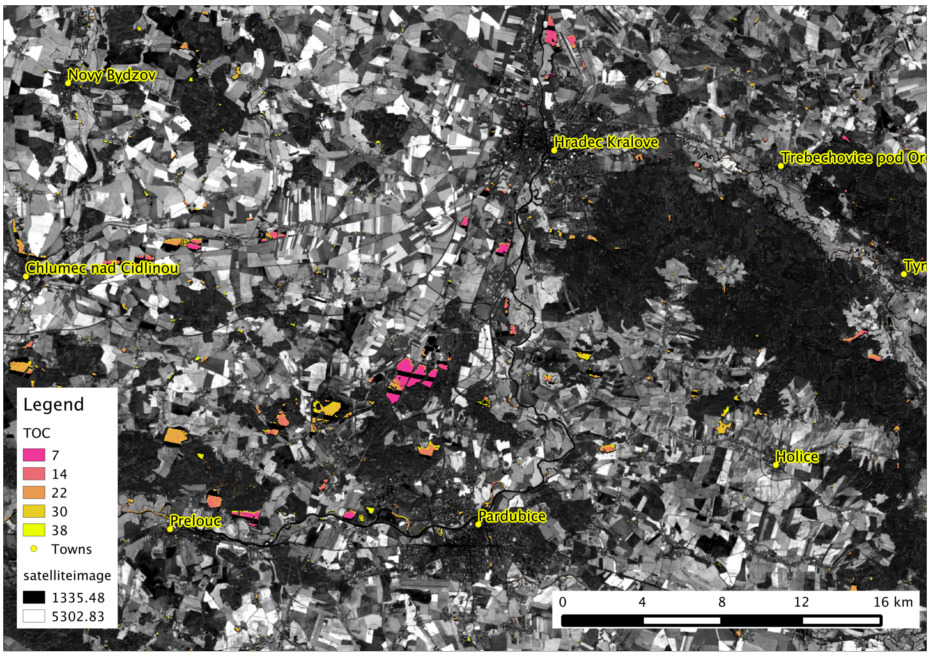

Figure 62: Model (33.58(L3/L1)-6.0159) map showing the levels of TOC for 2013.05.09*

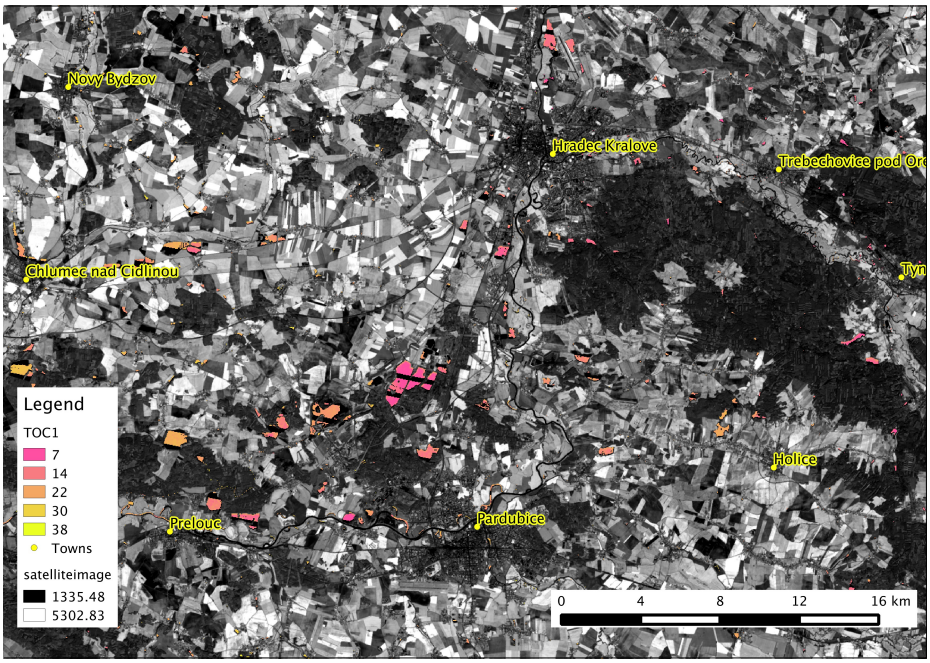

Figure 63:Model (10^(0.9279(L3/L1)+0.4906)) map showing the levels of TOC for 2013.05.09*

Chl-a (Figure 58, 59), can be an indicator of the level of phytoplankton development as collaborated by Baborowski et al [237]. The blue areas of the water bodies represent low levels of Chl-a 0-15 ug/l (Figure 58, 59). Dark green portions show averagely high levels of Chl-a (30-45 ug/l), with the light green parts showing portions with high levels of Chl-a (60 ug/l and more). TC showed a range of levels from 35 mg/l to 90 mg/l. The yellow through to orange areas have low TC levels (35-48 mg/l), mid-levels from 62 to 76 mg/l (Figure 60, 61). The red (77-90 mg/l) depicts areas of the water bodies with relatively high levels of TC. TOC which encompasses the total amount of organic carbon, shows a range based of the models maps 7mg/l to 38 mg/l. 7 to 14 mg/l (Figure 62, 63) shows low levels of TOC in the water bodies, 22 to 30 mg/l shows mid levels of TOC and 30 to 38 mg/l shows high levels of TOC based of the models for TOC.

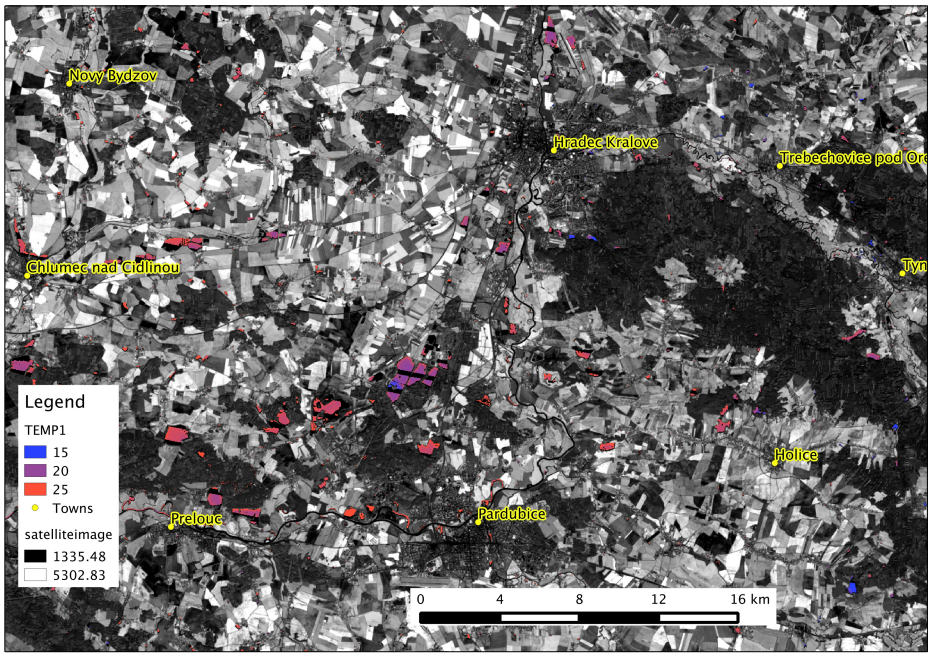

Figure 64: Model (0.0154(L62/L1)-27.05) map showing the levels of temperature for 2013.05.09*

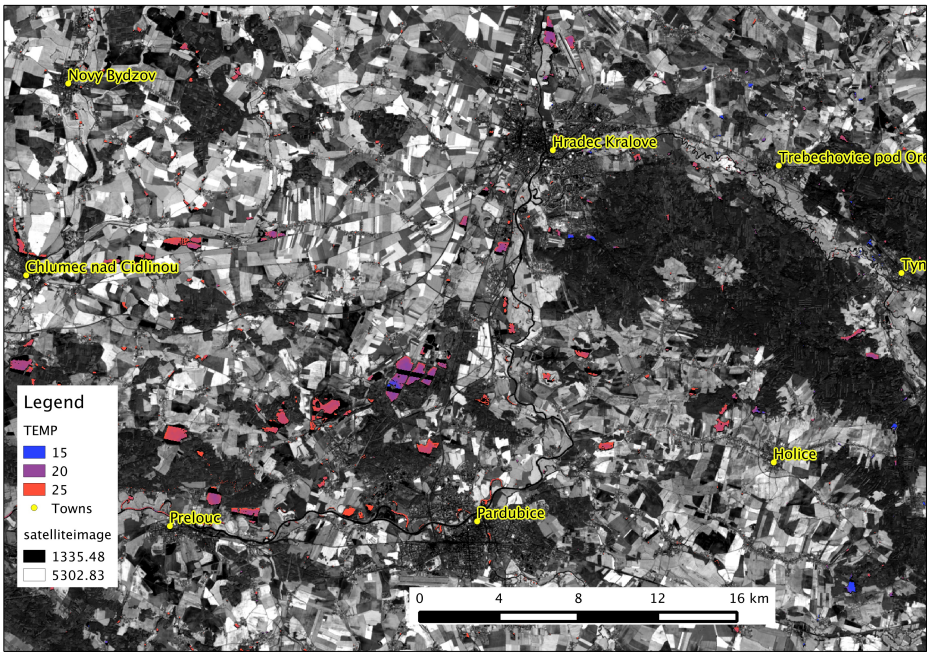

*Figure 65: Model (1.1203*L62-302.78) map showing the levels of Temperature for 2013.05.09*

The model maps for temperature depicts a range of 15 to 25 °C (Figure 64, Figure 65).

It is quite evident based on the model maps that in all cases the second best model performs similarly to the best one, although checking for the performance, r^2, RSME and NRSME may vary. It was realised that in some instances though a model's r^2 value value might be high the RSME and NRMSE, and especially performance chart shape can give a greater picture.

3.5 Validation of Models

There is always the need to verify the actual performances of developed models on independent data set. Some of the sampled data were retained as earlier mentioned for this particular process. The samples were collected on the 02.07 and 10.08 of 2015. In all 12 samples were taken for the validation, but two had to be removed due to clouds. The satellite data were smoothed and processed in the same way as in model creation. Validation of the models were based on the performance charts and the r^2 , RMSE and NRMSE values. This enabled the measurement of validity of the models created. Figure 66 shows the validation for

SDD taking into measured values for SDD and that of the estimated values based of the developed model. The model performance for Chl-a is shown in figure 67 plotting measured Chl-a values against estimated values based on the model developed for Chl-a. Figures 68, 69 and 70 and 71 show the validation for models of TC, TOC, TEMP and TN respectively. It is worth noting that most of the clear images were used for the model creation. Because of this not that many images usable were available for the model validation that is how come we have less sample space.

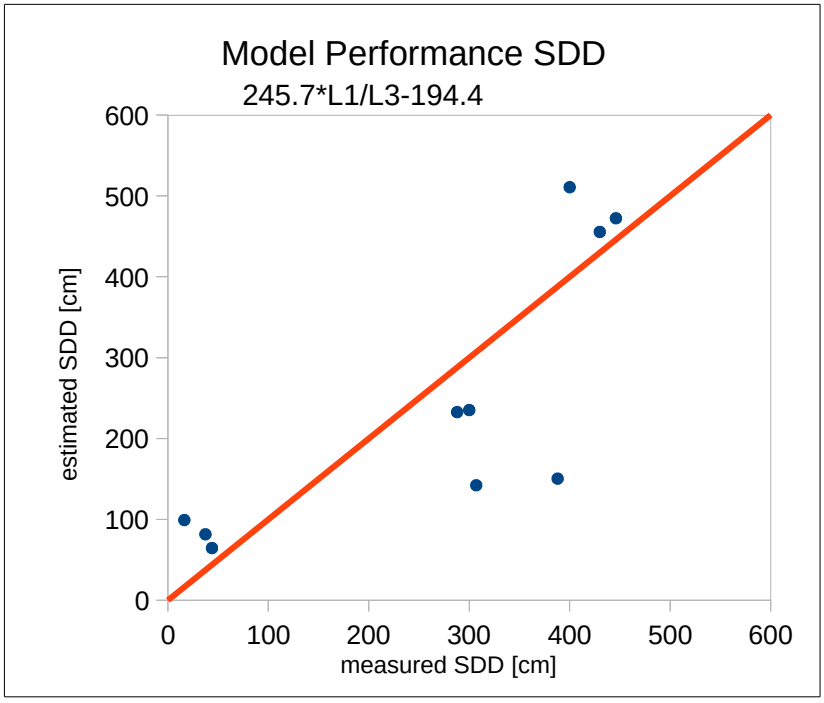

Figure 66: Model performance for SDD

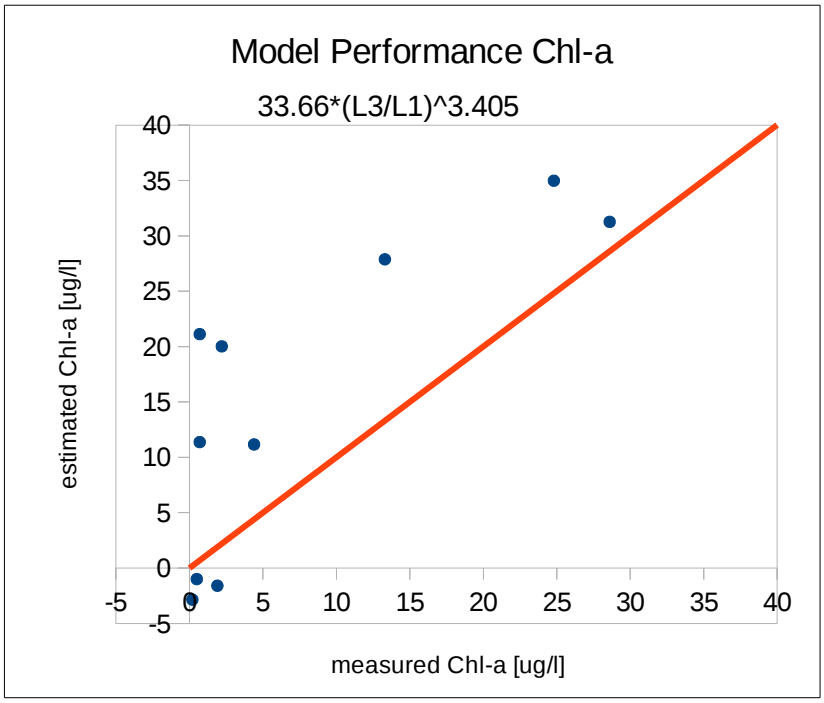

Figure 67: Model performance for Chl-a

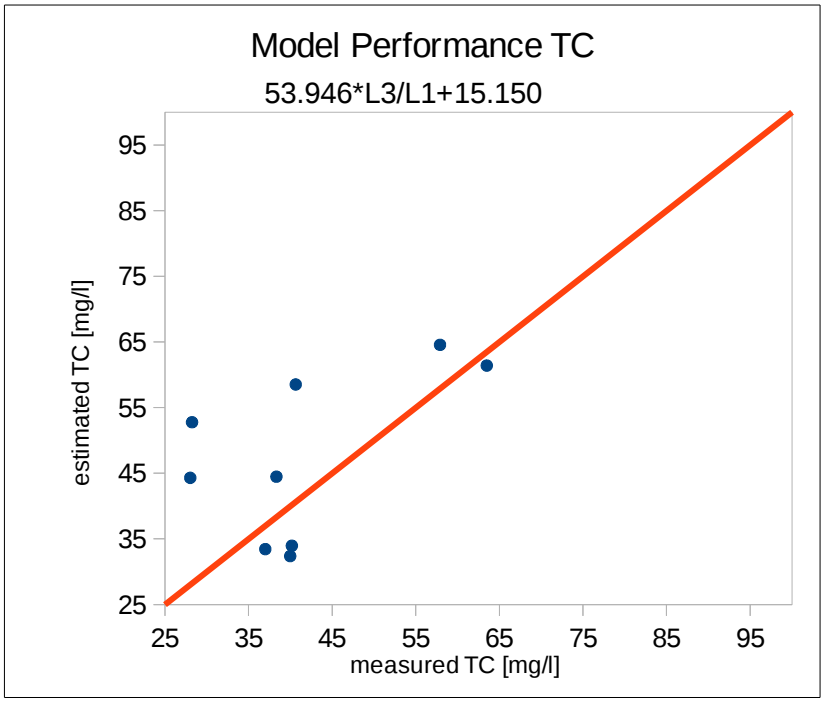

Figure 68: Model performance for TC

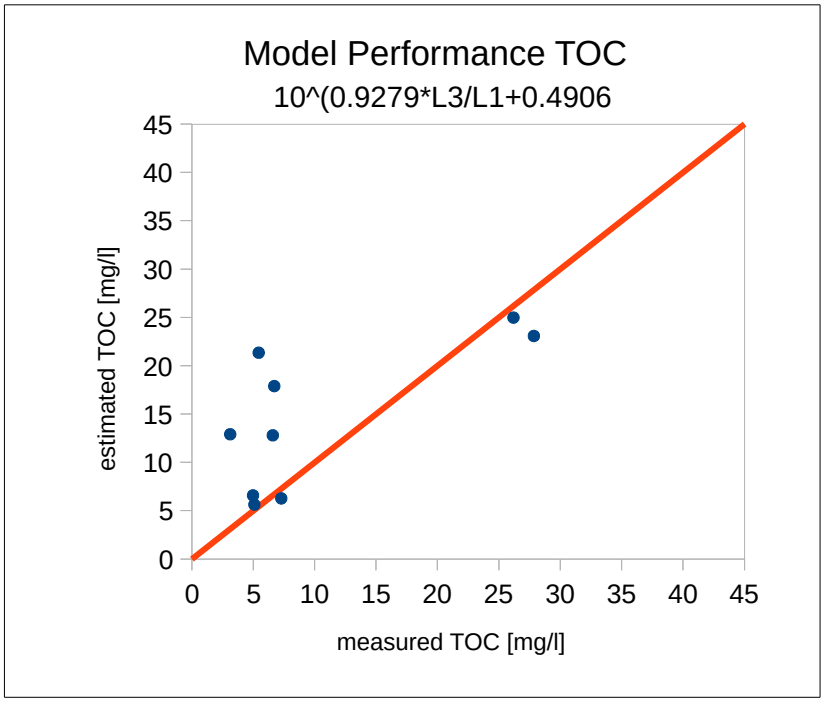

Figure 69: Model performance for TOC

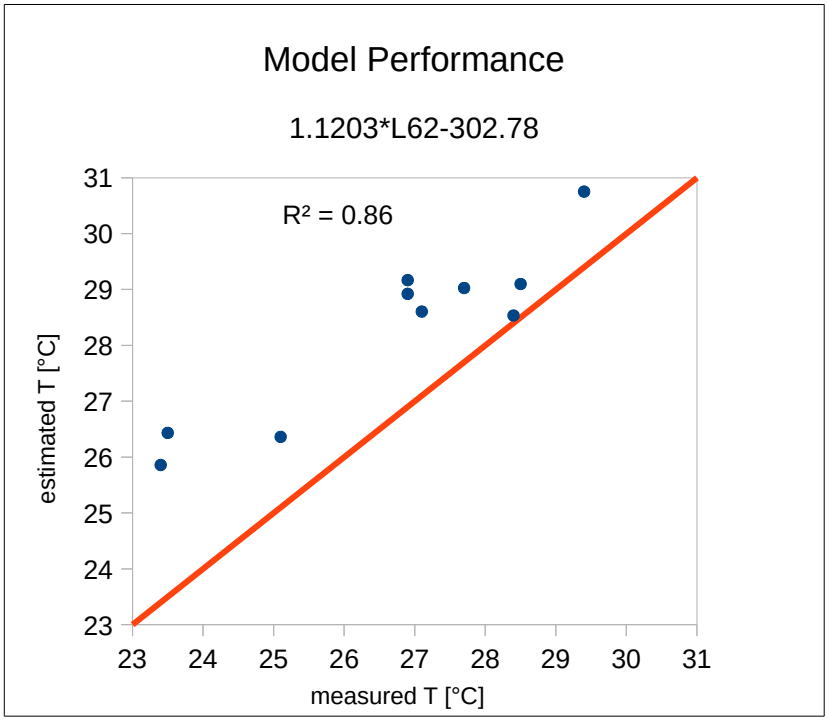

Figure 70: Model performance for Temp.

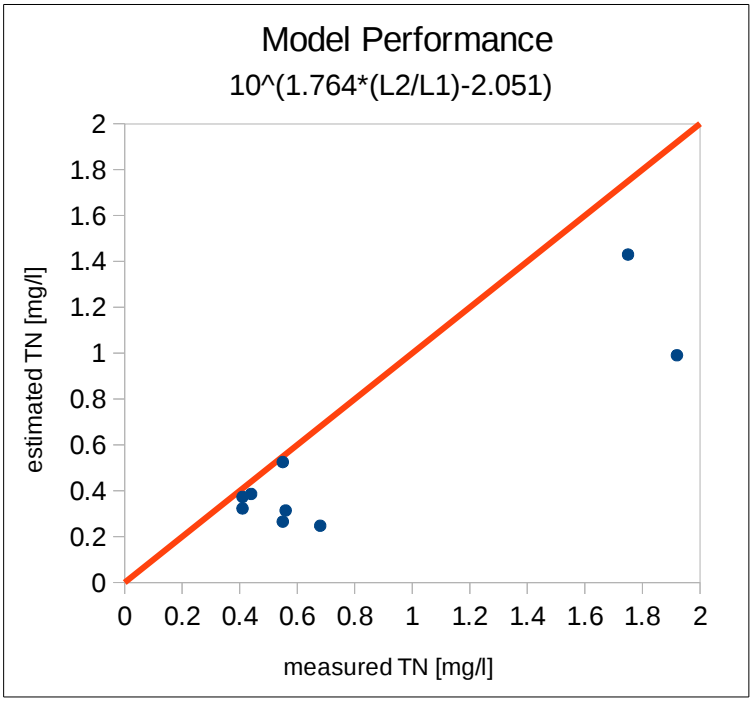

Figure 1: Model Performance for TN

The root mean square root error (RMSE) and normalised root mean square error (NRMSE) were calculated. The performance indicators are summarised in table table 13.

Table 13: Validation of models developed for water quality parameters

Parameter	Models	r^2	RMSE	NRMSE	n
SDD[cm]	245.7(L1/L3)-194.4	0.78	109.56	0.25	10
CHL-a[ug/l]	33.66*L3/L1^3.405	0.83	6.43	0.23	10
TC[mg/l]	53.946*(L3/L1)+15.150	0.3	14.35	0.45	10
TOC[mg/l]	10^(0.9279*(L3/L1)+0.4906	0.61	6.76	0.28	10
TN[mg/l]	10^(1.764*L2/L1-2.051)	0.81	0.38	0.27	10
TEMP[°C]	1.1203*L62-302.78	0.89	1.78	0.28	10

Comparing the models and the validations results based on tables 12 and 13, the margins between the performance figures of the models and the that of the validation are much as these differences were expected. However r^2 , NRMSE values for TC were unusually low as model value was 0.83 (table 12) and 0.13 whereas that of the model validation was 0.3 (table 13) which failed to yield a positive result, as both models with the best fit were tested but both failed to give a good validation. TOC had r^2, NRMSE values of 0.9, 0.12 (table 12), for the model validation r^2 0.61 and 0.28 (table 13) for the model validation. SDD had 0.77 and 0.17 (table 12) r^2 value for the model whereas 0.78 and 0.25 respectively (table 13) was recorded for model validation. In the case of Chl-a, the best r^2, NRMSE values were 0.82 and 0.13 (table 12) and r^2, NRMSE values for the model validation was 0.83, 8.35 (table 13) respectively. For temperature model r^2, NRMSE values was, 0.9 and 0.08 (12) and that of the model validation were 0.89 and 0.28 (table 13). It is worth noting that the model with the best fit for temperature failed to give a good validation but rather the second best did. For TN the best r^2, NRMSE values were 0.78 and 0.15 (table 12) and r^2, NRMSE values for the model validation was 0.81, 0.28 (table 13). Further validation is needed for these models in future research as more points are needed to further test them.

3.6 Application of Chl-a Model example

The models created were applied to surface water within the areas that the research covered to evaluate their application. The various seasons of the year were considered with the exception of winter.

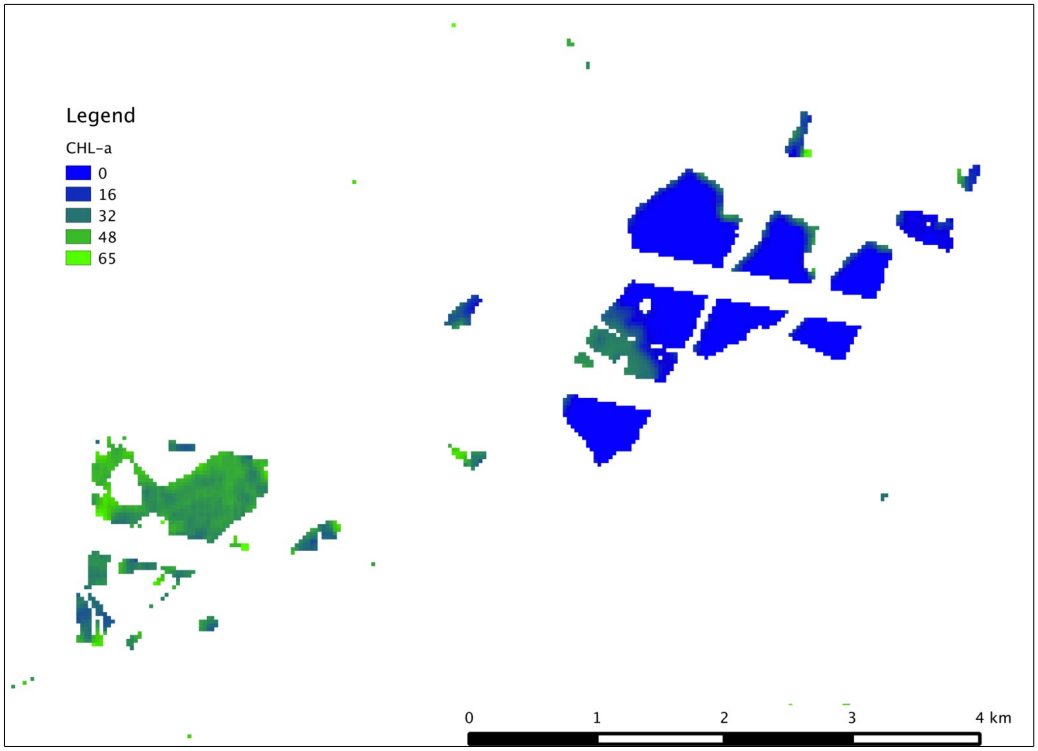

Figure 72: Model 33.66(L3/L1)^3.405 of Chl-a on Oplatil and Bohdanecsky rybnik on 2012.05.29*

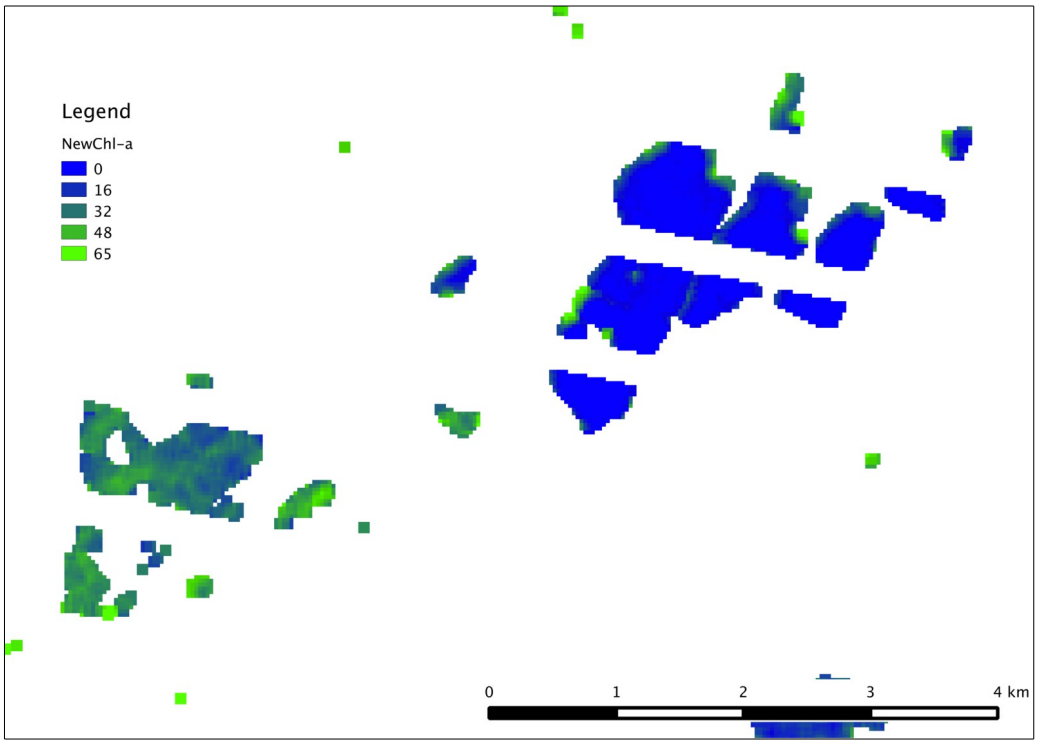

Figure 73: Model 33.66(L3/L1)^3.405 of Chl-a on Oplatil and Bohdanecsky rybnik on 2012.06.22*

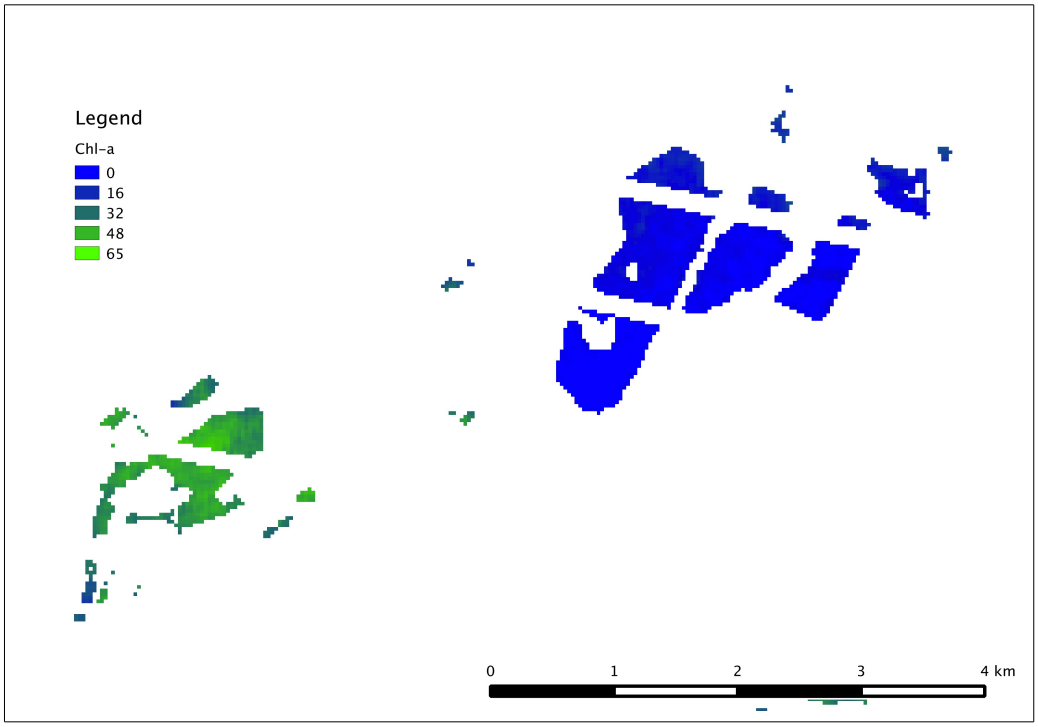

Figure 74: Model 33.66(L3/L1)^3.405 of Chl-a on Oplatil and Bohdanecsky rybnik on 2012.08.01*

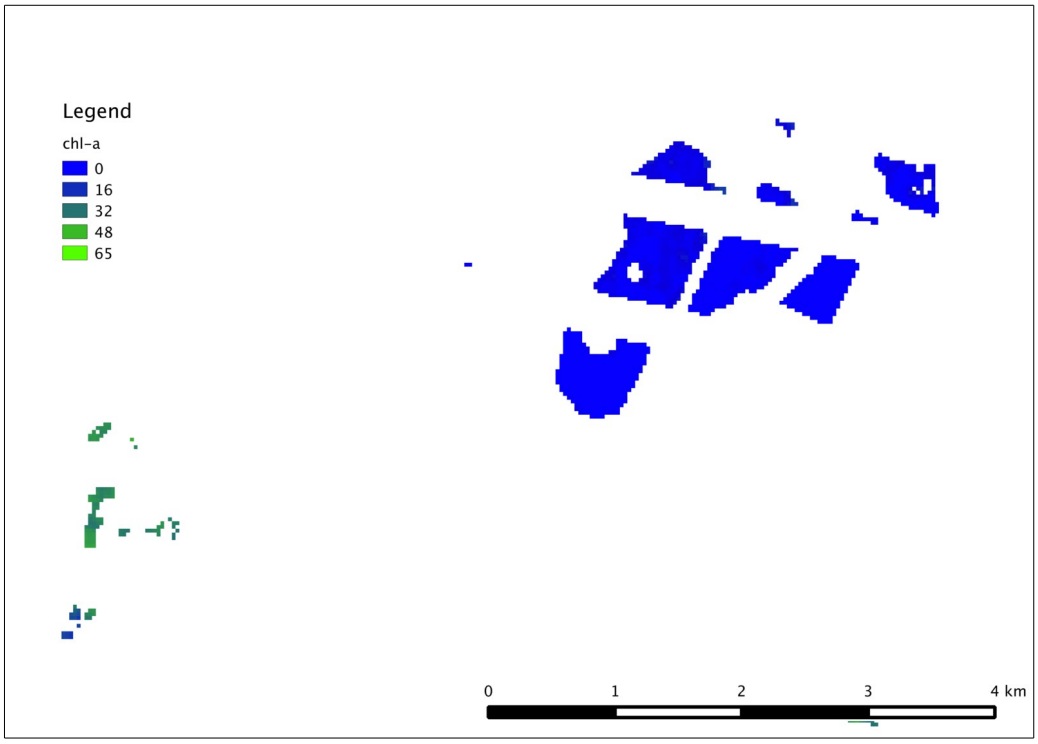

Figure 75: Model 33.66(L3/L1)^3.405 of Chl-a on Oplatil and Bohdanecsky rybnik on 2012.09.11*

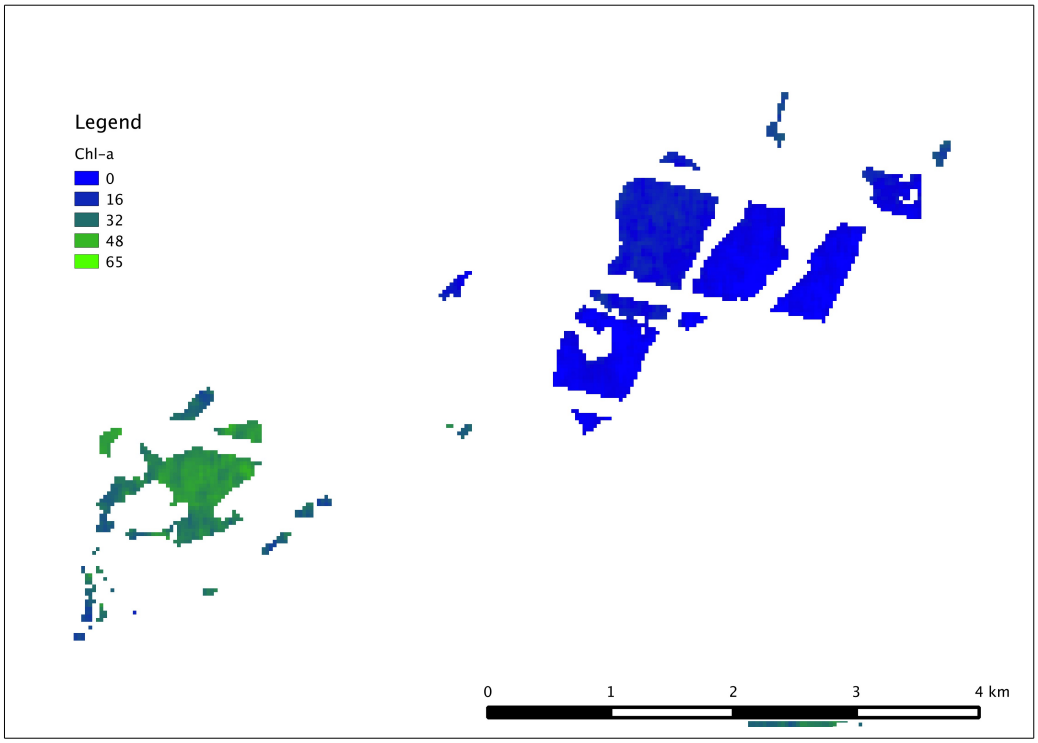

Figure 76: Model 33.66(L3/L1)^3.405 of Chl-a on Oplatil and Bohdanecsky rybnik on 18.09.2012*

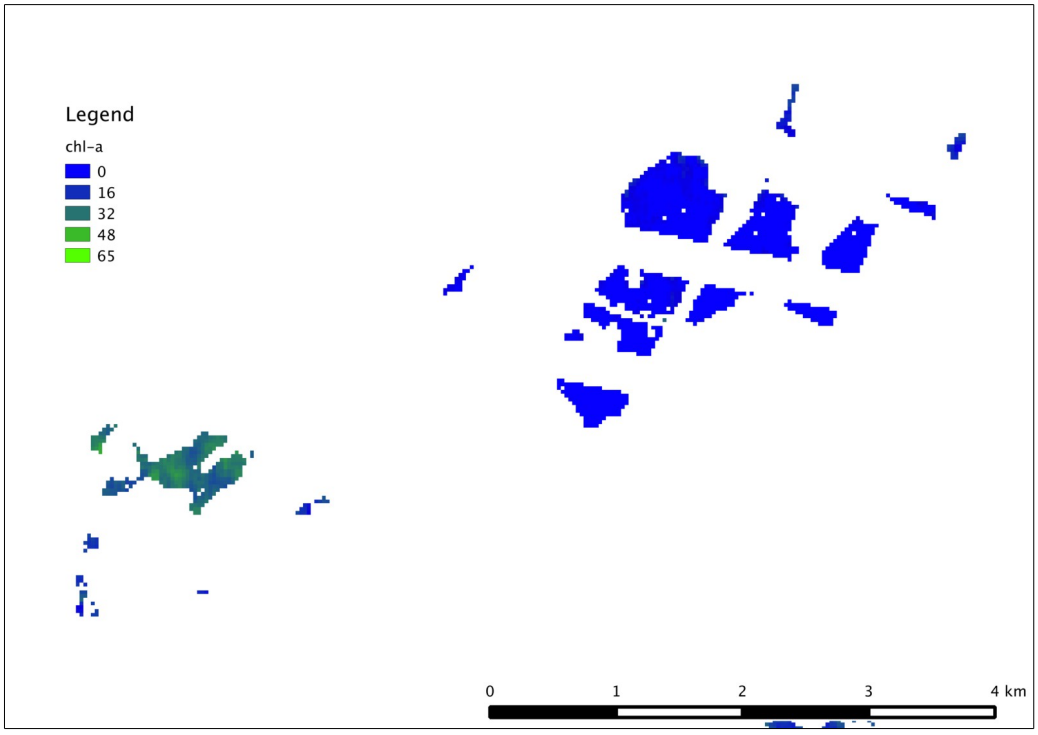

Figure 77: Model 33.66(L3/L1)^3.405 of Chl-a on Oplatil and Bohdanecsky rybnik on 2012.11.14*

The figures 72 to 77 show the levels of chlorophyll-a on Oplatil and Bohdanecsky rybnik during different seasons from May to November of 2012. The estimated levels of Chl-a were based on the model 33.66*(L3/L1)^3.405. Bohdanecsky rybnik is a protected national reserve as it serves as a breeding habitat for numerous species of birds. Based on models that have been developed the various water quality parameters of such water bodies could be estimated without disturbing the habitat of these birds. The average levels of Chl-a for the

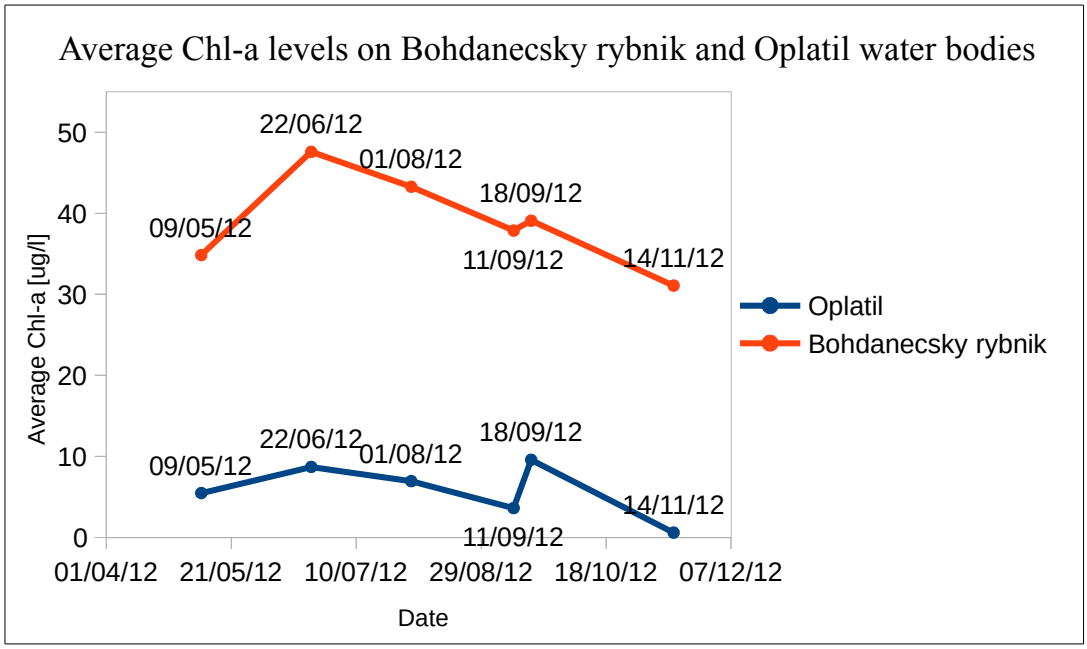

Figure 78: Average Chl-a levels for Bohdanecsky rybnik and Oplatil in 2012 based on Model developed for Chl-a.

Bohdanecsky rybnik and Oplatil water bodies were measured based on the model developed (33.66*(L3/L1)^3.405) for Chl-a. This was to estimated time line of Chl-a for the two water bodies, showing how the models really work. It estimates the averages of Chl-a in the two water bodies by measuring the whole water area of these water bodies and based on this, calculates the Chl-a average of each water body. The measurement of the Chl-a in each water body, relies on a vector layer created for Chl-a of all surface water bodies in the Czech Republic. The average for Bohdanecsky rybnik and Oplatil for 9th of May 2012 was 34.84 ug/l and 5.48 ug/l (Figure 78) respectively. For the 22nd of June the average measurements as per the

model were 8.71 ug/l, 47.58 ug/l. The next date (1st of August, 2012) showed 6.96 ug/l, 43.27 for Oplatil and Bohdanecsky rybnik. That for 11th of September averages for the two water bodies were 3.63 ug/l and 37.86 ug/l. 18th of September showed averages of 9.59 and 39.08 respectively. For the 14th of November the average Chl-a were 0.61 ug/l for Oplatil and 31.08 ug/l for Bohdanecsky rybnik. The highest average for Bohdanecsky rybnik was in June whereas that for Oplatil was in September. (Figure 78)

4 CONCLUSION AND RECOMMENDATIONS

In looking at the use of remote sensing as a tool for monitoring inland water bodies the following objectives were set. First to create a model for estimating the levels of inland water quality parameters based on Landsat ETM+ data. Secondly to assess the effects of smoothing on the models developed because of the sizes of the water bodies that were to be monitored. Thirdly to analyse the effects of atmospheric correction on the models that were developed.

In analysing data statistically values from TOAR images and values from atmospherically corrected images were those that were considered. The use of RGB band combination did aid the identification of areas covered by clouds, cloud shade and haze. This made it possible to identify and remove sample points which were affected by these phenomenon. This is evident in Figure 39 and Figure 40. The area of study had general cloudy conditions that sometimes made it next to impossible for the availability of clear images as in the case of works focusing on arid or coastal regions. The careful examination of of images and removal of problematic areas from the processing still makes it possible to build and use models from satellite imagery for the purpose.

It was further demonstrated that despite the size of an inland water body, it is possible to smooth images of them and that smoothing enhances the performance of the resultant model. This is possible when the right water only mask is applied. Atmospheric correction did also improve the overall quality values though in some situations it reduced correlation between measured values and those extracted from atmospherically corrected images as visible in table 10. Atmospherically corrected Landsat ETM+ images downloaded from USGS. These images were corrected based on the 6S algorithm as expounded by Masek et al [117].

From the models it is evident that most of the water quality parameters had varied r^2 values though in some it was low vis a vis bands and band combinations that falls within the range 450 (blue) – 690 (red) nm with the exception of temperature which was modelled based on thermal bands. Table 12 shows the two best models for each parameter analysed.

Though mostly small sized inland water bodies were monitored in this research it showed clearly that Landsat ETM+ data can be relied on for monitoring of inland water quality parameters as shown by the models developed. It is also worth mentioning that we relied on

Landsat ETM+ and not Landsat 8, because at the inception of our work it was the satellite in operation. Additionally it is the longest running environmental satellite in orbit and this allows the use of models to analyse trends in time (from the year of satellite launch to date). The procedures are applicable to other satellite images, example Landsat 8.

Monitoring of small inland water bodies based of Landsat imagery

Though this research went well there were a few challenges worth noting. Thick clouds caused a lot of data loss. Images with light clouds and haze could not be used even when a robust atmospheric correction was adopted to limit the effect of the cloud and haze over water bodies. Some of the samples could not be used due to the fact that on the day they were taken available satellite images were cloudy. With this problem, some of the samples could not be factored into our analysis. Also because of this issue the application of the models could not be done in evenly spaced intervals for whole year of any of the years under review. Long distances between the individual sampled water water bodies also made it time consuming sampling a number of water bodies within the day of overpass. In some occasions, though the weather was good not that many samples were taken due to the issue of time. One pertinent issue, is the fact that not all water quality parameters can monitored based remote sensing with the required precision based on this method. Also most of the parameters depend on similar band combinations. It suffices to say that concentration from the models for the parameters will have strong inter-correlation. In some situations that might not be the case as in reality parameters can behave independently. Example is SDD and Chl-a in situations of high turbidity not related to algae growth. Due to the afore mentioned reasons remote sensing can not solely be relied on but rather go hand in hand with traditional methods of inland water monitoring.

Benefits of this Research

Models developed for the inland water quality parameters analysed, can be used in estimating these parameters for other inland water bodies that are visible on the image used. Limiting in situ measurements reduces operational cost, time and energies spent monitoring inland water bodies.

Secondly similar water only masks could be developed as done in this research work so smoothing could be effectively done to limit the effect of noise on remotely sensed data for smaller inland water bodies. This will aid effective inland water management.

The models developed will help monitor special inland water bodies such those that serve as habitat or breeding spot without disturbance to the habitat. As demonstrated in the use of the models in estimating the levels of Chl-a on Bohdanecsky rybnik which is national reserve and a breeding place for different species of birds.

Last but not least models also helps in estimation of concentration not only for the areas that were sampled but rather for the whole water body. By this problematic areas of the water body could be identified.

Recommendations for Future work

The recommendations for future research to further enhance the findings made in this work are as follows.

Exploring further methods of atmospheric correction methods in order to improve the quality of data and develop models based on Landsat 8 OLI and Sentinel-2 MSI. Sentinel-2 has better spatial and temporal resolution which has the potential to greatly enhance usability of the models for monitoring small water bodies.

One other area that needs to be looked at is the measurement of wind currents during satellite overpass. Due to the size of the water bodies rapid changes could occur due to strong winds with respect to spectral properties of the water surface.

Exploring other methods of collecting in situ data such as building mini sampling stations on these water bodies. A lot of time was spent on collecting samples as the sampled water bodies in terms of distance were quite far apart. Juggling between these water bodies was tedious work adding the time spent in the laboratory meant a few samples could be worked on at a time.

Also further work needs to be done regarding inland water quality parameters based on classification of water body types. Example sand lakes, reservoirs, fish ponds, lakes only. To clearly identify the patterns of inland water quality parameters during the various seasons of the year.

From the research emphasis has been brought to the fact that the use of remote sensing in near real time monitoring of water quality has been shown to be a good alternative to in situ monitoring.

5 BIBLIOGRAPHY

[1] BARTRAM, J a R BALLANCE, ed. *Water quality monitoring a practical guide to the design and implementation of freshwater quality studies and monitoring programmes*. 1. ed. London [u.a.]: E & FN Spon, 1996. ISBN 0-419-21730-4.

[2] NATALE, O. E., R. M. BHARDWAJ, I. HODGSON a J. NIEMI. *WQ_Tech_Report_FINALDRAFT_United Nations Environmental Programme*. B.m.: United Nations Environmental Programme. 2012

[3] *Quebec inventory on Emissions*. B.m.: Ministry of of Sustainable Development, Environment and Parks. 2009

[4] CARDER K. L, F. R CHEN, Z. P LEE, S. K. HAWES a D KAMYKOWSKI. Semianalytic Moderate-Resolution Imaging Spectrometer Algoritms for Chlorophyll A and Absorption with Bio-Optical Domains Based on Nitrate-Depletion Temperatures. *Journal of Geographical Research*. 1999, **104**(C3), 5403–5421.

[5] MOREL, A a L PRIEUR. Analysis of variations in ocean color. *Limnology and Oceanography*. 1977, (22), 709-.

[6] BARUAH, P. J, M TAMURA, K OKI a H NISHIMURA. Neural Network Modelling of Surface Chlorophyll and Sediment Content in Inland Water from Landsat Thematic Mapper: Imagery Using Multidate Spectrometer Data in G. D. Gilbert, R. J. Frouin (Eds), Ocean Optics. In: *Remote Sensing and Underwater Imager*: *Ocean Optics*. Seattle,WA, USA: International Society For Optical Engineering, 2002, s. 205–212.

[7] PRIEUR, Louis a Shubha SATHYENDRANATH. An optical classification of coastal and oceanic waters based on the specific spectral absorption curves of phytoplankton pigments, dissolved organic matter, and other particulate materials. *Limnology and Oceanography*. 1981, **26**(4), 671–689.

[8] DEKKER, A. G., T. J. MALTHUS a E SEYHAN. Quantitative modeling of inland water quality for high-resolution MSS systems. *Geoscience and Remote Sensing, IEEE Transactions on*. 1991, **29**(1), 89–95.

[9] AKBAR, T. A., Q. A. HASSAN a G. ACHARI. A Remote sensing based framework for predicting water quality of different source waters. *The International Archives of Photogrammetry, Remote Sensing and Spatial Information Sciences*. 2010, **34**.

[10] GRAHAM, S. *Remote Sensing: Feature Articles* [online]. 1999 [vid. 2015-06-24]. Dostupné z: http://earthobservatory.nasa.gov/Features/RemoteSensing/

[11] BAUMANN, P. R. *History of Remote Sensing, Satellite Imagery* [online]. 2009 [vid. 2015-04-15]. Dostupné z: http://www.oneonta.edu/faculty/baumanpr/geosat2/RS%20History%20II/RS-History-Part-2.html

[12] 1 Course introduction. *Planetek Italia* [online]. 2012 [vid. 2015-04-15]. Dostupné z: http://www.planetek.it/eng/training_courses/online_manuals/on_line_course_of_remote_sensing/1_course_introduction

[13] BAUMANN, P. R. *History of Remote Sensing, Aerial Photography* [online]. 2014 [vid. 2015-06-24]. Dostupné z: http://www.oneonta.edu/faculty/baumanpr/geosat2/RS%20History%20I/RS-History-Part-1.htm

[14] RUFFNER, K. C. *Corona: America's first satellite program*. B.m.: Morgan James Publishing, 1995.

[15] DEKKER, G. A. a E. L. HESTIR. *Evaluating the Feasibility of Systematic Inland Water Quality Monitoring with Satellite Remote Sensing* [online]. Canberra, Australia: CSIRO, 2012. Water for a Healthy Country National Research Flagship. ISBN 978-0-643-10849-3. Dostupné z: https://publications.csiro.au/rpr/download?pid=csiro:EP117441&dsid=DS10

[16] COLWELL, R. N. Uses Limitations of Multi-Spectral Remote Sensing:In Proceedings of the Fourth symposium on Remote Sensing of Environment. 1966, 77–100.

[17] LANDGREBE, D. Computer-based remote sensing technology a look to the future. *Remote Sensing Environment*. 1976, **5**, 229–246.

[18] WHITE, L. P. *Ariel Photography and Remote Sensing for soil Survey*. B.m.: Clarendon Press, Oxford, 1977.

[19] BAUMANN, P.R. Introduction to Remote Sensing. In: [online]. B.m. 2010 [vid. 2015-04-15]. Dostupné z: http://www.oneonta.edu/faculty/baumanpr/geosat2/RS-Introduction/RS-Introduction.html

[20] JENSEN, J. R. *Remote Sensing of the environment: An Earth Resource Perspective.* B.m.: Prentice Hall, 2000.

[21] SCHOWENGERDT, R. A. *Remote Sensing: Models and Methods for image Processing*. 3. vyd. B.m.: Academic Press, 2006. ISBN 0-12-369407-8.

[22] CAMPBELL, J. B a R. H WYNNE. *Introduction to Remote Sensing*. 5th vyd. B.m.: Guilford Press, 2011. ISBN 1-60918-176-X.

[23] ARKARJUN. *Remote Sensing Illustration - Remote sensing - Wikipedia, the free encyclopedia* [online]. 2013 [vid. 2015-05-13]. Dostupné z: http://en.wikipedia.org/wiki/Remote_sensing#/media/File:Remote_Sensing_Illustration.jpg

[24] LIEW, S. C. *Principles of Remote Sensing - Centre for Remote Imaging, Sensing and Processing, CRISP* [online]. 2001 [vid. 2015-05-18]. Dostupné z: http://www.crisp.nus.edu.sg/~research/tutorial/sar_int.htm

[25] LIU, J. G a P MASON. *Essential Image processing and Geographical Information Systems for Remote Sensing*. B.m.: John Wiley and Sons, 2009.

[26] CAMPBELL, J.B. *Introduction to Remote Sensing*. 3rd vyd. B.m.: The Guilford Press, 2002. ISBN 1-57230-640-8.

[27] MOUNT HOLYOKE COLLEGE. *Introduction to Remote Sensing and Image Processing* [online]. 2011 [vid. 2015-06-24]. Dostupné z: https://www.mtholyoke.edu/courses/tmillett/course/geog205/files/remote_sensing.pdf

[28] *Landsat 7 Science Data Users Handbook*. B.m.: National Aeronautics and Space Administration. 2011

[29] ESTES, E. *Fundamentals of Image interpretation. In Manual of Remote Sensing*. Falls Church, Virginia: American Society of Photogrammetry, 1975.

[30] LILLESAND, T a R. W KIEFER. *Remote Sensing and Image Interpretation*. 2nd vyd. B.m.: Wiley, 1987. ISBN 0-471-84517-5.

[31] MAINI, K and V AGRAWAL. *Satellite Technology: Principles and Applications*. 2nd vyd. B.m.: John Wiley and Sons, 2011. ISBN 1-119-95727-3.

[32] QUADRI, S. A and SIDEK., O. Image quality improvement of low-resolution camera using data fusion technique. In: *4th International Conference on Digital Image Processing-ICDIP*. Kualar Lumpur. 2012.

[33] GATRELL, A. *Concepts of space and geographical data In:Longley, P., Goodchild, M., Maguire, D., Rhind, D. (Eds.), Geographic Information Systems*. 1st vyd. West Sussex, UK: Wiley, 1991.

[34] SABINS, F. F. *Remote Sensing: Principles and Interpretation*. 3rd vyd. B.m.: Waveland Press, 2007. ISBN 1478610085.

[35] MATHER, P. M a M KOCH. *Computer Processing of Remotely-Sensed Images*. 4th vyd. New Jersey: Wiley-Blackwell, 2011.

[36] SABINS, F. F. *Remote Sensing Laboratory Manual*. 3. vyd. B.m.: Kensall/Hunt, 1997. ISBN 0-7872-2543-6.

[37] WEBSTER, J. G a H EREN. *Measurement, Instrument, and Sensors Handbook: Electromagnetic, Optical, Radiation, Chemical and Biomedical Measurement*. 2nd vyd. B.m.: CRC Press, 2014. ISBN 1-4398-4891-2.

[38] VERBYLA, D. L. *Satellite Remote Sensing of Natural Resources*. 1. vyd. B.m.: CRC Press, 1995. Mapping Science. ISBN 1-56670-107-4.

[39] HASAN, S. M. *Remote sensing* [online]. 2011 [vid. 2015-05-13]. Dostupné z: http://www.slideshare.net/merdevie/remote-sensing-10526190

[40] TOWNSHEND, J. R. G. *The spatial resolving power of earth resources satellites: A review (NASA technical memorandum)*. B.m.: NASA, Goddard Space Flight Center, 1980. NASA technical memorandum.

[41] TOWNSHEND, J. R. G a C. O JUSTICE. Towards operational monitoring of terrestrial systems by moderate-resolution remote sensing. *Remote Sensing of Environment*. 2002, **83**(1), 351–359.

[42] BILLINGSLEY, F. C. *Data Processing and reprocessing in Manual of Remote Sensing*. B.m.: American Society of Photogrammetry, 1983.

[43] AL-WASSAI, F.A a N. V. KALYANKAR. Major limitations of satellite images. *Arxiv.org* [online]. 2013 [vid. 2015-05-07]. Dostupné z: http://arxiv.org/abs/1307.2434

[44] RASHEED, T a C JURGENS. *Remote Sensing of Urban and Suburban Areas*. Illustrated. B.m.: Springer Science and Business Media, 2010.

[45] YANG, C, D WONG, Q MIAO a R YANG. *Advance Geoinformamtion Science*. Illustrated. B.m.: CRC Press, 2010.

[46] MATHER, P. M. *Computer Processsing of Remotely-Sensed Images: An Introduction*. 3. vyd. B.m.: John Wiley and Sons, 2004.

[47] WANG, G a Q WENG. *Remote Sensing of Natural Resources*. Illustrated. B.m.: CRC Press, 2013. Remote Sensing Applications. ISBN 1-4665-5692-7.

[48] JENSEN, J. R. *Remote sensing of the Environment: An Earth Resource Perspective*. 2nd vyd. B.m.: Prentice Hall, 2006. ISBN 10: 0131889508.

[49] BHATTI, A. M. *Modelling and monitoring of suspended matter in surface waters using remotely sensed data*. Kochi, Japan, 2008. University of Technology.

[50] YUAN, M. Temporal GIS and applications. In: *Encyclopedia of GIS* [online]. B.m.: Springer, 2008 [vid. 2015-05-07], s. 1147–1150. Dostupné z: http://link.springer.com/10.1007/978-0-387-35973-1_1373

[51] GIBSON, C. C., E OSTROM a T AHN. The concept of scale and the human dimensions of global change: a survey. *Ecological economics*. 2000, **32**(2), 217–239.

[52] NATURAL RESOURCES CANADA. Satellite Characteristics: Orbits and Swaths | Natural Resources Canada. *Natural Resources Canada* [online]. 2014 [vid. 2015-05-13]. Dostupné z: http://www.nrcan.gc.ca/earth-sciences/geomatics/satellite-imagery-air-photos/satellite-imagery-products/educational-resources/9283

[53] BECVAR, M. Introduction to Remote Sensing. In: [online]. Prague. [vid. 2015-05-11]. Dostupné z: http://storm.fsv.cvut.cz/on_line/enen/ENEN_12_remote_sensing.pdf

[54] FALKNER, E a D MORGAN. *Aerial mapping: methods and applications*. 2nd ed. Boca Raton [Fla.]: Lewis, 2002. ISBN 1-56670-557-6.

[55] Remote Sensing, Satellite Imaging Technology | Satellite Imaging Corp. *satellite imaging corporation* [online]. 2014 2001 [vid. 2015-05-13]. Dostupné z: http://www.satimagingcorp.com/services/resources/characterization-of-satellite-remote-sensing-systems/

[56] EMEIS, Stefan. *Surface-Based Remote Sensing of the Atmospheric Boundary Layer*. B.m.: Springer Science and Business Media, 2010. ISBN 90-481-9340-0.

[57] SMITH, G. M a P. J CURAN. Signal-to-noise ratio required for the estimation of Foliar biochemical concentrations. *International Journal of Remote Sensing*. 1996, **17**(5), 1031–1058.

[58] SMITH, G. M a P. J CURAN. Methods of estimating image siganl-to-noise ratio. *Advances in Remote Sensing and GIS Analysis*. 1999, 61–74.

[59] MATHER, P. M. *Computational methods of multivariate analysis in physical geography*. B.m.: John Wiley and Sons, 1976.

[60] EUROPEAN SPACE AGENCY. Radiometric - Resolutions - Sentinel-2 MSI - User Guides - Sentinel Online. *ESA sentinel online* [online]. 2015 2000 [vid. 2015-05-11]. Dostupné z: https://sentinel.esa.int/web/sentinel/user-guides/sentinel-2-msi/resolutions/radiometric

[61] NAVULUR, K. *Multispectral image analysis using the object-oriented paradigm*. B.m.: CRC Press, 2006. Remote Sensing Applications. ISBN 1-4200-4306-4.

[62] SINGHAL, B. B. S a R. P GUPTA. *Applied Hydrogeology*. 2nd vyd. B.m.: Springer Science and Business Media, 2010.

[63] LANDGREBE, D. A a E MALARET. Noise in Remote-Sensing System: The Effect on Classification Error. *IEEE Geoscience and Remote Sensing*. 1986, **GE-24**, 294–300.

[64] AL-AMRI, S. S, N. V KALYANKAR a S. D KHAMITKAR. A comparative study of removal noise from remote sensing image. *arXiv preprint arXiv:1002.1148* [online]. 2010 [vid. 2015-04-29]. Dostupné z: http://arxiv.org/abs/1002.1148

[65] Remote Sensing Phenology: Data Smoothing. *USGS* [online]. [vid. 2015-04-27]. Dostupné z: http://phenology.cr.usgs.gov/methods_data.php

[66] VAIPHASA, Chaichoke. Consideration of smoothing techniques for hyperspectral remote sensing. *ISPRS Journal of Photogrammetry and Remote Sensing*. 2006, **60**(2), 91–99.

[67] BHOSALE, N. P a R. R MANZA. Analysis of effect of noise removal filters on noisy remote sensing images. *International Journal of Scientific & Engineering Research (IJSER)(10)*. 2013, 1511–1514.

[68] CORNER, B. R., R. M. NARAYANAN a S. E. REICHENBACH. Noise estimation in remote sensing imagery using data masking. *International Journal of Remote Sensing*. 2003, **24**(4), 689–702.

[69] RANI, V a P KAMBOJ. A brief study of various noise model and filtering techniques. *Journal of global research in computer science*. 2013, **4**(4), 166–171.

[70] AFROSE, Z. Relaxed Median Filter: A Better Noise Removal Filter for Compound Images. *International Journal on Computer Science & Engineering*. 2012, **4**(7).

[71] CHAN, R.H., CHUNG-WA a M. NIKOLOVA. Salt-and-pepper noise removal by median-type noise detectors and detail-preserving regularization. *IEEE Transactions on Image Processing*. 2005, **14**(10), 1479–1485.

[72] YOUNG, I. T, J. J GERBRANDS a L. J VAN VLIET. *Fundamentals of image processing*. Delft: TU Delft, Faculty of Applied Physics, Pattern Recognition Group, 1995. ISBN 90-75691-01-7.

[73] LILLESAND, T. M a R. W KIEFER. *Remote Sensing and Image interpretation*. 3rd vyd. B.m.: Wiley, 1994. ISBN 0-471-57783-9.

[74] WENG, Q. *An Introduction to Contemporary Remote Sensing*. B.m.: McGraw-Hill Professional, 2012. ISBN 0-07-174012-0.

[75] WEMMERT, C., A. PUISSANT, G. FORESTIER a P. GANCARSKI. Multiresolution Remote Sensing Image Clustering. *IEEE Geoscience and Remote Sensing Letters*. 2009, **6**(3), 533–537.

[76] LARK, R. M. A reappraisal of unsupervised classification, II: optimal adjustment of the map legend and a neighbourhood approach for mapping legend units. *International Journal Remote Sensing*. 1995, **16**(8), 1445–1460.

[77] MATHER, P. M a B TSO. *Classification Methods for Remotely Sensed Data*. 2nd vyd. B.m.: CRC Press, 2009.

[78] HARALICK, R. M, K SHANMUGAM a I DINSTEIN. 04309314.pdf. *IEEE Transactions on Systems, Man and Cybernetics*. 1973, **SMC-3**(6), 610–621.

[79] SABINS JNR, F.F. *Remote Sensing: Principles and Interpretation.* 2. vyd. New York: W.H. Freeman & Co, 1987.

[80] KANELLOPOULOS, L. Neurocomputation in Remote Sensing Data Analysis: Proceedings of concerted Action COMPARES;(connectionist methods of Pre-processing and Analysis of Remote Sensing Data). *Springer Science and Business Media*. 1997, 2–29.

[81] GONZALEZ, R. C a R. E WOODS. *Digital Image Processing*. 3rd vyd. B.m.: Addison-Wesley Pub, 1992. ISBN 0-201-50803-6.

[82] TAMIM, A. Smoothing Techniques in Image Processing. In: [online]. B.m. 2009 [vid. 2015-05-21]. Dostupné z: http://www.scribd.com/doc/21424720/Smoothing-Techniques-in-Image-Processing#scribd

[83] PRATT, W. K. *Digital image processing PIKS inside*. 3rd vyd. New York; Chichester: John Wiley & Sons, 2001. ISBN 0-471-22132-5.

[84] PRATT, W. K. *Digital Image Processing*. B.m.: John Wiley and Sons, 1991.

[85] KUAN, D. T, A. A SAWCHUK, T. C STRAND a P CHAVEL. Adaptive Noise Smoothing Filter for Images with Signal-Dependent Noise. *IEEE Transactions on Pattern Analysis and Machine Intelligence*. 1985, **PAMI-7**(2), 165–177.

[86] HE, K, J SUN a X TANG. Guided image filtering. In: *Computer Vision–ECCV 2010* [online]. B.m.: Springer, 2010 [vid. 2015-05-21], s. 1–14. Dostupné z: http://link.springer.com/chapter/10.1007/978-3-642-15549-9_1

[87] MANCUSO, M. Non-linear image filter for filtering noise - Google Patents [online]. US6108455 A. 2000. [vid. 2015-05-21]. Dostupné z: https://www.google.com/patents/US6108455

[88] SIVASUNDARI, S, R. S KUMAR a M KARNAN. PERFORMANCE ANALYSIS OF IMAGE FILTERING ALGORITHMS FOR MRI IMAGES. *International Journal of Research in Engineering and Technology*. 2014, **03**(05), 438–440.

[89] HWANG, H a R. HADDAD. Adaptive median filters: new algorithms and results. *Image Processing, IEEE Transactions on*. 1995, **4**(4), 499–502.

[90] UNIVERSITY OF AUCKLAND. Image Filtering_2up.pdf. In: [online]. B.m. 2010 [vid. 2015-05-21]. Dostupné z: https://www.cs.auckland.ac.nz/courses/compsci373s1c/PatricesLectures/Image%20Filtering_2up.pdf

[91] FU, F, F WALKER, W ALMAGUER a J KINCAID. *Wiener Filtering and Image Processing* [online]. [vid. 2015-05-25]. Dostupné z: https://www.clear.rice.edu/elec431/projects95/lords/wiener.html

[92] KAILATH, T. *Lectures on Weiner and Kalman Filtering*. 2nd vyd. B.m.: Springer, 2014. ISBN 3-7091-2804-8.

[93] MIAO, J. G a M. A CLEMENTS. *Digital Signal Processing and Statistical Classification*. Illustrated. B.m.: Artech House, 2002. ISBN 1-58053-135-0.

[94] HAMZA, A. B, P LUQUE-ESCAMILLA, J MARTÍNEZ-AROZA a R ROMÁN-ROLDÁN. Removing noise and preserving details with relaxed median filters. *Journal of Mathematical Imaging and Vision*. 1999, **11**(2), 161–177.

[95] KO, S a Y. H LEE. Center weighted median filters and their applications to image enhancement. *Circuits and Systems, IEEE Transactions on*. 1991, **38**(9), 984–993.

[96] JA'JA', J. *Atmospheric Correction* [online]. 1995 [vid. 2015-06-10]. Dostupné z: http://www.umiacs.umd.edu/labs/GC/atmo/

[97] FALLAH-ADL, H, J JAJA, S LIANG, Y. J KAUFMAN a J TOWNSHEND. Efficient algorithms for atmospheric correction of remotely sensed data. In: *Supercomputing, 1995. Proceedings of the IEEE/ACM SC95 Conference* [online]. B.m.: IEEE, 1995, s. 12–12 [vid. 2015-06-10]. Dostupné z: http://ieeexplore.ieee.org/xpls/abs_all.jsp?arnumber=1383146

[98] HADJIMITSIS, D.G., G PAPADAVID, A AGAPIOU, K THEMISTOCLEOUS, M. G HADJIMITSIS, A RETALIS, S MICHAELIDES, N CHRYSOULAKIS, L TOULIOS a C. R. I CLAYTON. Atmospheric correction for satellite remotely sensed data intended for agricultural applications: impact on vegetation indices. *National Hazards Earth Systems Science*. 2010, **10**, 89–95.

[99] SLATE, P. N. *Remote Sensing optics and optical systems*. White-Plains, New York: Addison-Wesley, 1980.

[100] LU, D., P. MAUSEL, E. BRONDIZIO a E. MORAN. Assessment of atmospheric correction methods for Landsat TM data applicable to Amazon basin LBA research. *International Journal of Remote Sensing* [online]. 2002, **23**(13), 2651–2671. ISSN 0143-1161, 1366-5901. Dostupné z: doi:10.1080/01431160110109642

[101] FRASER, R. S a Y. J KAUFMAN. The Relative Importance of Aerosol Scattering and Absorption in Remote Sensing. *IEEE Geoscience and Remote Sensing*. 1985, **GE-23**(5), 625–633.

[102] FRASER, R. S, O. P BAHETHI a A. H AL-ABBAS. *NASA Technical Reports Server (NTRS) - The effect of the atmosphere on the classification of satellite observations to identify surface features* [online]. 1977 [vid. 2015-06-10]. Dostupné z: http://ntrs.nasa.gov/search.jsp?R=19770066545

[103] HADJIMITSIS, D. G., C. R. I. CLAYTON a V. S. HOPE. An assessment of the effectiveness of atmospheric correction algorithms through the remote sensing of some reservoirs. *International Journal of Remote Sensing* [online]. 2004, **25**(18), 3651–3674. ISSN 0143-1161, 1366-5901. Dostupné z: doi:10.1080/01431160310001647993

[104] HADJIMITSIS, D. G., C CLAYTON a A RETALIS. On the darkest pixel atmospheric correction algorithm: a revised procedure applied over satellite remotely sensed images intended for environmental applications. In: [online]. B.m.: SPIE, 2004, s. 464–471 [vid. 2015-06-11]. Dostupné z: doi:10.1117/12.511520

[105] CHAVEZ, P. S. Image-based atmospheric corrections-revisited and improved. *Photogrammetric engineering and remote sensing*. 1996, **62**(9), 1025–1035.

[106] BAUGH, W. M a D.P GROENEVELD. Empirical proof of the empirical line. *International Journal Remote Sensing*. 2008, **29**(3), 665–672.

[107] KARPOUZLI, E. a T. MALTHUS. The empirical line method for the atmospheric correction of IKONOS imagery. *International Journal of Remote Sensing* [online].

2003, **24**(5), 1143–1150. ISSN 0143-1161, 1366-5901. Dostupné z: doi:10.1080/0143116021000026779

[108] SMITH, G. M a E. J MILTON. The use of the empirical line method to calibrate remotely sensed data to reflectance. *International Journal of remote sensing*. 1999, **20**(13), 2653–2662.

[109] MORAN, M. S., R. BRYANT, K. THOME, W. NI, Y. NOUVELLON, M. P. GONZALEZ-DUGO, J. QI a T. R. CLARKE. A refined empirical line approach for reflectance factor retrieval from Landsat-5 TM and Landsat-7 ETM+. *Remote Sensing of Environment*. 2001, **78**(1), 71–82.

[110] VAUDOUR, E., J. MOEYS, J. M. GILLIOT a Y. COQUET. Spatial retrieval of soil reflectance from SPOT multispectral data using the empirical line method. *International Journal of Remote Sensing* [online]. 2008, **29**(19), 5571–5584. ISSN 0143-1161, 1366-5901. Dostupné z: doi:10.1080/01431160802060920

[111] KNEIZYS, F. X, E. P. SHETTLE, L. W. ABREU, J. H. CHETWYND a G. P. ANDERSON. *Users guide to LOWTRAN 7* [online]. B.m.: DTIC Document. 1988 [vid. 2015-06-15]. Dostupné z: http://oai.dtic.mil/oai/oai?verb=getRecord&metadataPrefix=html&identifier=ADA206773

[112] BERK, A.L, G.P ANDERSON, L. S BERNSTEIN, P. K ACHARYA, H. DOTHE, M. W MATTHEW, S ADLER-GOLDEN, J. H CHETWYND JR, S. C RICHTSMEIER, B PUKALL a OTHERS. MODTRAN4 radiative transfer modeling for atmospheric correction. In: *SPIE's International Symposium on Optical Science, Engineering, and Instrumentation* [online]. B.m.: International Society for Optics and Photonics, 1999, s. 348–353 [vid. 2015-06-15]. Dostupné z: http://proceedings.spiedigitallibrary.org/proceeding.aspx?articleid=995156

[113] GUANTER, L, R RICHTER a H KAUFMANN. On the application of the MODTRAN4 atmospheric radiative transfer code to optical remote sensing. *International Journal of Remote Sensing* [online]. 2009, **30**(6), 1407–1424. ISSN 0143-1161, 1366-5901. Dostupné z: doi:10.1080/01431160802438555

[114] GAO, B. C, K. B HEIDEBRECHT a A. F. H GOETZ. Derivation of scaled surface reflectances from AVIRIS data. *Remote Sensing of Environment*. 1993, **44**, 145–163.

[115] TANRE, D, C DEROO, P DUHAUT, M HERMAN, J.J MORCRETTE, J PERBOS a P. Y DESCHAMPS. Technical note Description of a computercode to simulate the satellite signal in the solar spectrum: the 5S code. *International Journal of Remote Sensing*. 1990, **11**(4), 659–668.

[116] VERMOTE, E. F, D TANRÉ, J.L DEUZÉ, M HERMAN a J. J MORCETTE. Second simulation of the satellite signal in the solar spectrum, 6S: An overview. *Geoscience and Remote Sensing, IEEE Transactions on*. 1997, **35**(3), 675–686.

[117] MASEK, J.G., E.F. VERMOTE, N.E. SALEOUS, R. WOLFE, F.G. HALL, K.F. HUEMMRICH, F. GAO, J. KUTLER a T.-K. LIM. A Landsat Surface Reflectance Dataset for North America, 1990–2000. *IEEE Geoscience and Remote*

Sensing Letters [online]. 2006, **3**(1), 68–72. ISSN 1545-598X. Dostupné z: doi:10.1109/LGRS.2005.857030

[118] RITCHIE, J. C, J.R MCHENRY, F.R SCHIEBE a R. B WILSON. The relationship of reflected solar radiation and the concentration of sediment in the surface water of reservoirs,. *Remote sensing of Earth Resources*. 1974, **III**, 57–72.

[119] SCHIEBE, F. R, J. A HARRINGTON JR a J. C RITCHIE. Remote sensing of suspended sediments: the Lake Chicot, Arkansas project. *International Journal Remote Sensing*. 1992, **13**(8), 1487–1509.

[120] HARDING, L. W, E. C ITSWEIRE a W. E ESAIAS. Algorithm development for recovering chlorophyll concentrations in the Chesapeake Bay using aircraft remote sensing, 1989-91. *Photogrammetric engineering and Remote sensing*. 1995, **61**(2), 177–185.

[121] LESHT, B, R. P BARBIERO a G. J WARREN. A band-ratio algorithm for retrieving open-lake chlorophyll values from satellite observations of the Great Lakes. *Journal of Great Lakes Research*. 2013, **39**(1), 138–152.

[122] RUNDQUIST, D. C, L HAN, J. F. SCHALLES a J. S PEAKE. Remote Measurement of Algal Chlorophyll in surface Waters: The Case for the first Derivative of Reflectance Near 690 nm. *Photogrammetric Engineering and Remote Sensing* [online]. 1996, **62**(2), 195–200. Dostupné z: doi:10.1016/j.jglr.2012.12.007

[123] NOVOA, S, G CHUST, V VALENCIA, Jean-Marie FROIDEFOND a D MORICHON. Estimation of chlorophyll-a concentration in waters over the continental shelf of the Bay of Biscay: a comparison of remote sensing algorithms. *International Journal of Remote Sensing* [online]. 2011, **32**(23), 8349–8371. Dostupné z: doi:10.1080/01431161.2010.540588

[124] YU, G, W YANG, B MATSUSHITA, R LI, Y OYAMA a T FUKUSHIMA. Remote Estimation of Chlorophyll-a in Inland Waters by a NIR-Red-Based Algorithm: Validation in Asian Lakes. *Remote Sensing*. 2014, **6**(4), 3492–3510.

[125] HE, W, S CHEN, X LIU a J CHEN. Water Quality in Slightly Polluted Inland Water Body. *Front. Environmental Science Engineering China*. 2008.

[126] HELLWEGER, F.L., P. SCHLOSSER, U. LALL a J.K. WEISSEL. Use of satellite imagery for water quality studies in New York Harbor. *Estuarine, Coastal and Shelf Science* [online]. 2004, **61**(3), 437–448. Dostupné z: doi:10.1016/j.ecss.2004.06.019

[127] SUDHEER, K. P, I CHAUBEY a V GARG. Lake Water Quality Assessment from Landsat Thematic Mapper Data using neutral Network: An approach to optimal band combination selection. *Journal of The American Water Resources association* [online]. 2006, **42**(6), 1683–1695. Dostupné z: doi:10.1111/j.1752-1688.2006.tb06029.x

[128] PAPOUTSA, C a D. G. HADJIMITSIS. Remote Sensing for Water Quality Surveillance in Inland Waters: The Case Study of Asprokremmos Dam in Cyprus.

In: *Remote Sensing of Environment: Integrated Approaches*. London, UK: IntechOpen, 2013, s. 131–152. ISBN 978-953-51-1152-8.

[129] LIU, Yansui, Md Anisul ISLAM a Jay GAO. Quantification of shallow water quality parameters by means of remote sensing. *Progress in Physical Geography* [online]. 2003, **27**(1), 24–43. ISSN 14770296, 03091333. Dostupné z: doi:10.1191/0309133303pp357ra

[130] WANG, Y, H XIA, J FU a G SHENG. Water quality change in reservoirs of Shenzhen, China: detection using Landsat/TM data. *Science of The Total Environment*. 2004, 195–206.

[131] BREZONIK, P, K. D MENKEN a M BAUER. Landsat-based Remote Sensing of Lake Water Quality Characteristics, Including Chlorophyll and Colored Dissolved Organic Matter (CDOM). *Lake and Reservoir Management* [online]. 2005, **21**(4), 373–382. Dostupné z: doi:10.1080/07438140509354442

[132] BRAGA, C. Z. F, A. W SETZER a L DRUDE DE LACERDA. Water Quality Assessment with Simultaneous Landsat-5 TM Data at Guanabara Bay, Rio de Janeiro, Brazil. *Remote Sensing Environment* [online]. 1993, **45**(1), 95–106. Dostupné z: doi:10.1016/0034-4257(93)90085-c

[133] MEYBECK, M, V KIMSTACH a R HELMER. *Strategies fro water quality assessment, Water Quality Assessments- A Guide to Use of Biota, Sediment and Water in Environmental Monitoring- Second Edition, UNESCO*. B.m.: The University Press, Cambridge. 1996

[134] BUKATA, R. P, J. H JEROME, A. S KONDRATYEV a D. V POZDNYAKOV. *Optical Properties and Remote Sensing of Inland and Coastal Waters*. Illustrated. B.m.: CRC Press, 1995. ISBN 0-8493-4754-8.

[135] Chapter 5 Water Quality Conditions | Monitoring & Assessment | US EPA. *United States Environmental Protection Agency* [online]. 2012 [vid. 2015-04-15]. Dostupné z: http://water.epa.gov/type/rsl/monitoring/vms50.cfm

[136] DEPARTMENT OF WATER, WESTERN AUSTRALIA. *Water Quality monitoring program Design: A guideline to the development of surface water quality monitoring programs* [online]. B.m.: Department of Water, Western Australia. 2009 [vid. 2015-04-27]. Dostupné z: http://www.water.wa.gov.au/PublicationStore/first/87153.pdf

[137] EUROPEAN COMMISSION a DIRECTORATE-GENERAL FOR THE ENVIRONMENT. *Guidance on surface water chemical monitoring under the water framework directive No 19. No 19.* Luxembourg: OPOCE, 2009. ISBN 978-92-79-11297-3.

[138] WALK, Stream Habitat, Streamside BIOSURVEY a Macroinvertebrate ASSESSMENT. Volunteer Stream Monitoring: A Methods Manual [online]. 1997 [vid. 2015-04-16]. Dostupné z: http://vwvw.krisweb.com/biblio/gen_usepa_xxxx_1997_841b97003.pdf

[139] BARTRAM, J a R BALLANCE, ed. *Water quality monitoring a practical guide to the design and implementation of freshwater quality studies and monitoring programmes*. 1. ed. London [u.a.]: E & FN Spon, 1996. ISBN 0-419-22320-7.

[140] INTERNATIONAL STANDARDS ORGANIZATION. *Monitoring - ISO* [online]. [vid. 2015-05-01]. Dostupné z: http://www.iso.org/iso/home/search.htm?qt=monitoring&sort=rel&type=simple&published=on

[141] USALI, N a Mohd Hasmadi ISMAIL. Use of remote sensing and GIS in monitoring water quality. *Journal of sustainable development*. 2010, **3**(3), p228.

[142] WEBBER, C. I. *Biological field and Laboratory Methods for Measuring the Quality of Surface Waters and Effluents*. 1973. 00000

[143] UNESCO, ed. *Facing the challenges*. Paris: UNESCO [u.a.], 2012. World Water Assessment Programme, Vol. 3. ISBN 978-92-3-104235-5.

[144] O'NEIL, J. M, T. W DAVIS, M. A BURFORD a C. J GOBLER. The Rise of Harmful Cyanobacteria Blooms: The potential roles of eutrophication and climate change. Harmful Algae. 2012, **14**, 313–334.

[145] OGASHAWARA, I a Max MORENO-MADRIÑN. Improving Inland Water Quality Monitoring through Remote Sensing Techniques. *ISPRS International Journal of Geo-Information* [online]. 2014, **3**(4), 1234–1255. ISSN 2220-9964. Dostupné z: doi:10.3390/ijgi3041234

[146] MEYBECK, M., D CHAPMAN a R HELMER. *Global Freshwater Quality: A First Assessment.* B.m.: Blackwell Reference, Oxford, 1989.

[147] LINDELL, Tommy, ed. *Manual for monitoring European lakes using remote sensing techniques*. Luxembourg: Off. for Off. Publ. of the Europ. Communities, 1999. EUR, 18665. ISBN 92-828-5390-X.

[148] ZHANG, Y., J. PULLIAINEN, S. KOPONEN a M. HALLIKAINEN. A semi-empirical algorithm of water transparency at the Green wavelength band of optical remote sensing. *Progress In Electromagnetics Research*. 2002, **37**, 191–203.

[149] BABAN, S. M. J. Detecting water quality parameters in Norfolk Broads, U.K, Using Landsat imagery. *International Remote Sensing*. 1993, **14**, 1247–1267.

[150] WU, C. F, J. P WU, J. G QI, L. S ZHANG, H. Q HUANG, L. P LOU a Y. X CHEN. Empirical estimation of total Phosphorus concentration in the mainstream of the Qiantang River in China using Landsat TM data. *International Journal of Remote Sensing*. 2010, **31**, 2309–2324.

[151] TYRRELL, T. The relative influence of nitrogen and phosphorus on oceanic primary production. *Nature*. 1999, (400), 525–531.

[152] SCHINDLER, D. W. The evolution of phosphorus limitation in lakes. *Science*. 1977, (195), 260–266.

[153] EDMUNSON, W. T. Phosphorus, nitrogen and algae in Lake Washington after diversion of sewage. *Science*. 1970, (169), 690–691.

[154] REIF, Molly. *Remote Sensing for Inland Water Quality Monitoring: A US Army Corps of Engineers Perspective*. B.m.: United States Army Cops of Engineers. 2011.

[155] ERDMANN, E. S a S. S GREB. Research And Monitoring Of Lake Water Quality Using Remote Sensing. In: . Winsconsin. 2013.

[156] WANG, F. L, T KUNG a R. B VAN ASDALE. . Applications of Landsat-5 TM imagery in assessing and mapping water quality in Reelfoot Lake, Tennessee. *International Remote Sensing*. 2006, **27**, 5269–5283.

[157] KOPONEN, S, J PULLIAINEN, K KALLIO a M HALLIKAINEN. Lake water quality classification with airborne hyper spectral spectrometer and simulated MERIS data. *Remote Sensing of Environment*. 2002, **79**, 51–59.

[158] LILLESAND, T. M, W. L JOHNSON, R. L DEUELL, O. M LINDSTROM a D. E MEISNER. Use of Landsat data to predict the trophic state of Minnesota lakes. *Photogrammetric Engineering & Remote Sensing*. 1983, **49**, 219–229.

[159] JERLOV, N.G. *Marine Optics*. 2. vyd. Amsterdam, The Neatherlands: Elsevier Scientific Publishing Company, 1976. Elsevier Ocenography, 14.

[160] RITCHIE, Jerry C., Paul V. ZIMBA a James H. EVERITT. Remote sensing techniques to assess water quality. *Photogrammetric Engineering & Remote Sensing*. 2003, **69**(6), 695–704.

[161] REDMAN, C. L. Human dimensions of ecosystems. *Ecolo-Systems*. 1999, **2**, 516–526.

[162] FISHER, J a U KRONFIELD. Sun-simulated chlorophyll fluorescence: Influence of oceanic properties. *International Journal of Remote Sensing*. 1990, **11**(12), 2125–2147.

[163] PURKIS, S a V KLEMIS. *Remote Sensing and Global Environmental Change*. 1. vyd. B.m.: Wiley-Blackwell, 2011. ISBN 1-4051-8225-3.

[164] HAN, L a K. J JORDAN. Estimating and mapping chlorophyll-a concentration in the Pensacola Bay, Florida using Landsat ETM+ data. *International Journal of Remote Sensing* [online]. 2005, **26**(23), 5245–5254. ISSN 01431161. Dostupné z: doi:10.1080/01431160500219182

[165] LEE, G. F a A JONES-LEE. *Alternative approaches for Trophic state classification for water quality management part I: suitability of existing trophic state classification systems.* 1995

[166] GERMAN INSTITUTE OF STANDARDIZATION. *TP-Total Phosphorus - LAR AG* [online]. 2009 2004 [vid. 2015-05-04]. Dostupné z: http://www.lar.com/fr/products/tnb-tp-analysis/tp-total-phosphorus.html

[167] GRIESBACH, S. J a R. H PETERS. *The effects of analytical variation on estimates of phosphorus concentration in surface waters. Lake and Reservoir Management*. 1991.

[168] RIGLER, G. H. *A dynamic view of phosphorus cycle in lakes. In: E. J. Griffith, A. Beeton, J. M. Spencer and D. T. Mitchell (eds),Environmental Phosphorus Handbook*. eds. B.m.: John Wiley and Sons, 1973.

[169] INTERGRATED LAND MANAGEMENT BUREAU BRITISH COLUMBIA, CANADA. *WaterQualityParameterDefinitions.pdf* [online]. 1998 [vid. 2015-05-04]. Dostupné z: https://www.owrb.ok.gov/quality/monitoring/bump/pdf_bump/SOPs_for_streams/WaterQualityParameterDefinitions.pdf

[170] NIXON, S. W. Coastal Marine Eutrophication: A definition, social causes and future concerns. *Ophelia*. 1995, **41**, 199–219.

[171] CONLEY, J.D, H. W PEARL, R. W HOWARTH, D. F BOESCH, S. P SEITZINGER, K. E HAVENS, C LANCELOT a G. E LIKENS. Controlling Eutrophication: Nitrogen and Phosphorus. *Science*. 2009, **323**(5917), 1014–1015.

[172] SEKER, S, E AYAZ a E TRKCAN. Elman's recurrent neural network applications to condition monitoring in nuclear power plant and rotating machinery. *Engineering Application Artificial Intelligence*. 2003, **16**, 647–656.

[173] PETERS, R. H. The role of prediction in Limnology. *Limnology and Oceanography*. 1986, **31**, 1143–1159.

[174] KUTSER, T, H ARST, T MILLER, L KAARMANN a A MILLIUS. Telespectrometrical estimation of water transparency, chlorophyll-a and total phosphorus concentration of Lake Peipsi. *International Journal of Remote Sensing*. 1995, **16**(16), 3069–3085.

[175] UNITED STATES EBNVIRONMENTAL AGENCY. *5.5 Turbidity | Monitoring & Assessment | US EPA* [online]. 1995 [vid. 2015-05-04]. Dostupné z: http://water.epa.gov/type/rsl/monitoring/vms55.cfm

[176] TANANAEV, N. I a M.V DEBOLSKIY. Turbidity observations in sediment flux studies: Examples from Russian rivers in cold environments. *Geomorphology*. 2014, **218**, 63–71.

[177] PAVELICH, M. Patricia. Turbidity studies at the national water quality laboratory. In: *Turbidity and other surrogates workshop* [online]. 2002 [vid. 2015-05-05]. Dostupné z: http://www.comm-tec.com/library/technical_papers/various/pavelich.pdf

[178] Missouri Department of Natural Resources. *Missouri Department of Natural Resources* [online]. 1991 [vid. 2015-05-05]. Dostupné z: http://dnr.mo.gov/env/esp/waterquality-parameters.htm#Turbidity

[179] ZHANG, Qingguo, M. G MULLER, J WU a M. S FELD. Turbidity-free fluorescence spectroscopy of biological tissue. *Optics Letters*. 2000, **25**, 1451–1453.

[180] KHORRAM, S, Heather CHESHIRE, A. L GERACI a G LA ROSA. Water quality mapping of Augusta Bay, Italy from Landsat-TM data. *International Journal of Remote Sensing*. 1991, **12**, 803–808.

[181] COX, R. M, R. D FORSYTHE, G. E VAUGHAN a L. L OLMSTED. Assessing Water Quality in Catawba River Reservoirs Using Landsat Thematic Mapper Satellite Data, Lakes Reservoirs. *Reservoir Management*. 1998, **14**, 405–416.

[182] SWANSON, H a R ZURAWELL. *Steele Lake Water Quality Monitoring* [online]. Alberta, Canada: Environmental monitoring and Evaluation Branch, Environmental Assurance Division Alberta Environment. 2006 [vid. 2015-04-20]. Dostupné z: http://www.assembly.ab.ca/lao/library/egovdocs/2006/alen/159474.pdf

[183] DOKULIL, Martin. Impact of climate warming on European inland waters. *Inland Waters* [online]. 2014, **4**(1), 27–40. ISSN 20442041, 2044205X. Dostupné z: doi:10.5268/IW-4.1.705

[184] IPCC. Projections of Future Changes in Climate - AR4 WGI Summary for Policymakers. *Intergovernmental Panel On Climate Change* [online]. 2007 [vid. 2015-05-06]. Dostupné z: https://www.ipcc.ch/publications_and_data/ar4/wg1/en/spmsspm-projections-of.html

[185] HASSAN, Q. K. a K. M. RAHMAN. Applicability of remote sensing-based surface temperature regimes in determining deciduous phenology over boreal forest. *Journal of Plant Ecology* [online]. 2013, **6**(1), 84–91. ISSN 1752-9921, 1752-993X. Dostupné z: doi:10.1093/jpe/rts010

[186] BREZONIK, P. L, L. G OLMANSON, J. C FINLAY a M. E BAUER. Factors affecting the measurement of CDOM by remote sensing of optically complex inland waters. *Remote Sensing of Environment* [online]. 2015, **157**, 199–215. ISSN 00344257. Dostupné z: doi:10.1016/j.rse.2014.04.033

[187] SCHWARZ, J. N, P KOWALCZUK, S KACZMAREK, G. F COTA, B. G MITCHELL, M KAHRU, F. P CHAVEZ, A CUNNINGHAM, D MCKEE, Peter GEGE a OTHERS. Two models for absorption by coloured dissolved organic matter (CDOM). *Oceanologia* [online]. 2002, **44**(2) [vid. 2015-04-13]. Dostupné z: http://yadda.icm.edu.pl/agro/element/bwmeta1.element.agro-article-3da30bf9-9204-479b-83bd-a9c585e0df38

[188] CORBETT, Catherine A. Colored Dissolved Organic matter (CDOM) workshop summary [online]. 2007 [vid. 2015-04-13]. Dostupné z: http://scholarcommons.usf.edu/basgp_report/2/

[189] GUÉGUEN, C., M.A. GRANSKOG, G. MCCULLOUGH a D.G. BARBER. Characterisation of colored dissolved organic matter in Hudson Bay and Hudson Strait using parallel factor analysis. *Journal of Marine Systems* [online]. 2011, **88**(3), 423–433. ISSN 09247963. Dostupné z: doi:10.1016/j.jmarsys.2010.12.001

[190] KHAN, M. G, Y TAKAHITO, A MATTALEB a D VIONE. *Photobiogeochemistry of Organic Matter:Principles and Practices in Water*. Illustrated. B.m.: Springer Science and Business Media, 2012.

[191] HANSELL, D. A a C. A CARLSON. *Biogeochemistry of Marine Dissolved Organic Matter*. B.m.: Academic Press, 2002.

[192] KIRK, J. T. O. *Light and Photosynthesis in Aquatic Ecosystem*. Britain: Cambridge University Press, 1994.

[193] SANIBEL-CAPTIVA CONSERVATION FOUNDATION. *SCCF RECON - Home* [online]. 2014 [vid. 2015-05-06]. Dostupné z: http://recon.sccf.org/

[194] BERNARD, B. B, H BERNARD a James M. BROOKS. Determination of total carbon, total organic carbon and inorganic carbon in sediments. *Online Cited fill in: Apr*. 2004, **15**, 2004.

[195] CORROSIONPEDIA. What is Total Carbon? - Definition from Corrosionpedia. *Corrosionpedia* [online]. [vid. 2015-05-06]. Dostupné z: http://www.corrosionpedia.com/definition/1101/total-carbon

[196] SEPA. ippc-s402-speciality-organics-issue-6.pdf. *Scottish Environmental Protection Agency* [online]. 2003 [vid. 2015-05-06]. Dostupné z: http://www.sepa.org.uk/media/61092/ippc-s402-speciality-organics-issue-6.pdf

[197] WATERSHEDCOUNCIL.ORG. Water Quality Monitoring Data Parameters. *Watershedcouncil* [online]. [vid. 2015-05-06]. Dostupné z: http://www.watershedcouncil.org/learn/water%20terminology/

[198] BRICKER, S.B., B. LONGSTAFF, W. DENNISON, A. JONES, K. BOICOURT, C. WICKS a J. WOERNER. Effects of nutrient enrichment in the nation's estuaries: A decade of change. *Harmful Algae* [online]. 2008, **8**(1), 21–32. ISSN 15689883. Dostupné z: doi:10.1016/j.hal.2008.08.028

[199] VAN DONK, E a J VAN DE BUND. Impact of submerged macrophytes including charophytes on phyto- and zooplankton communities: allelopathy versus other mechanisms. *Aquatic Botany*. 2002, **72**(3–4), 261–274.

[200] SMITH, Val H. Eutrophication of freshwater and coastal marine ecosystems a global problem. *Environmental Science and Pollution Research*. 2003, **10**(2), 126–139.

[201] GUILDFORD, S. J a Robert E. HECKY. Total nitrogen, total phosphorus, and nutrient limitation in lakes and oceans: Is there a common relationship? *Limnology and Oceanography*. 2000, **45**(6), 1213–1223.

[202] SCHINDLER, D. W., R. E. HECKY, D. L. FINDLAY, M. P. STAINTON, B. R. PARKER, M. J. PATERSON, K. G. BEATY, M. LYNG a S. E. M. KASIAN. Eutrophication of lakes cannot be controlled by reducing nitrogen input: results of a 37-year whole-ecosystem experiment. *Proceedings of the National Academy of Sciences*. 2008, **105**(32), 11254–11258.

[203] BHATTI, A. M, D RUNDQUIST, J SCHALLES, M STEELE a M TAKAGI. QUALITATIVE ASSESSMENT OF INLAND AND COASTAL WATERS BY USING. In: *Networking the World with Remote Sensing*: *TS-16 Water*. Kyoto, Japan: International Society for Photogrammetry and Remote Sensing, 2010, s. 415–420.

[204] KRITIKOS, H, L YORINKS a H SMITH. Suspended solids analysis using ERTSA data. *Remote Sensing of Environment*. 1974, **3**, 69–80.

[205] TAO, Jing. *SEASONAL VARIABILITY OF TOTAL SUSPENDED MATTER IN MINAS BASIN, BAY OF FUNDY* [online]. Nova Scotia, 2013 [vid. 2015-05-06]. Dalhousie University Halifax,. Dostupné z: http://dalspace.library.dal.ca/bitstream/handle/10222/35458/Tao-Jing-MSc-OCEA-August-2013.pdf?sequence=1

[206] ZHANG, M, J TANG, Q DONG, Q. T SONG a Jing DING. Retrieval of total suspended matter concentration in the Yellow and East China Seas from MODIS imagery. *Remote Sensing of Environment* [online]. 2010, **114**(2), 392–403. ISSN 00344257. Dostupné z: doi:10.1016/j.rse.2009.09.016

[207] MAY, C. L, J. R KOSEFF, L. V LUCAS, J. E CLOEM a D. H SCHOELLHAMER. Effects of Spatial and Temporal variability of turbidity on phytoplankton blooms. *Marine Ecology Progress*. 2003, 254, 111–128.

[208] BALL, A. S, M WILLIAMS, D VINCENT a J ROBINSON. Algal growth control by a barley straw extract. *Bioresource Technology*. 2001, **77**, 177–181.

[209] HARRIS, G. A Nutrient Dynamics Model for Australian Waterways, LandUse, Catchment Biogeochemistry and Water Quality in Australian Rivers, Lakes and Estuaries. *Australia State of the Environment Technical Paper Series (Inland Waters)*. 2001, 2.

[210] ENVIRONMENTAL PROTECTION AUTHORITY. *Western Australia Water Quality Guidelines for Fresh and Marine Waters: ANZECC/AWRC 1992* [online]. 0730956415. 1992. Dostupné z: http://epa.wa.gov.au/EPADocLib/1396_B711.pdf

[211] GALLOWAY, J. N, A. R TOWNSEND, J. W ERISMAN, M BEKUNDA, Z CAI, J. R FRENEY, L. A MARTINELLI, S. P SEITZINGER a M. A SUTTON. Transformation of the Nitrogen Cycle: Recent Trends, Questions and Potential Solutions. *Science*. 2008, **320**, 889–892.

[212] CHILDERS, D. L, J CORMAN, M EDWARDS a J. J ELSER. Sustainability Challenges of Phosphorus and Food: Solutions from Closing the Human Phosphorus Cycle. *BioScience* [online]. 2011, **61**(2), 117–124. ISSN 00063568, 15253244. Dostupné z: doi:10.1525/bio.2011.61.2.6

[213] METSON, G. S, E. M BENNETT a J.J ELSER. The role of diet in phosphorus demand. *Environmental Research Letters* [online]. 2012, **7**(4), 044043. ISSN 1748-9326. Dostupné z: doi:10.1088/1748-9326/7/4/044043

[214] CUI, S., Y. SHI, P. M. GROFFMAN, W. H. SCHLESINGER a Y.-G. ZHU. Centennial-scale analysis of the creation and fate of reactive nitrogen in China (1910-2010). *Proceedings of the National Academy of Sciences* [online]. 2013, **110**(6), 2052–2057. ISSN 0027-8424, 1091-6490. Dostupné z: doi:10.1073/pnas.1221638110

[215] DODDS, W. K, W. W BOUSKA, J. L EITZMANN, T. J PILGER, K. L PITTS, A. J RILEY, J. T SCHLOESSER a Darren J. THORNBRUGH. Eutrophication of U.S. Freshwaters: Analysis of Potential Economic Damages. *Environmental Science & Technology* [online]. 2009, **43**(1), 12–19. ISSN 0013-936X, 1520-5851. Dostupné z: doi:10.1021/es801217q

[216] CHAPRA, S. C. *surface water-quality modelling*. B.m.: Waveland Press, 2008. ISBN 1-4786-0830-7.

[217] ART, H.W. *A dictionary of ecology and environmental science*. 1. vyd. New York: Henry Holt and Company, 1993.

[218] RMB ENVIRONMENTAL LABORATORIES. *Lake Trophic States - RMBEL* [online]. 2015 [vid. 2015-06-22]. Dostupné z: http://rmbel.info/lake-trophic-states-2/

[219] POKORNY, Daniel, Eva ROLECKOVA, Jana JANKOVA a Jan RAUCHER. *REPORT ON WATER MANAGEMENT IN THE CZECH REPUBLIC.* [online]. 2013 [vid. 2015-09-09]. Dostupné z: http://eagri.cz/public/web/file/273506/Modra_zprava_ENG_web.pdf

[220] DATT, B. Remote sensing of chlorophyll a, chlorophyll b, chlorophyll a+ b, and total carotenoid content in eucalyptus leaves. *Remote Sensing of Environment*. 1998, **66**(2), 111–121.

[221] KUKLA, G. Analysis of historical development of landscape with special view to water component. *Rural Landscaping*. 2007.

[222] DEPARTMENT OF ENVIRONMENTAL SERVICES. *Layman's Guide for Measuring a Lake's State* [online]. B.m.: New Hampshire Environmental services. 1997 [vid. 2015-06-22]. Dostupné z: http://des.nh.gov/organization/commissioner/pip/factsheets/bb/documents/bb-27.pdf

[223] HAN, Luoheng. Spectral reflectance with varying suspended sediment concentrations in clear and algae-laden waters. *Photogrammetric Engineering and Remote Sensing*. 1997, **63**(6), 701–705.

[224] JONES, R. A a G. F LEE. Chlorophyll-a raw water quality parameter. *American Water Works Association Journal*. 1982, 490–494.

[225] INTERNATIONAL ORGANIZATION FOR STANDARDIZATION. *ISO 10260:1992 - Water quality -- Measurement of biochemical parameters -- Spectrometric determination of the chlorophyll-a concentration* [online]. 1992 [vid. 2015-06-25]. Dostupné z: http://www.iso.org/iso/catalogue_detail.htm?csnumber=18300

[226] INTERNATIONAL ORGANISATION FOR STANDARDIZATION. *ISO 8245:1999,Water Quality: Guidelines for the determination of total organic carbon (TOC) and dissolved organic carbon (DOC)*. B.m.: International Organisation for Standardization. 1999. 00000

[227] SKALAR. *Formacs SERIES | Total Organic Carbon (TOC) and Total Nitrogen analyzers* [online]. 2015 [vid. 2015-06-25]. Dostupné z: http://www.skalar.com/analyzers/total-organic-carbon-toc-and-total-nitrogen-tn-analyzers/

[228] CSUROS, M. *Environmental Sampling and Analysis: Lab Manual*. B.m.: CRC Press, 1997.

[229] ADREFOUET, S, R BINDSCHANDLER, E BROWN DE COLSTOUN, M CHOATE, W CHOMENTOWSKI, J CHRISTOPHERSON, B DOOM, D. K HALL, C HOLIFIELD, S HOWARD, C KRANENBURG, Scott LEE, J. G MASEK, M. S MORAN, F MUELLER-KARGER, D OHLEN, D PALANDRO, J PRICE, J QI, B REED, J SAMEK, P SCARAMUZZA, D SKOLE, J SCHOTT, J STOREY, K THOME, D TORRES-PILLIZA, J VOGELMANN, D WILLIAMS, C WOODCOCK a B WYLIE. *Preliminary assessment of the value of Landsat 7 ETM+ Data following scan line corrector Malfunction*. B.m.: United State Geological Survey. 2003

[230] OLMANSON, L. G., M. E. BAUER a P. L. BREZONIK. A 20-year Landsat water clarity census of Minnesota's 10,000 lakes. *Remote Sensing of Environment* [online]. 2008, **112**(11), 4086–4097. ISSN 00344257. Dostupné z: doi:10.1016/j.rse.2007.12.013

[231] CHANDER, G, B. L MARKHAM a D. L HELDER. Summary of current radiometric calibration coefficients for Landsat MSS,TM, ETM+m and EO-1 ALI sensors. *Remote Sensing of Environment*. 2009, **113**(5), 893–903.

[232] GAO, B. C. NDWI-A Normalized Difference Water Index for Remote Sensing of Vegetation Liquid Water From Space. *Remote Sensing Environment*. 1996, **58**, 257–266.

[233] COHEN, L, L MANION a K MORRISON. *Research Methods in Education*. 6. vyd. B.m.: Routledge, Taylor & Francis, 2007. ISBN 0-415-37410-3.

[234] EFRON, B a R. J TIBSHIRANI. *An introduction to the Bootstrap*. Monographs on statistics and Applied Probability 57. B.m.: Springer Science and Business Media, 1993. ISBN 978-0-412-04231-7.

[235] OLMANSON, Leif G., Patrick L. BREZONIK a Marvin E. BAUER. Airborne hyperspectral remote sensing to assess spatial distribution of water quality characteristics in large rivers: The Mississippi River and its tributaries in Minnesota. *Remote Sensing of Environment* [online]. 2013, **130**, 254–265. ISSN 00344257. Dostupné z: doi:10.1016/j.rse.2012.11.023

[236] WU, M, W ZHANG, X WANG a D LUO. Application of MODIS satellite data in monitoring water quality parameters of Chaohu Lake in China. *Environmental Monitoring and Assessment*. 2009, **148**, 255–264.

[237] BABOROWSKI, M, V SIMEONOV a J. W EINAX. Assessment of Water Quality in the Elbe River at Flood Water Conditions Based on Cluster Analysis, Principle Components Analysis, and Source Apportionment. *CLEAN - Soil, Air, Water*. 2012, **40**(4), 373–380. ISSN 18630650.

[238] RMBEL. *Chlorophyll-a - RMBEL* [online]. [vid. 2015-06-24]. Dostupné z: http://rmbel.info/chlorophyll-a/

[239] ARAYA, Y. Filtering, Enhancement, and Extraction. *Erin's Remote Sensing Blog* [online]. 2011 [vid. 2015-05-18]. Dostupné z: http://remotesensor.blogspot.cz/

[240] OHIO WESLYAN UNIVERSITY. *The Nutrients - Eutrophication of Lake Erie* [online]. [vid. 2015-05-13]. Dostupné z: https://sites.google.com/a/owu.edu/lake-erie-eutrophication/what-is-eutrophication/the-nutrients

[241] TESTO. *Testo 110 - 1 Channel NTC Thermometer | Testo Limited Instruments* [online]. 2015 [vid. 2015-06-24]. Dostupné z: http://www.testolimited.com/testo-110-1-channel-ntc-thermometer

[242] LIEW, S. C. *Effects of Atmosphere: Optical and Infrared Remote Sensing* [online]. 2001 [vid. 2015-06-08]. Dostupné z: http://www.crisp.nus.edu.sg/~research/tutorial/optical.gif

[243] TURNER, W, S SPECTOR, N GARDINER, M FLADELAND, E STERLING a M STEININGER. Remote sensing for biodiversity science and conservation. *Trends in Ecology & Evolution* [online]. 2003, **18**(6), 306–314. ISSN 01695347. Dostupné z: doi:10.1016/S0169-5347(03)00070-3

[244] *Woodward Wednesday 3: Chlorophyll a — B.R.S.M.* [online]. [vid. 2015-06-22]. Dostupné z: http://brsmblog.com/woodward-wednesday-3-chlorophyll-a/

[245] TURNER, Woody, Sacha SPECTOR, Ned GARDINER, Matthew FLADELAND, Eleanor STERLING a Marc STEININGER. Remote sensing for biodiversity science and conservation. *Trends in Ecology & Evolution* [online]. 2003, **18**(6), 306–314. ISSN 01695347. Dostupné z: doi:10.1016/S0169-5347(03)00070-3

[246] SHAPLEY, Patricia. *Chlorophyll.jpg (JPEG Image, 424 × 304 pixels)* [online]. 2012 [vid. 2015-06-22]. Dostupné z: http://butane.chem.uiuc.edu/pshapley/GenChem2/A4/Chlorophyll.jpg

[247] FLOOD, Neil. Continuity of Reflectance Data between Landsat-7 ETM+ and Landsat-8 OLI, for Both Top-of-Atmosphere and Surface Reflectance: A Study in the Australian Landscape - See more at: http://www.mdpi.com/2072-4292/6/9/7952/htm#sthash.IvV7rGSs.dpuf [online]. nedatováno. Dostupné z: http://www.mdpi.com/2072-4292/6/9/7952/htm

[248] MARTINEC, Emil. *Noise, Dynamic Range and Bit Depth in Digital SLRs* [online]. 2008 [vid. 2015-05-25]. Dostupné z: http://theory.uchicago.edu/~ejm/pix/20d/tests/noise/

[249] BIOCHROM. *Biochrom Libra S22 UV/Vis Spectrophotometer - Biochrom* [online]. [vid. 2015-06-25]. Dostupné z: http://www.biochrom.co.uk/product/48/biochrom-libra-s22-uv-vis-spectrophotometer.html

[250] UNIVERSITY OF MARYLAND. *Atmospheric Correction* [online]. 1995 [vid. 2015-06-08]. Dostupné z: http://www.umiacs.umd.edu/labs/GC/atmo/

[251] *Photon noise* [online]. [vid. 2015-05-25]. Dostupné z: http://aas.aanda.org/articles/aas/full/1999/01/ds1570/img45.gif

[252] QUANTUM SCIENTIFIC IMAGING. Understanding CCD Read Noise. *Quantum Scientific Imaging* [online]. 2008 2006 [vid. 2015-05-25]. Dostupné z: http://qsimaging.com/ccd_noise.html:

6 APPENDICES

6.1 Various functions used in developing models

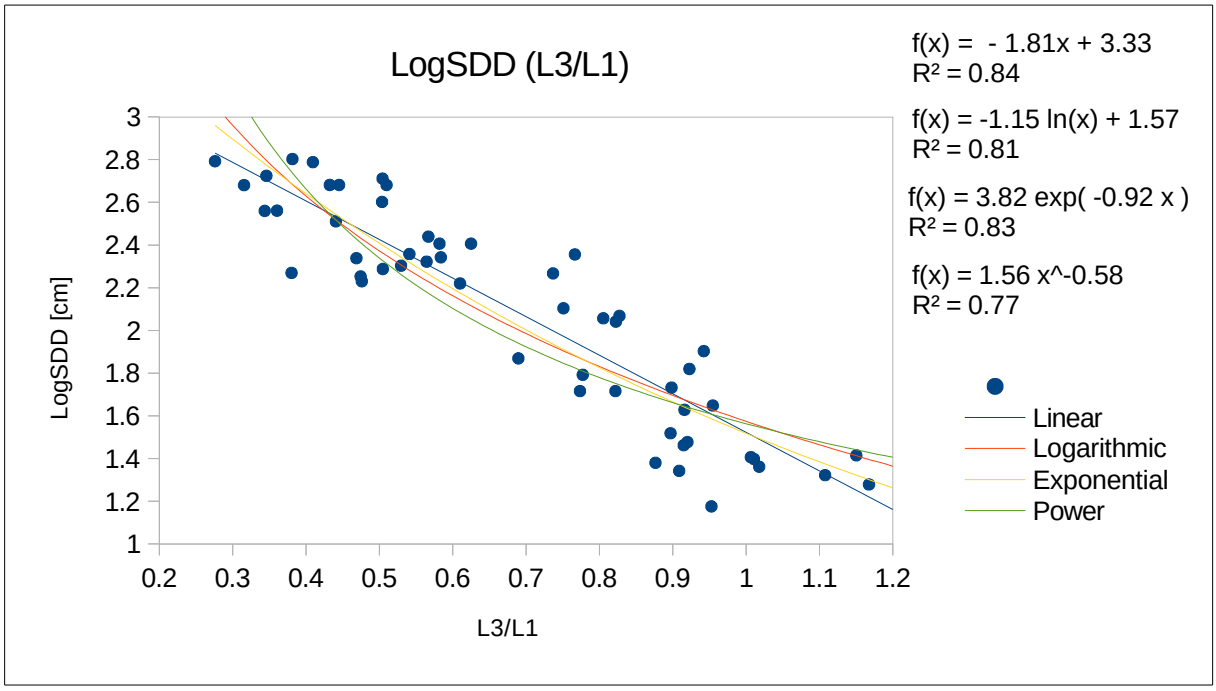

Figure 79: Model Chart for SDD showing the functions used in developing models

6.2 Table showing the r^2 values for Measured parameters

Parameter	L1	L2	L3	L4	L5	L7
R^2 chl-a	0.01	0.30	0.38	0.23	0.01	0.01
R^2 log chl-a	0.01	0.25	***0.50***	0.13	0.02	0.03
TC [mg/l]	0.02	0.10	0.27	0.16	0.00	0.04
Log TC	0.03	0.11	0.29	0.18	0.00	0.05
TOC [mg/l]	0.09	0.38	0.38	0.36	0.02	0.01
LogTOC	0.13	***0.45***	***0.42***	0.29	0.00	0.01
TN [mg/l]	0.07	0.04	0.13	0.20	0.08	0.00
LogTN [mg/l]	0.04	0.01	0.07	0.08	0.09	0.00
T [°C]	0.15	0.00	0.00	0.13	0.01	0.00
Log T	0.12	0.01	0.00	0.12	0.02	0.00
Secchi [cm]	0.10	0.28	***0.49***	0.06	0.01	0.02
Log Secchi	0.05	0.37	***0.64***	0.15	0.00	0.03

Parameter	L1/L2	L1/L3	L1/L4	L1/L5	L1/L7	L2/L1
R^2 chl-a	0.35	0.36	0.16	0.00	0.02	***0.51***
R^2 log chl-a	0.35	***0.66***	0.11	0.00	0.00	***0.45***
TC [mg/l]	0.22	0.32	0.26	0.03	0.04	0.26
Log TC	0.25	0.34	0.27	0.02	0.04	0.30
TOC [mg/l]	0.39	***0.41***	0.39	0.02	0.00	***0.53***
LogTOC	***0.54***	***0.52***	***0.42***	0.02	0.00	***0.64***
TN [mg/l]	0.18	0.20	0.17	0.02	0.01	0.26
LogTN [mg/l]	0.07	0.12	0.04	0.06	0.04	0.12
T [°C]	0.21	0.03	***0.42***	0.00	0.00	0.19
Log T	0.24	0.03	***0.42***	0.01	0.01	0.19
Secchi [cm]	***0.66***	***0.75***	0.22	0.00	0.02	***0.64***
Log Secchi	***0.59***	***0.72***	0.24	0.01	0.06	***0.69***

Parameter	L2/L3	L2/L4	L2/L5	L2/L7	L3/L1	L3/L2
R^2 chl-a	0.16	0.00	0.11	0.16	***0.52***	0.20
R^2 log chl-a	***0.44***	0.02	0.07	0.11	***0.66***	***0.47***
TC [mg/l]	0.25	0.06	0.09	0.10	***0.44***	0.31
Log TC	0.26	0.06	0.08	0.10	***0.48***	0.32
TOC [mg/l]	0.17	0.09	0.05	0.08	***0.60***	0.23
LogTOC	0.19	0.05	0.10	0.11	***0.66***	0.24
TN [mg/l]	0.15	0.04	0.00	0.00	0.35	0.19
LogTN [mg/l]	0.11	0.00	0.02	0.01	0.21	0.14
T [°C]	0.01	0.14	0.05	0.03	0.06	0.00
Log T	0.01	0.11	0.06	0.04	0.05	0.01
Secchi [cm]	0.34	0.02	0.17	0.13	***0.70***	***0.41***
Log Secchi	***0.41***	0.00	0.20	0.20	***0.84***	***0.52***

6.3 Model charts and their model performance scatter plots for second best models.

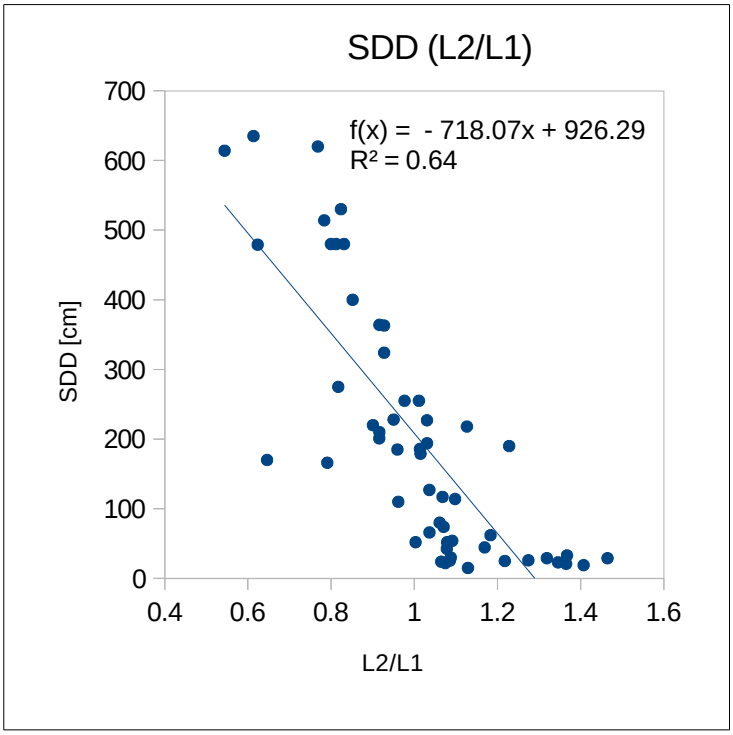

Figure 80:Model chart of SDD

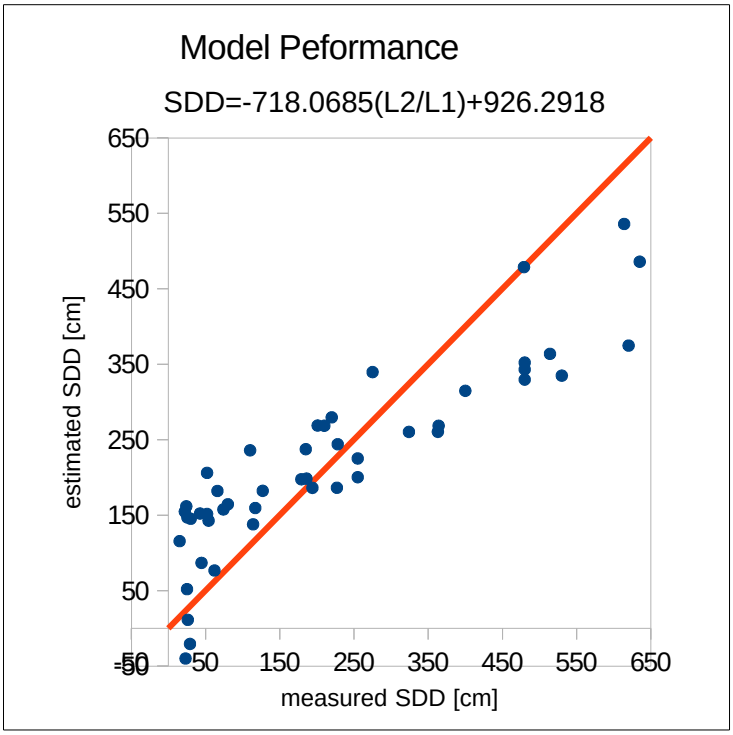

Figure 81: Scatter plot for Model Performance of SDD

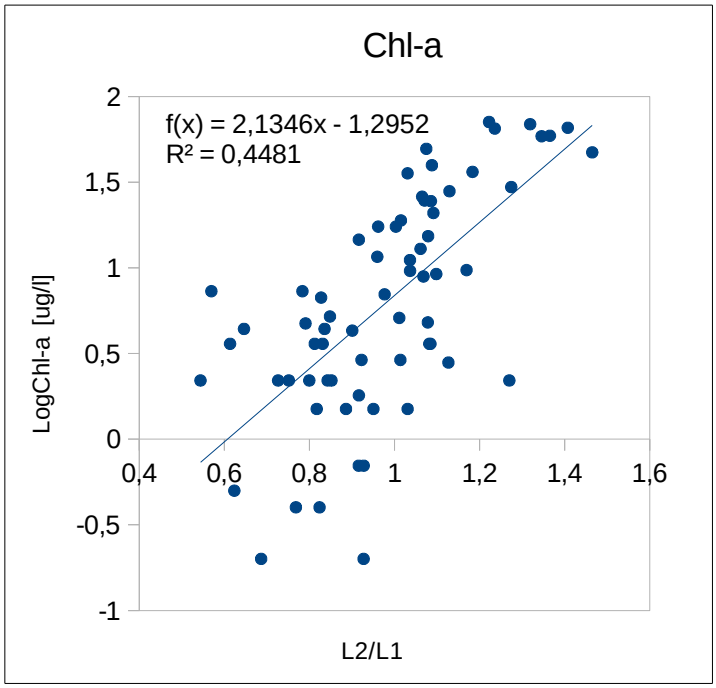

Illustration 2 part 1:Model chart for Chl-a

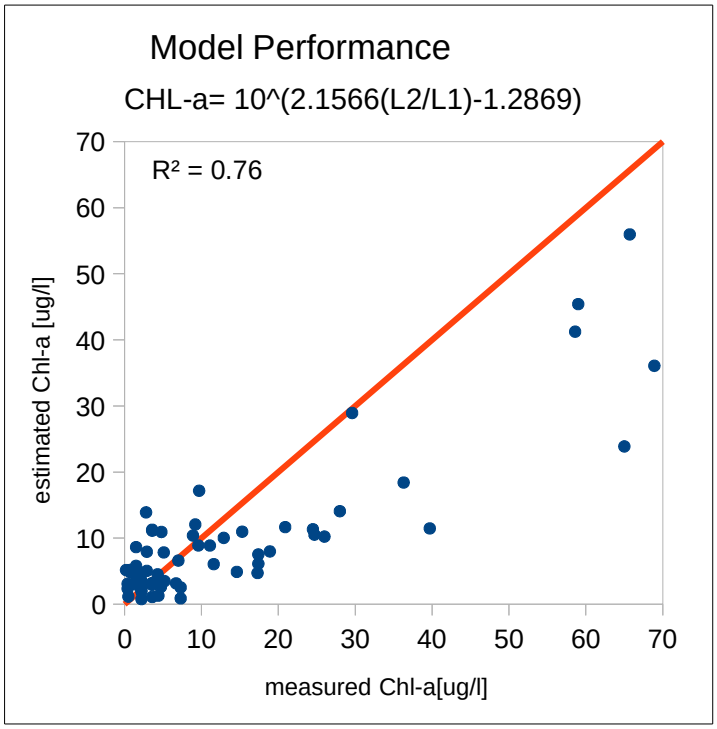

Illustration 2 part 2: Scatter plot for Model Performance of Chl-a

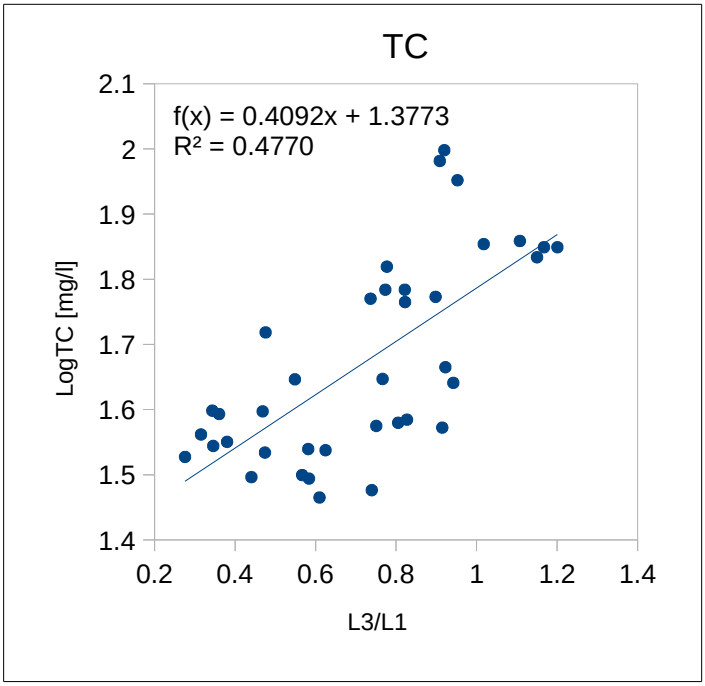

Illustration 3 part 1: Model chart for TC

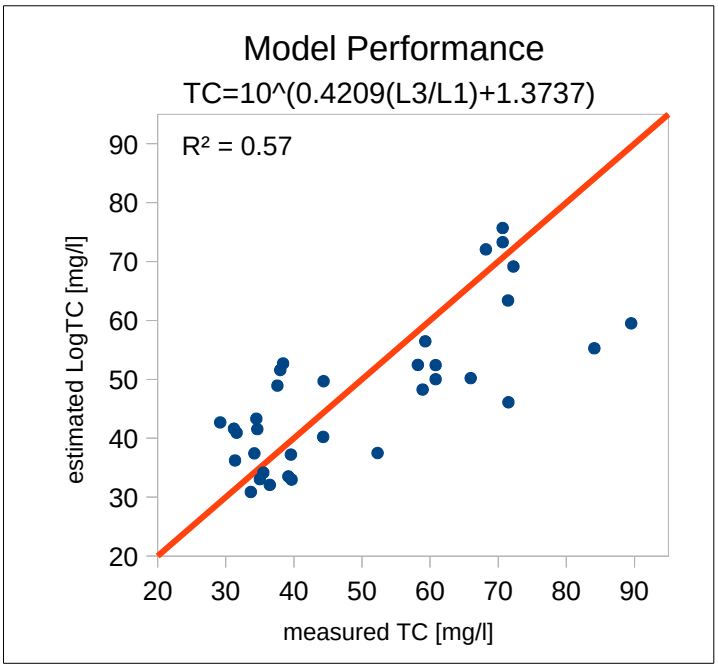

Illustration 3 part 2: Scatter plot for Model Performance of TC

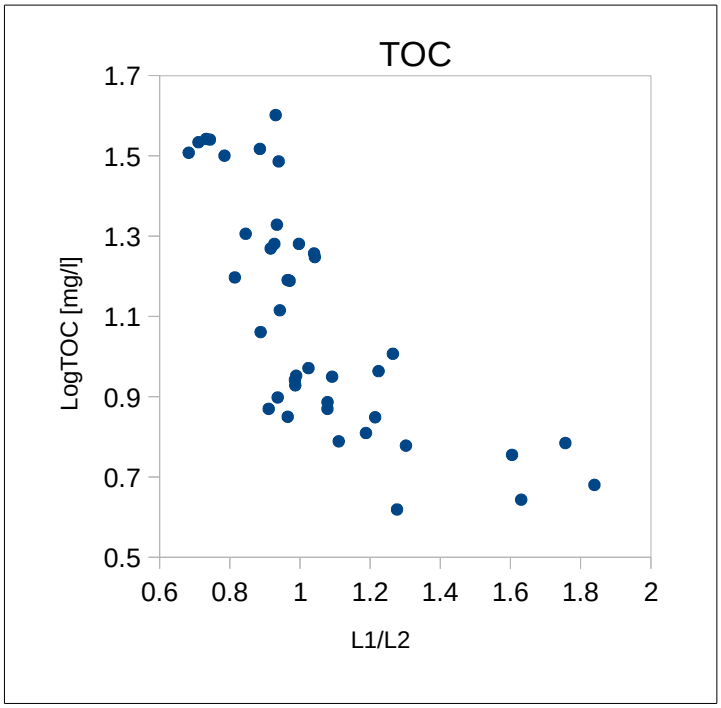

Illustration 4 part 1: Model chart for TOC

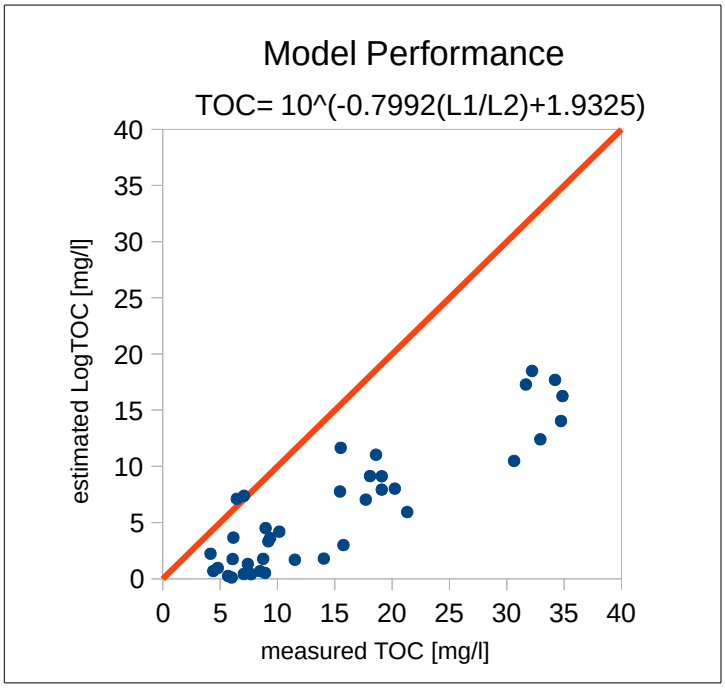

Illustration 4 part 2: Scatter plot for Model Performance of TOC

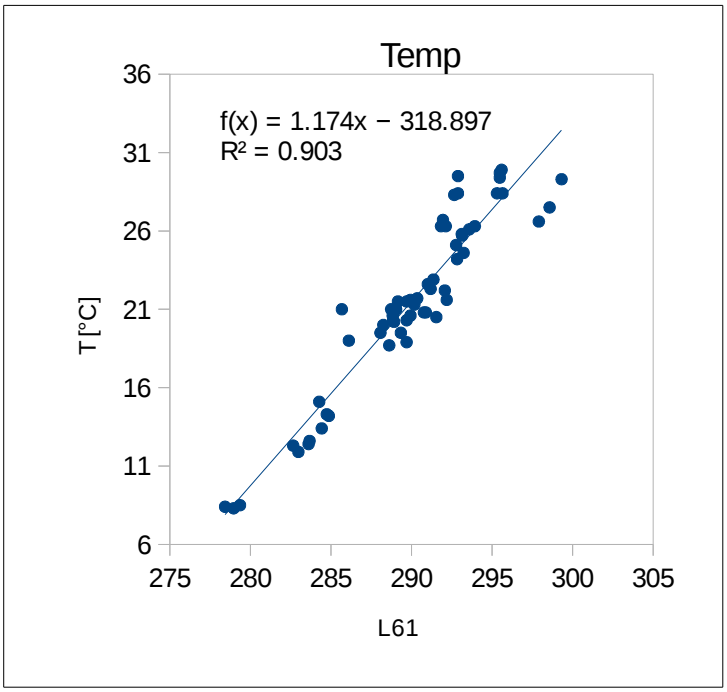

Illustration 5 part 1:Model chart for T

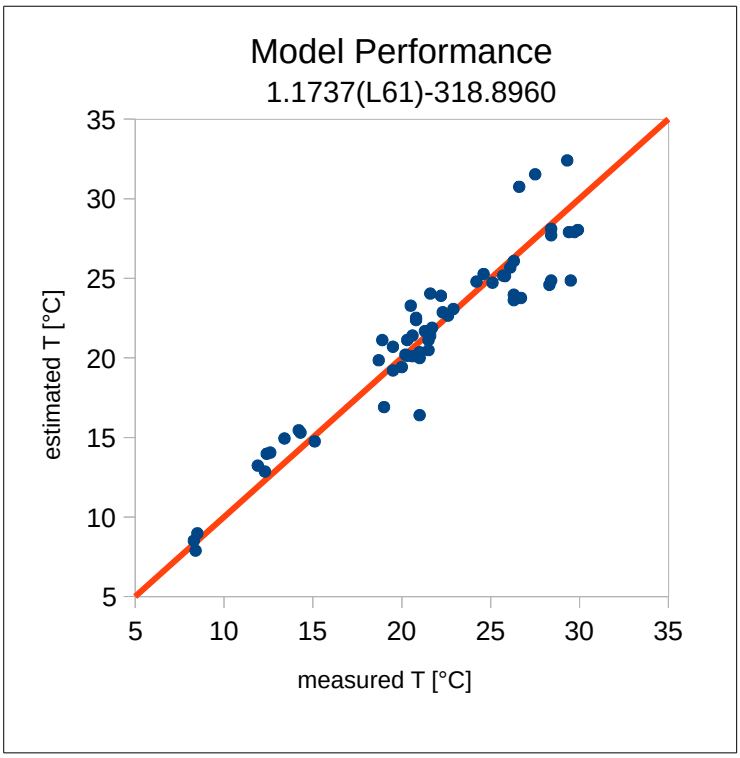

Illustration 5 part 2:Scatter plot for Model Performance of T

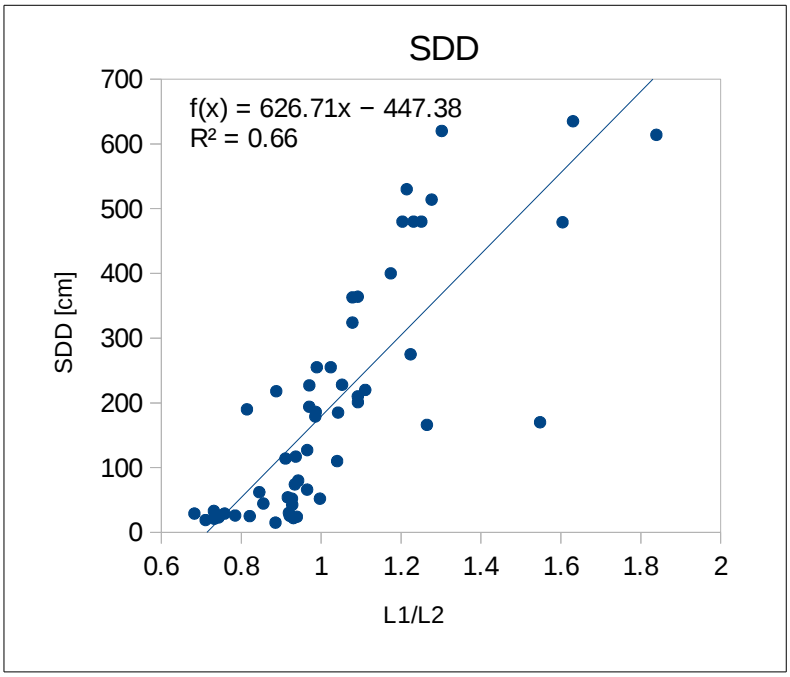

Illustration 6 part 1: Model chart for SDD

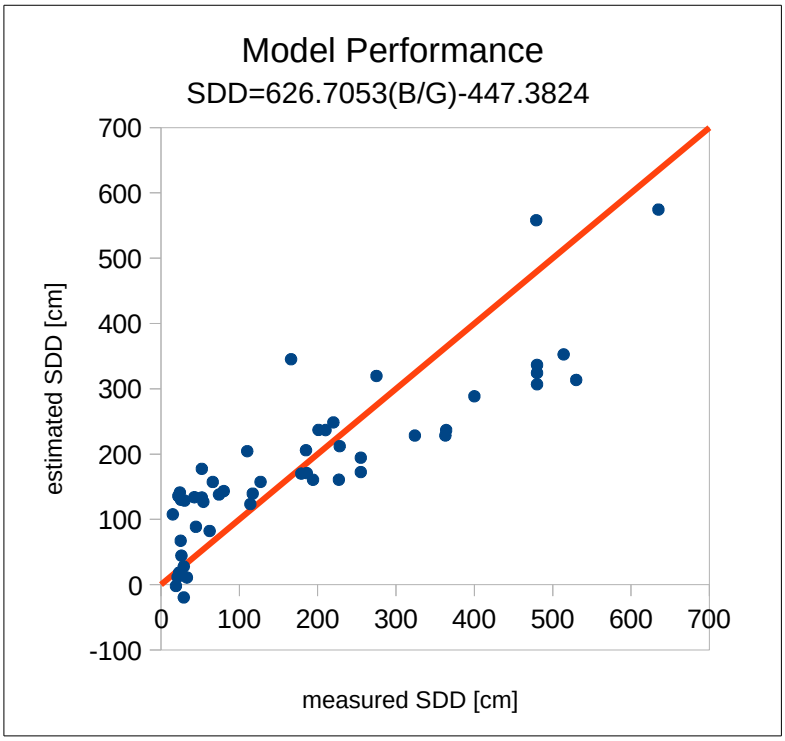

Illustration 6 part 2: Scatter plot for Model Performance of SDD

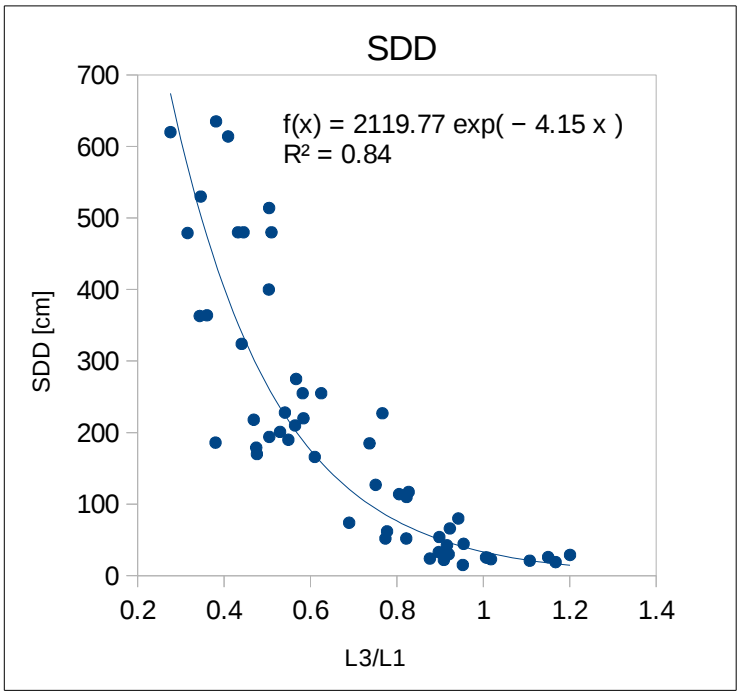

Illustration 7 part 1: Model chart for SDD

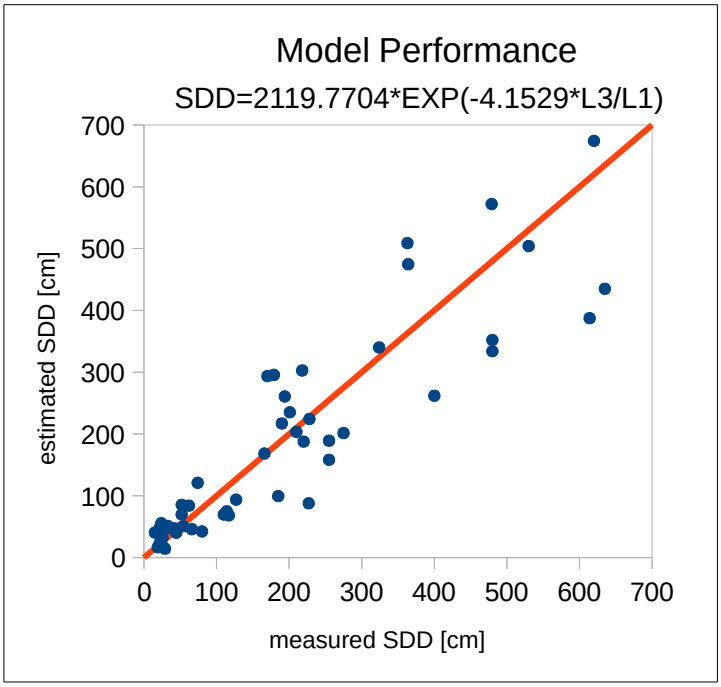

Illustration 7 part 2: Scatter plot for Model Performance of SDD

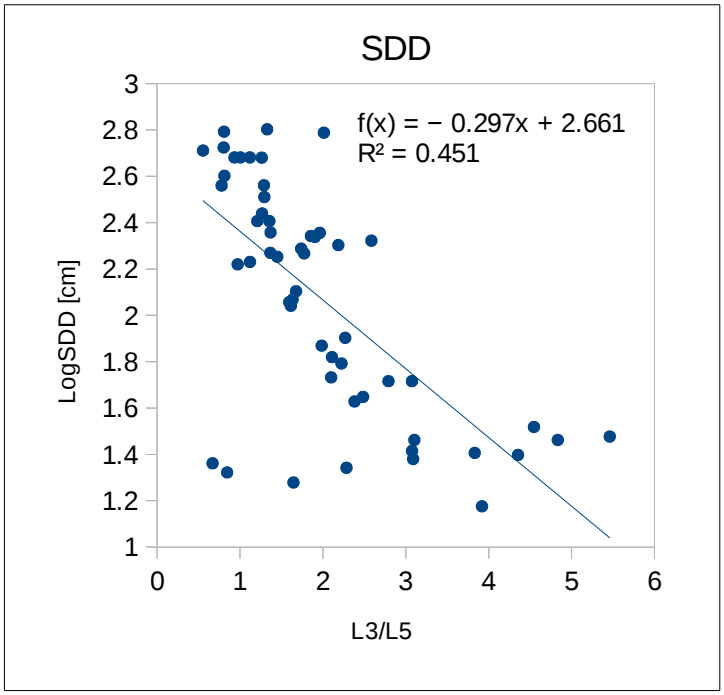

Illustration 8 part 1: Model chart for SDD

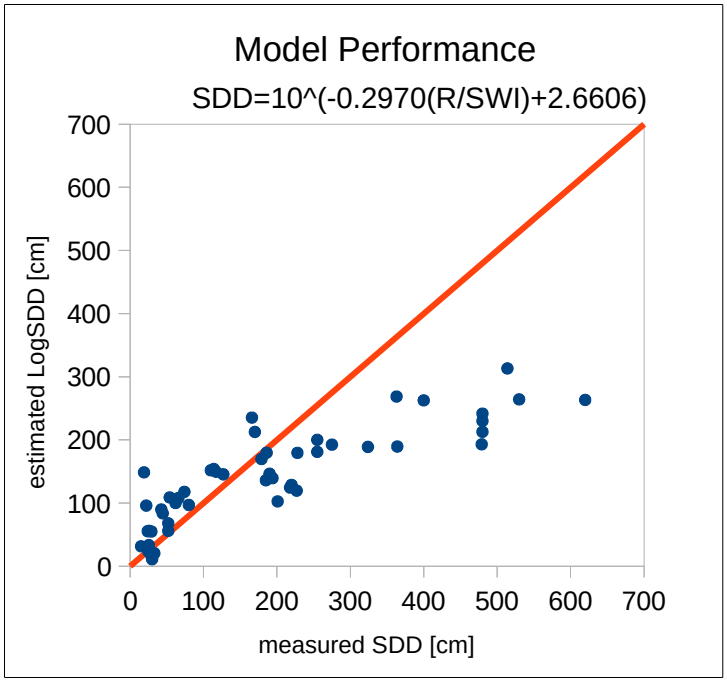

Illustration 8 part 2: Scatter plot for Model Performance of SDD

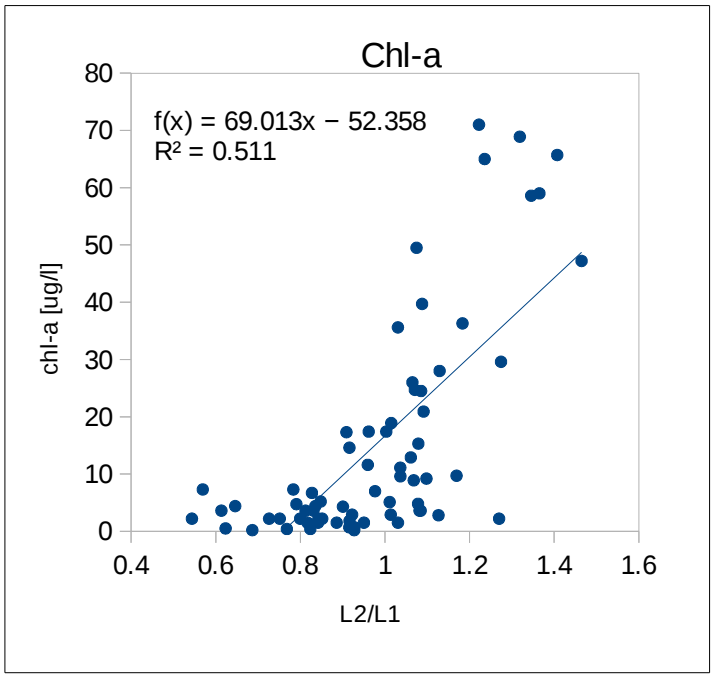

Illustration 9 part 1: Model chart for Chl-a

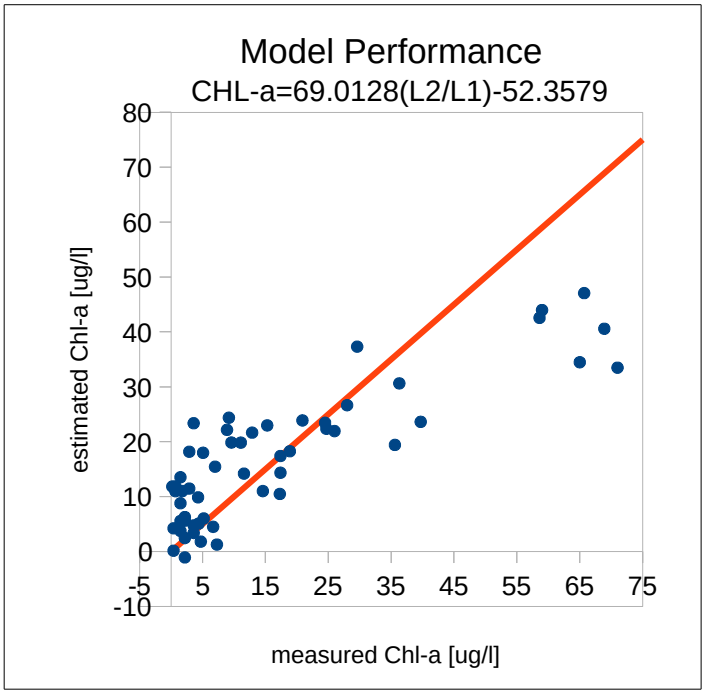

Illustration 9 part 2: Scatter plot for Model Performance of Chl-a

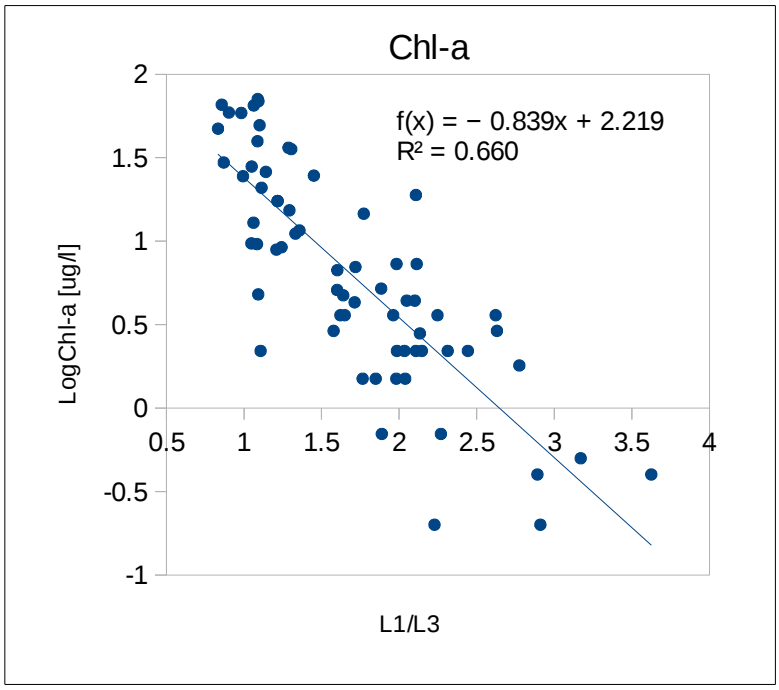

Illustration 10 part 1: Model chart for Chl-a

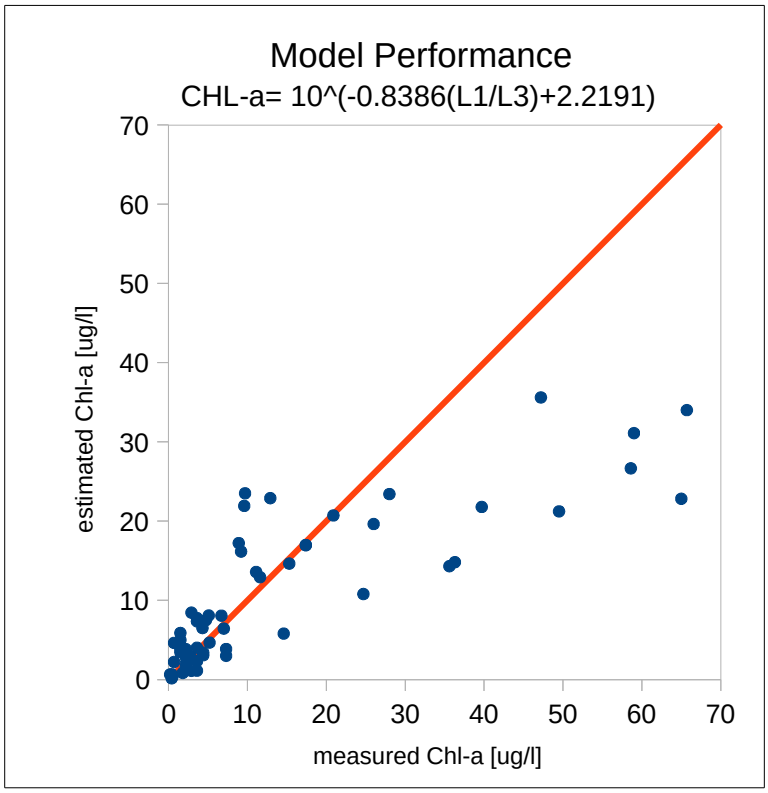

Illustration 10 part 2: Scatter plot for Model Performance of Chl-a

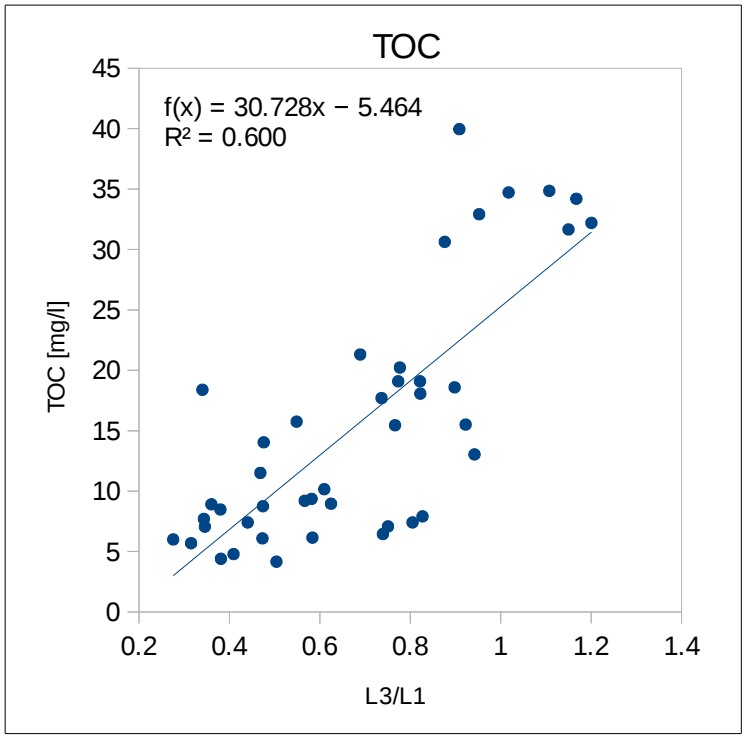

Illustration 11 part 1: Model chart for TOC

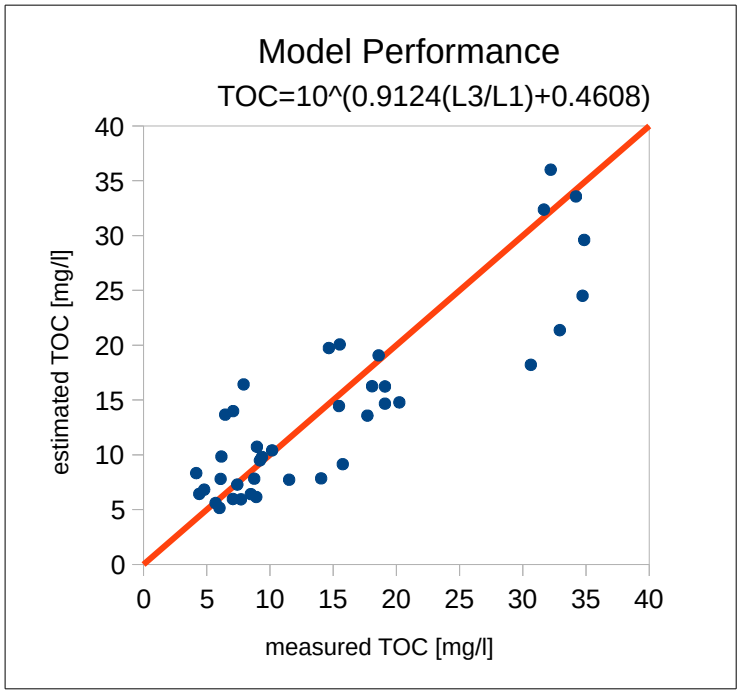

Illustration 11 part 2: Scatter plot for Model Performance of TOC

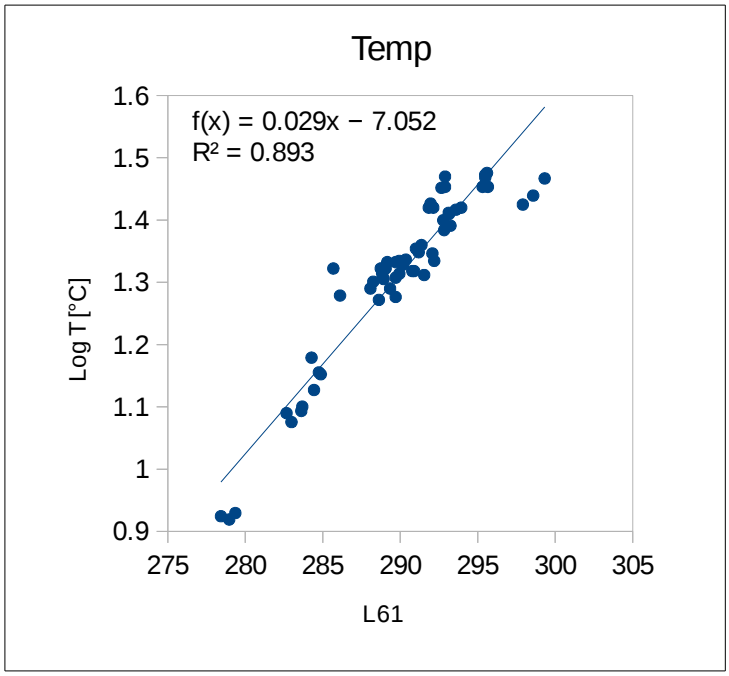

Illustration 12 part 1: Model chart for T

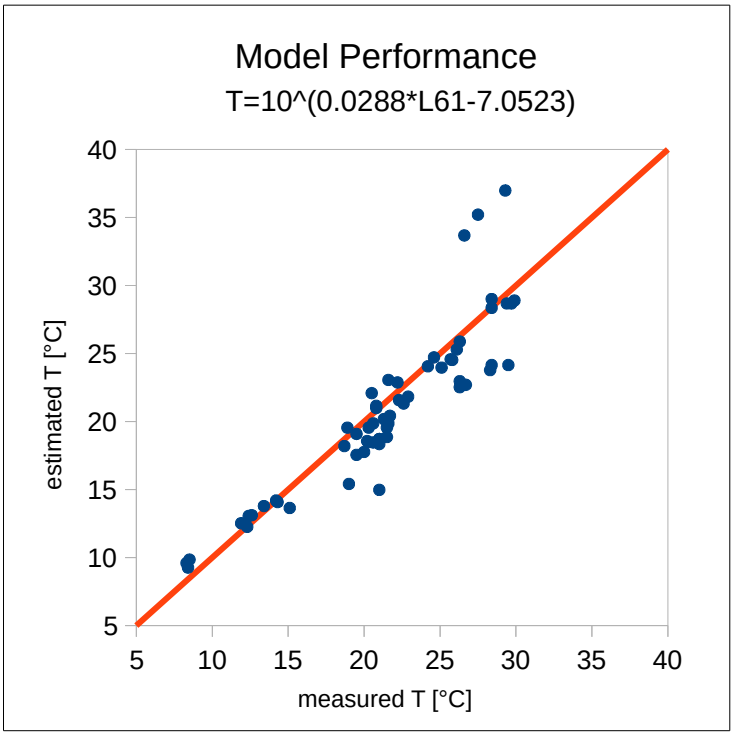

Illustration 12 part 2: Scatter plot for Model Performance of T

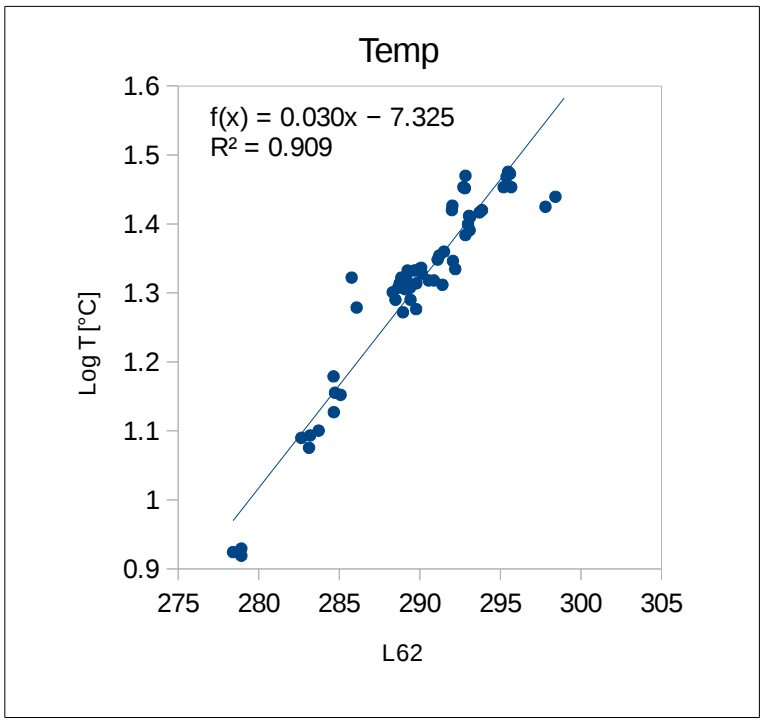

Illustration 13 part 1: Model chart for T

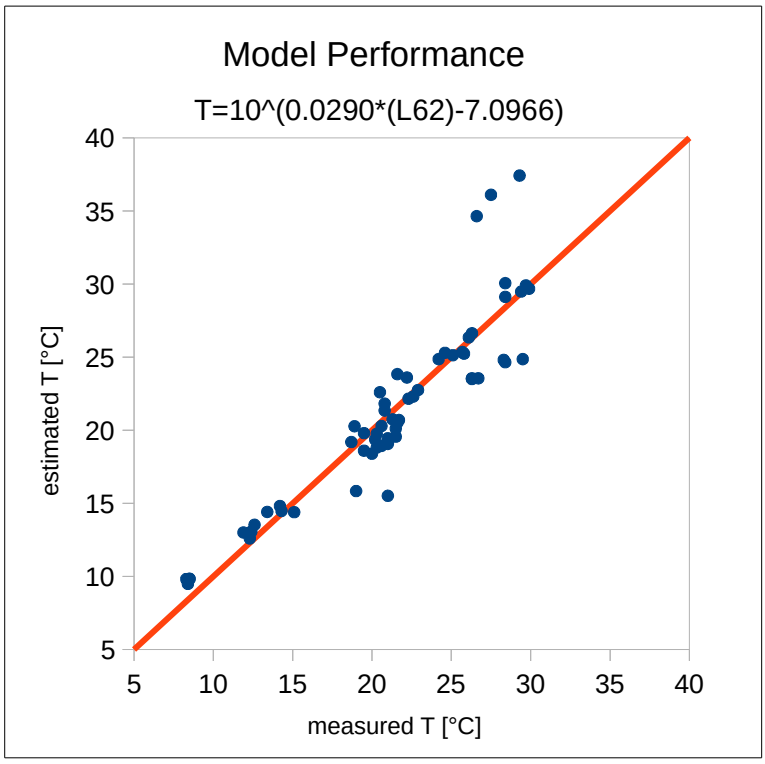

Illustration 13 part 2: Scatter plot for Model Performance of T

6.4 Unsmoothed Top of Atmosphere Reflectance

Parameter	L1/L2	L1/L3	L1/L4	L1/L6	L3/L1	L4/L1	L62/L1
R^2 chl-a [ug/l]	0.2547	0.2811	0.0858	0.0535	0.2837	0.1387	0.0722
R^2 log chl-a [ug/l]	0.1622	0.1997	0.0258	0.0200	***0.4293***	0.0541	0.0280
TC [mg/l]	0.1469	0.2051	0.0454	0.1033	0.2767	0.0633	0.1133
Log TC	0.1020	0.1605	0.3172	0.0360	***0.4231***	0.3059	0.0440
TOC [mg/l]	0.3164	0.3667	0.2046	0.1734	***0.4425***	0.2584	0.2085
LogTOC	0.3452	***0.4168***	***0.4447***	0.2814	***0.5592***	***0.4410***	0.2860
TN [mg/l]	0.1290	0.1646	0.0531	***0.4249***	0.2107	0.1221	***0.4320***
LogTN [mg/l]	0.0282	0.0401	0.0167	0.3642	0.0918	0.0504	0.3553
T [°C]	0.2258	0.2466	0.3674	0.3563	0.0526	0.2973	0.3228
Log T [°C]	0.2300	0.2519	***0.4192***	***0.4129***	0.0615	0.3039	0.3496
SDD [cm]	0.3509	***0.4073***	0.1324	0.2013	***0.5480***	0.1125	0.1880
Log SDD [cm]	***0.4221***	***0.4747***	0.1972	0.1224	***0.6588***	0.1991	0.1224